Interactions of Water Droplets in Organic Media

by

Hadi Afsaneh

A thesis submitted in partial fulfillment of the requirements for the degree of

Master of Science

in

Chemical Engineering

Department of Chemical and Materials Engineering

University of Alberta

Abstract

Emulsion droplets are present in various systems and their dynamic behaviors are important to the design of efficient processes in different biological and industrial applications. Studying the interaction mechanisms of deformable droplets provides fundamental insights into many unsolved problems in the field of droplet dynamics. Also, the properties of the thin liquid film between droplets during their interactions is of significant importance in the stability of emulsions. During the past few years, oil-in-water systems have been the center of attention in many theoretical and experimental studies due to their numerous applications, and hence, the dynamic behaviors of oil droplets inside aqueous solutions are well understood. However, water-in-oil systems are relatively new and require more studies to fully appreciate the underlying interaction mechanisms of water droplets within surrounding oil phases. Our investigations show that the Stokes–Reynolds–Young–Laplace model, as the currently established model for the study of droplet interaction in a medium, does not describe the experimental force versus piezo-displacement data for two water droplets inside a pure oil medium in the literature, and a further relatively long-ranged attractive force is required to explain these observations. In this study, we hypothesize that the source of the unexplored long-ranged force pertains to the presence of charges at the interface of the water drops with the oil phase. We propose fixed-surface-charge–bulk-dipole attraction, or charge–dipole interaction for short, as a new interaction force between water-in-oil droplets and then derive an equation for its disjoining pressure to add into the current Stokes–Reynolds–Young–Laplace model. The numerical results demonstrate that the force versus piezo-displacement curves deviate

from experimental data in the literature in the absence of charge–dipole attraction while they are in excellent agreement with experimental data when charge–dipole attraction is included. Furthermore, we mathematically prove that electric double layer and surface electrostatic interactions are absent between two water droplets inside a pure organic phase as suggested by the experimental data, and therefore van der Waals and charge–dipole interactions are the only intermolecular and surface forces between water drops immersed within a pure oil medium. Our mathematical derivations show that although charges are present at the interface of water with a pure oil phase, no electrostatic interaction is present. This research indicates that charge–dipole attraction can adequately explain the unexplained attractive force observed in literature and provides a critical foundation for the study of water-in-oil emulsions with significant implications in different industries.

Preface

Chapters 1 to 4 of this thesis have been published or are under preparation for publication. I performed all the research under the direction and supervision of J. A. W. Elliott.

Chapter 2 and the Appendix of this thesis, with minor modifications, has been published as H. Afsaneh and J. A. W. Elliott. "Charge–Dipole Attraction as a Surface Interaction between Water Droplets Immersed in Organic Phases". *Langmuir* 2022 38 (43), 13121–13138. J. A. W. Elliott conceived the idea. H. Afsaneh performed the research under the supervision of J. A. W. Elliott and wrote the first draft of the manuscript. Both authors contributed to the final manuscript. https://pubs.acs.org/doi/full/10.1021/acs.langmuir.2c01828

Chapters 1, 3, and 4 of this thesis, with modifications, are under preparation for publication.

To my family

Acknowledgments

To Dr. Janet Elliott, thank you for your infinite care and boundless support of my professional and academic development throughout my graduate studies. Your enthusiasm in the course of research, your careful supervision, and your commitment to teaching and research are purely encouraging.

To Drs. Hongbo Zeng and Anthony Yeung who willingly accepted to be the members of my examining committee, thank you for your time in reading my work, your kind guidance, and your helpful advice.

To all present members of Dr. Elliott's research group, Soheil Rezvani, Hikmat Binyaminov, and Julia Grenke that I have had the pleasure of meeting, thank you for sharing your knowledge, experience, advice, and our daily talks.

To all my friends, especially Rasool Mohammadi, that I have been lucky to meet and to get to know, thank you all for your friendship, your supports, and all our daily chats.

To my beloved parents, Eisa Afsaneh and Parvin Mohammadi that have always warmly supported me with my decisions, encouraged me to pursue my dreams, and have always had faith in me, to my brother, Alireza Afsaneh, that has always been the closest friend to me, thank you all for believing in me and being there for me.

To the Natural Sciences and Engineering Research Council of Canada (NSERC) and the University of Alberta, thank you for your financial support that made this research possible.

Finally, to God that has given me such power to overcome difficulties and led me to the right path, thank you for hearing my voice and always being with me.

Table of Contents

List of Figures

List of Tables

List of Symbols

Latin Symbols

Physical parameter	Description, unit
a	radius of the ring during integration, m
A_{H}	nonretarded Hamaker constant, J
$B(\theta)$	constant value associated with the behavior of the three-phase contact line of the droplet on a surface, unitless
d	a length in the derivation of the initial condition (i.e., eq (2.4))
e	elementary charge, C
E	interaction energy per unit area between two surfaces, $\mathrm{J/m^2}$
f	volume fraction of a component, $\mathrm{m^3/m^3}$
F	force per unit area between two surfaces, $\mathrm{N/m^2}$
$F(t)$	overall instantaneous interaction force between two surfaces, N
F_{CC}	surface electrostatic force between two surfaces, N
g	gravitational acceleration of the Earth, $\mathrm{m/s^2}$
$G(t)$	characteristic length associated with the interaction force, m
$h(r,t)$	film thickness, m
h_0	minimum separation or film thickness between two spherical droplets at all times, m

h_{i}	initial apex separation or film thickness at drop head, m
$\hbar$	reduced Planck's constant, J s
k_{B}	Boltzmann constant, $\mathrm{J}/(\mathrm{kg\ K})$
K	spring constant of the cantilever, $\mathrm{N/m^2}$
l	thickness of a plate during integration, m
m	mass, kg
mol	number of moles, mol
M	molar mass, kg/mol
n	refractive index, unitless
N	number density or molecular density, $\mathrm{m^{-3}}$
N'	number of surface charges per unit area, $\mathrm{m^{-2}}$
N_{A}	Avogadro's number, $\mathrm{mol^{-1}}$
$p(r,t)$	hydrodynamic pressure in the thin film confined between two surfaces relative to the bulk fluid, Pa
Q	electric charge, C
r	radial coordinate in the film, m
r_{f}	radial length of the film, m
r_{m}	rim radius, m
R	unperturbed harmonic mean radius of the two interacting droplets, m
S	integral over a ring of radius a, $\mathrm{m^{-2}}$
t	time, s
T	absolute temperature, K
T_{c}	temperature, ℃

u	electric dipole moment, C m
u_{f}	velocity profile of the draining film confined between two droplets, m/s
v_{e}	main electronic absorption frequency in the ultraviolet (UV) region, s^{-1}
V	drive velocity of the droplet, m/s
$w(\rho)$	interaction free energy between a single charge and a single dipole, J
x	mole fraction of a component, mol/mol
$X(t)$	displacement function of the cantilever with time, m
z	vertical coordinate, m
Z	valency, unitless

Greek Symbols

Physical parameter	**Description, unit**
α	a constant value in the constant volume boundary condition for two drops, unitless
δ	a region occupied by charges near the surface
Δh	film thickness difference, m
ΔX	piezo-displacement, m
$\Delta\rho_{\mathrm{f}}$	density difference between the two phases, $\mathrm{kg/m}^3$
ε_0	dielectric permittivity of the free space, F/m
ε_{r}	relative permittivity of the medium, unitless
θ	contact angle of the droplet on a surface, °
κ^{-1}	Debye length, m
λ_{CD}	charge–dipole constant, $\mathrm{J/m}^4$

μ	dynamic viscosity of the film, Pa s
$\Pi(\mathrm{r},\mathrm{t})$	disjoining pressure in the film, Pa
Π_{CC}	disjoining pressure due to surface electrostatic interaction, Pa
Π_{CD}	disjoining pressure due to charge–dipole interaction, Pa
Π_{EDL}	disjoining pressure due to electric double layer interaction, Pa
Π_{vdW}	disjoining pressure due to van der Waals interaction, Pa
ρ	distance between the interacting species, m
ρ_∞	number density (i.e., concentration) of charges or ions in the solution far from the surface, m^{-3}
ρ_{f}	density, $\mathrm{kg/m}^3$
ρ_z	number density (i.e., concentration) of charges or ions in the solution, m^{-3}
σ	interfacial tension, $\mathrm{N/m}^2$
σ_{c}	surface charge density, $\mathrm{C/m}^2$
τ_{f}	shear stress at the droplet–liquid interface, Pa
ϕ	an angle in the derivation of the initial condition (i.e., eq (2.4))
ψ	electric potential, V
ψ_0	surface potential, V
ψ_{m}	potential at the midplane, V

Subscripts

b	bottom
CC	surface-charge–surface-charge
CD	charge–dipole

cr	critical
EDL	electric double layer
P	point P
t	top
vdW	van der Waals

Dimensionless Numbers

Bo	Bond number
Ca	capillary number

Abbreviations

AFM	atomic force microscope
CC	surface-charge–surface-charge
CD	fixed-surface-charge–bulk-dipole or charge–dipole
DFA	dynamic force apparatus
DLVO	Derjaguin–Landau–Verwey–Overbeek
EDL	electric double layer
pH	potential of hydrogen
PDE	partial differential equation
SFA	surface force apparatus
SRYL	Stokes–Reynolds–Young–Laplace
vdW	van der Waals

Chapter 1

Introduction

1.1 Background

Emulsion droplets are ubiquitous in our daily life, and their dynamics are relevant in many applications, such as those in the oil industry,[1,2] pharmaceuticals,[3,4] and food science.[5,6] An emulsion can be simply formed via agitating two immiscible or partially miscible liquids, leading to the appearance of liquid–liquid interfaces or deformable droplets (e.g., water-in-oil or oil-in-water droplets) within the system. The status of these drops inside emulsions is of significant importance in terms of their interaction with other drops or components, for instance, solid particles, surfactants, and polymers;[7–9] hence, they play a paramount role in the path to design efficient processes.

In systems containing droplets, the curved interface that separates the two immiscible phases results in a pressure difference across the interface, called the Laplace pressure. This is in contrast to immiscible liquids separated by a flat interface which have the same pressure. Laplace pressure

is proportional to the interfacial tension and inversely proportional to the radius of curvature. When the radius of the drop reaches the microscale or nanoscale level, the role of curvature becomes more remarkable and alters the behavior of the system. As a result, Laplace pressure becomes important in studying the interaction mechanisms between small drops or between small drops and other components.

The interactions between two droplets are governed by a number of forces that appear at small separations. According to Figure 1.1, when two spherical drops are far apart, no interaction is present;[10] however, when they approach one another, and the separation between the droplet interfaces becomes smaller, the liquid film between them is drained to the sides due to the hydrodynamic pressure, and the droplets begin to interact. At this stage, the hydrodynamic pressure becomes comparable to the Laplace pressure, and the droplets deform accordingly.[11] At much smaller separations, around 100 nm, the intermolecular and surface forces come into play and govern the stability of the drops through the corresponding imparted pressures,[12,13] i.e.,

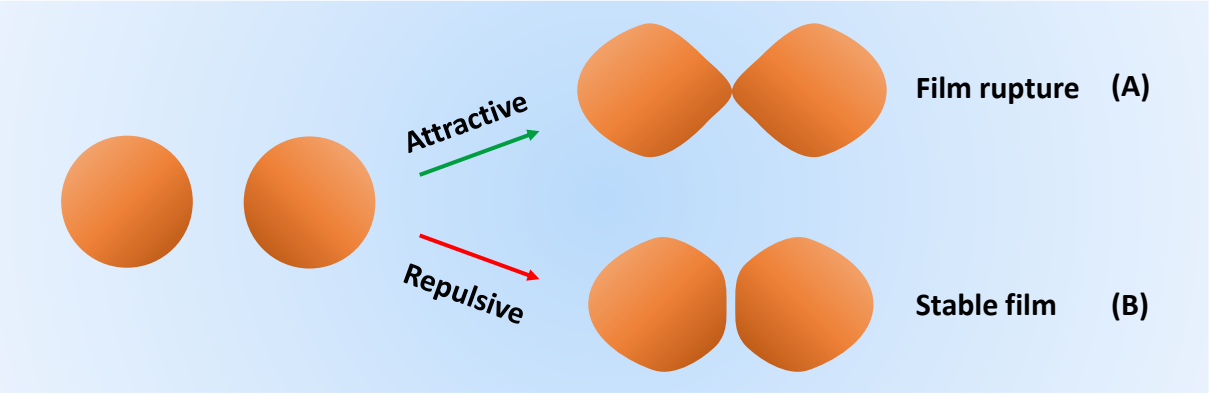

Figure 1.1 Schematic illustration of two general cases that appear during the interaction of two drops within a medium. (A) Attractive surface forces dominate at small separations and induce the coalescence of the droplets. (B) Repulsive surface forces dominate at small separations and result in the formation of a stable film between the droplets.

disjoining pressures, where the concept was first introduced by Derjaguin in 1936.[14,15] These surface forces can either be attractive or repulsive depending on the nature of the interaction force. If attractive surface forces, such as van der Waals (vdW) forces, dominate the interaction, then the confined film between the drops will rupture, and the drops will coalesce (Figure 1.1A), whereas repulsive surface forces, such as electric double layer (EDL) and steric forces, lead to the stabilization of the confined film. In this case, no droplet coalescence occurs, and the interface of the droplets form a flat shape within the interaction zone (Figure 1.1B).

Experimental techniques provide a strong foundation to study the interactions between droplets. Various tools, such as the surface force apparatus (SFA),[16,17] the dynamic force apparatus (DFA),[18,19] and the atomic force microscope (AFM),[20,21] have been implemented to measure the interactions between millimeter to micron sized droplets in various polar and organic systems. However, these techniques cannot distinguish the contributions of different surface forces because they can only measure the total interaction force between the droplets. As a result, alternative and complementary methods are required to realize the contributions of hydrodynamic forces and various surface forces, such as vdW and EDL interactions, to the total interaction force. In recent years, theoretical methods have been implemented to model the behavior of drops inside a medium,[17,22,23] and a strong theoretical framework has been developed. Many years ago, the importance of liquid drainage and droplet deformation became apparent through the work of many scientists. Among them, Thomas Young,[24] Pierre-Simon Laplace,[25] Carl Friedrich Gauss,[26] Josef Stefan,[27] and Osborne Reynolds,[22] made tremendous efforts in this path. The Stefan–Reynolds[22,27] model can be used for the film thinning between two perfectly flat surfaces. However, this model cannot be implemented for the film drainage and surface deformations of drops, and an alternative model is required. Ivanov et al.[28] for the first time introduced the well-known Stokes–Reynolds–

Young–Laplace (SRYL) model and formulated it mathematically. This model can capture the film drainage and surface deformations using coupled partial differential equations (PDEs). Also, this model can provide the ability to effectively evaluate the temporal magnitude of each force present and identify their role during the interaction using Derjaguin's approximation.[17,29] As a result, during the past few decades, the so-called SRYL model has been applied to various droplet–droplet[30,31] and droplet–solid[32,33] systems.

In the earliest studies, oil droplets were considered in aqueous solutions, and the role of various surface forces, such as vdW and EDL forces, were investigated. Shi et al.[34] studied the interaction of two oil drops in different aqueous solutions containing NaCl and asphaltenes using an AFM, and reported the interaction force versus time diagrams. For instance, their force versus time diagram and drop profile for two pure toluene droplets in 1 mM NaCl solution show that at nanometer separations, the EDL interaction is dominant, and a stable film forms between the toluene droplets. In a very similar study Shi et al.[35] used the same approach to investigate the interaction of an oil drop with a flat solid surface in different aqueous solutions and provided the force versus piezo-displacement diagrams. The results of their force versus piezo-displacement and drop profile interacting with mica as the solid surface for pure toluene and heptol droplets show that the EDL force is the dominant surface interaction at very small separations, and a stable film forms between the droplets and the solid surface. In general, in systems containing water as the continuous medium, ions are dispersed inside the continuous phase, and thus, an electric double layer forms around the surfaces. This repulsive interaction dominates the system and does not allow attractive vdW interactions to cause the coalescence of the drops or attachment of drops to solid surfaces. Hence, in most aqueous systems, a stable film can be observed between the surfaces.

The presence of water-in-oil systems in various processes has made their study a necessity. Studies on water-in-oil systems have been less abundant compared to those on oil-in-water systems, and thus, more attention needs to be focused on the physics of water drop interaction inside oil media. As a result, during the past few years, the interaction mechanisms of water-droplet–water-droplet[31,36–39] and water-droplet–solid-surface[32] have been investigated, and some aspects of their interaction have been identified. However, most of these studies are experimental, and almost no theoretical foundations are provided.[31,37–39] For instance, Shi et al.[37] studied the interaction of two water droplets suspended in a pure oil phase or in an asphaltene-containing oil phase, and observed that a relatively long-ranged attractive force exist between the water drops. Moreover, Xie et al.[38] focused their investigation on the interaction of two water drops within pentol (a mixture of pentane and toluene at a volume ratio of 1:1) as the organic phase. Also, Mao et al.[31] investigated the interaction of two water droplets within a different oil phase, namely n-dodecane, in the presence or absence of pH-responsive nanoparticles. For water droplets suspended in pure n-dodecane, they did not utilize the Hamaker constant calculated from Lifshitz theory in their computations, and instead they performed the fitting for Hamaker constant, meaning that if they had carried out the simulations using the Hamaker constant found by Lifshitz theory, their numerical results would deviate from the experimental data. In other words, an additional attractive force is required to fully explain the experimental observations. Sun et al.[39] chose toluene as the oil phase and studied the interactions of relatively larger water drops compared to the previous studies mentioned here inside either pure or polymer- or surfactant-containing toluene. Most of these studies do not provide any theoretical foundation on the interaction of water drops through an organic phase. Also, the theoretical fitting for the Hamaker constant provided by Mao et al. does not explain the actual physics during the interaction of two water drops inside a pure oil

phase. Furthermore, our investigations show that implementing the SRYL model with the conventional surface forces (i.e., only vdW forces) does not describe the experimental observations made in the literature, and a further relatively long-ranged attractive force is required to explain these observations. The research gap we found in the literature is fundamental since it pertains to the physics of many applications, such as those in the oil industry. As a result, new explorations are required to fully understand the physics of water droplet interaction inside surrounding oil phases.

Several studies have reported that charges are present at the interface of water with other fluids, such as oil or air. Tammet et al.[40] observed the presence of negative charges at the interface of water droplets with air, and Chaplin reported that when deionized water is in contact with air, the number of surface charges per unit area are approximately 10^{15} m^{-2}.[41] Moreover, a number of studies reported that the surfaces of water droplets are charged when they are submerged in oil phases (i.e., nonpolar) with different permittivities, and the number of these surface charges per unit area is of the order of 10^{13}–10^{14} m^{-2}.[42–45]

Here, we hypothesize that the unexplained additional interaction between water droplets in oil is related to the presence of surface charges at the interface of water drops with organic phases and propose that fixed surface charges of one water droplet interact with dipoles within the bulk of another water droplet, i.e., a fixed-surface-charge–bulk-dipole (CD) interaction. Since the SRYL model requires the disjoining pressure term, we develop an equation for the disjoining pressure of this CD interaction and incorporate it in the current SRYL model. This step allows us to better investigate the behavior of water droplets in different organic phases and understand the mechanism of their interaction.

1.2 Thesis Scope

The physics of water drop interaction within organic phases, such as toluene, pentol, and n-dodecane, is still incomplete due to the shortcomings in the use of the conventional Stokes–Reynolds–Young–Laplace (SRYL) model for such systems. As a result, a reliable theory is required to accurately describe the fundamentals of water droplet interaction through a surrounding oil phase. The main objective of this thesis is to develop a new theory that sufficiently explains the interaction mechanism of water drops in pure organic phases with useful implications in various industries and then apply it to analyze different experimental results for water drops suspended in oil phases reported in the literature. In summary, this thesis has the following objectives:

1) Explore the literature to find useful force versus piezo-displacement or force versus time data for the interaction between two water drops inside various pure oil phases (e.g., toluene, pentol, n-dodecane) and implement them in the study.
2) Collect various input parameters and system properties from the literature papers that report the force data. In the case that the essential properties, such as dynamic viscosity, have not been provided by the papers, we use data from other literature sources at temperatures at which the experiments had been carried out.
3) Perform simulations using the SRYL model with van der Waals (vdW) contributions as the only disjoining pressure and analyze the force results and the degree of deviation of conventional theoretical simulations from the experimental data. It is worth mentioning that since there are no ions inside the pure oil phase, no electric double layer (EDL) disjoining pressure is present.
4) Develop a new theory based on fixed-surface-charge–bulk-dipole (CD), or charge–dipole interaction for short, and derive a disjoining pressure equation.

5) Perform simulations using the SRYL model by adding the newly introduced CD interaction with the number of surface charges per unit area as the only fitting parameter during force calculations to the SRYL model and compare the fit values with independent measurements and calculations of their value in the literature. In other words, attractive vdW and CD disjoining pressures are the only disjoining pressures in the simulations.
6) Draw the spatiotemporal thicknesses of the thin oil film confined between two water droplets and also droplets profile at nanometer separations and explain the droplets coalescence mechanism.
7) Draw various pressure profiles, such as hydrodynamic and disjoining pressures, and analyze the pressure distributions along the droplet profile.

This thesis consists of five chapters that provide new knowledge on the interaction mechanisms of water droplets within oil phases and seeks to boost the current understating of such systems.

Chapter 1 provides a basic overview on the current status of droplet dynamics and significance of the study of water droplets in surrounding oil phases. In this chapter, the research gap present in the literature is introduced, and the objectives of the thesis are presented.

Chapter 2 outlines a new theory that provides a foundation for the study of water-in-oil systems and sufficiently describes the behavior observed in such systems. The developed theory is tested against two different literature cases in which two water droplets interact in pure toluene or pentol as the oil phase.

Chapter 3 extends our understandings of the developed theory from Chapter 2 to two other cases in which two water drops interact in pure n-dodecane or toluene as the oil phase.

Chapter 4 expands on the reasons why the EDL interaction is not present between two water drops within a pure oil phase, and that why the experimental data from the literature suggest that the electrostatic interaction is zero, from a mathematical point of view.

Chapter 5 summarizes the work presented in this thesis and highlights the main outcomes.

Chapter 2

Charge–Dipole Attraction as a Surface Interaction Force between Water Droplets Immersed in Organic Phases[1]

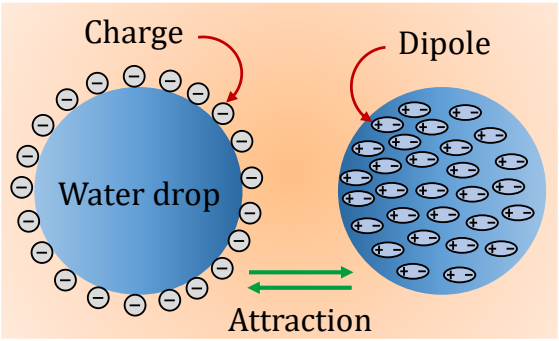

[1] This Chapter and the Appendix, with minor modifications, have been reproduced with permission from H. Afsaneh and J. A. W. Elliott. "Charge–Dipole Attraction as a Surface Interaction between Water Droplets Immersed in Organic Phases". *Langmuir* 2022 38 (43), 13121-13138. https://pubs.acs.org/doi/full/10.1021/acs.langmuir.2c01828

Abstract

The dynamic behavior of emulsion droplets during their interactions with one another or with solid surfaces plays a paramount role in their ultimate stability in various applications. While the interaction of oil droplets through a surrounding aqueous phase is well understood, recent studies on the interaction of water droplets through a surrounding pure organic phase showed the presence of an unexplained attraction between water droplets at relatively long ranges. In this research study, we propose fixed-surface-charge–bulk-dipole attraction as a new interaction force between water-in-oil droplets and then derive an equation for its disjoining pressure. The behavior of water droplets in the presence and absence of this charge–dipole interaction was numerically quantified using the Stokes–Reynolds–Young–Laplace model and compared to the experimental data. Numerically calculated net force curves are in excellent agreement with experimental data from the literature when charge–dipole attraction is included, while they deviate in its absence. In addition, the water droplet and thin oil film profiles in the presence and absence of charge–dipole attraction were calculated and compared. This research indicates that charge–dipole attraction can adequately explain the mysterious force observed in some studies, which demonstrates its unexplored potential to capture the physical properties and dynamic behavior of water droplets in organic phases with useful implications to unravel unidentified interactions between emulsion droplets in different industries.

2.1 Introduction

In recent years, the importance of droplet dynamics has been increasingly recognized in a variety of biological and industrial processes, such as those in cosmetics,[46,47] therapeutics,[48,49] food,[50,51] and oil[1,52] industries. In these processes, emulsion stability, i.e., the status of droplets inside a

second immiscible liquid, is a critical factor. The underlying mechanisms of droplet attraction or repulsion must be understood to design processes with high efficiencies.[7,53] In some applications, such as targeted drug or gene delivery, the droplets need to remain stable (separate from one another) to efficiently deliver therapeutic agents to the target site, while in other applications, such as bitumen production, the presence of water-in-oil or oil-in-water droplets is undesirable, and they need to be removed by destabilization (coalescence).[18] From the thermodynamic perspective, in these applications, surface-active elements, for example, surfactants, solid particles, polymers, and lipids, can adsorb on the surface of the droplets and dramatically alter their interfacial properties, ultimately influencing droplet interactions.[7,29,54] As a result, the interfaces of droplets need to be closely managed to result in the desirable outcome (i.e., either separate or coalesced).

Unlike solid particles, droplets can readily deform in response to external forces. The shape of the droplets is governed by the interplay between several droplet properties and external phenomena. The droplet properties include the interfacial tension and droplet size, exerting their influence in the Laplace pressure. The external phenomena can be either related to the hydrodynamic pressure in the draining liquid film, originating from the approach velocity of the droplets, or the disjoining pressure due to the intrinsic interactions between approaching droplet surfaces or between approaching droplets and solids.[11] The eventual stability and behavior of the emulsions are determined by the intermolecular and surface forces that generally come into effect when the thickness of the thin liquid film confined between the droplets or between the droplets and solids is below 100 nm.[11] Basically, attractive surface interactions, such as van der Waals (vdW) and hydrophobic forces, tend to thin and rupture the confined thin film, destabilizing the emulsion. In contrast, repulsive surface interactions, such as electric double layer (EDL) and steric forces, result in stable films, stabilizing the emulsion.

Diverse experimental tools have been implemented to directly measure the interaction forces between bubbles, droplets, and solids (either dispersed solid particles or flat solid surfaces). Among them, the dynamic force apparatus (DFA),[19] atomic force microscope (AFM),[55] and surface force apparatus (SFA)[56] are the most widely utilized tools for measuring the intermolecular and surface interactions. In addition, theoretical models have proven to be powerful assets in the numerical computation of the underlying interaction mechanisms between various surfaces.[57] These experimental and numerical techniques have been applied to various pairs of systems immersed in aqueous or organic phases, and different intermolecular and surface interactions have been identified.

The interaction of bubbles with other components is of great interest in many applications, such as mineral floatation.[58] Therefore, in the earliest studies, the interaction force between a cantilever-anchored spherical particle and a bubble was measured in a surrounding aqueous phase via an AFM.[23,59] Then, these studies were extended to different combinations of bubbles and/or solid surfaces immersed in aqueous phases to elucidate the interface behavior and discern different force interactions between interfaces. Hence, numerous investigations were carried out on bubble–bubble,[60–62] bubble–solid,[63,64] and solid–solid[65] systems in later studies.

Since droplets are important components of abundant systems, tremendous efforts have been made to understand the fundamentals of their physical behavior during their interaction with other droplets or components. The earliest investigations were focused on droplets submerged in aqueous phases. Examining the interaction between spherical particles (or colloidal probes) and oil droplets can be considered as one of the foundational studies that brought droplets into the center of attention.[55,66,67] Later on, the interaction mechanisms in droplet–solid[68,69] and droplet–droplet[30,70,71] systems were explored within systems with water as the continuous phase. Although

the number of studies on droplet-in-water systems has been substantial, less attention has been paid to droplet-in-oil systems, and thus, a deeper understanding is required. Water-in-oil systems can be composed of various pairs of constituents, for instance, droplet–solid,[18] droplet–particle,[32,72] and droplet–droplet[36,73] pairs. Hence, understanding the interaction mechanisms between different components in water-in-oil systems can be advantageous for various applications.

Recently, a long-range attractive force between two micron-sized water droplets in organic phases was observed via an AFM, and the source of this unexpected force is unknown.[37] Moreover, the studies on the interaction between water droplets inside various surrounding oil phases were experimental, and no theoretical foundations were provided.[37,38] As a result, these observations demonstrate a research gap in the literature, and new explorations are required to unravel the source of this mysterious force. Several studies have reported the presence of charges on the interface of water.[40–42,45] For instance, Tammet et al. observed that water droplets in air carry negative charges on the interface by means of electric mobility spectrometry under atmospheric conditions and in the laboratory, having important implications in atmospheric physics.[40] Furthermore, Chaplin reported the presence of negative surface charges for deionized water in contact with air of approximately 10^{15} surface charges per m^2.[41] Schoeler et al. observed the presence of positive surface charges for systems containing pure water microdroplets submerged in silicone and paraffin oils with experiments by means of video optical microscopy and molecular dynamics simulations.[42] The result of their study showed that the surface charge density of water droplets directly after addition to the oil phase was of the order of 10^{-6} C/m^2,[42] which is equivalent to about 10^{13} elementary surface charges per m^2. By implementing the relatively simple models provided by Leunissen et al.[43] using confocal microscopy imaging and modified Poisson–Boltzmann theory and Zwanikken and van Roij using modified Poisson–Boltzmann theory,[44] de

Graaf et al. showed that the number of surface charges per unit area for micron-sized water droplets in various oil phases containing colloidal particles is of the order of 10^{13}–10^{14} m^{-2}.[45] Also, the numerical calculations using Poisson–Boltzmann theory by de Graaf et al. for micron-sized water droplets suspended in oils with different relative permittivities demonstrate that the number of charges per unit area is of the order of 10^{13}–10^{14} m^{-2}.[45]

In this study, we hypothesize that the source of the unexplained additional force between water droplets in oil pertains to the surface charges present at the interface and propose that there is an interaction between the fixed surface charges of one water droplet and dipoles within the bulk of another water droplet, i.e., a fixed-surface-charge–bulk-dipole (CD) interaction. We develop an equation for this CD interaction and incorporate it in the current Stokes–Reynolds–Young–Laplace (SRYL) model to accurately capture the behavior of water droplets in different organic phases and compare the results with measurements reported in the literature.

In the following sections, we review the SRYL model (applicable to droplets, bubbles, and solid surfaces), which includes the hydrodynamic, vdW, and EDL forces that dominate the interaction of oil-in-water droplets. We validate our computational method and input parameters by comparison with experiments for oil-in-water droplets. For water-in-oil drops, because the continuous phase is nonpolar, there are no EDL forces. We introduce the CD force and show that this force when added to hydrodynamic and vdW forces explains the water-in-oil experiments in the literature.

2.2 System Definition and Governing Equations

2.2.1 Model Configuration

The system to be investigated computationally is composed of an AFM probe, where a micron-sized water droplet is anchored to its tipless cantilever (water droplet probe), and a second water droplet is placed on a substrate under the first droplet (Figure 2.1A). The droplets are perfectly aligned to create an axisymmetric system and ensure a head-on collision. The entire components are surrounded by a continuous oil phase to create a water-in-oil system. Figure 2.1B shows the side-view schematics of the water droplet probe along with the essential parameters utilized to calculate the dynamic interaction force between water-in-oil droplets. Note that while our main interest is the water-in-oil system shown in Figure 2.1, we will also describe and make calculations for the inverse, that is, an oil-in-water system in the validation computations.

2.2.2 Review of Stokes–Reynolds–Young–Laplace (SRYL) Model

The underlying mechanism of the drainage of the thin film between two surfaces can be approximated based upon the Stokes–Reynolds–Young–Laplace (SRYL) model.[74] The SRYL model is a robust time-dependent theoretical model implemented to calculate the interaction force between droplets, bubbles, and solid surfaces. It has been shown that the theoretical prediction or fitting of experimental AFM, DFA, and SFA results can be accomplished using the SRYL model for various droplet–droplet[75] and droplet–solid[35] systems. In particular, this model leads to promising outcomes for oil-in-water systems.[76] The model is composed of two main equations: the Stokes–Reynolds equation and the augmented Young–Laplace equation. The former simulates the film drainage between two surfaces while the latter captures the deformation of the interfaces

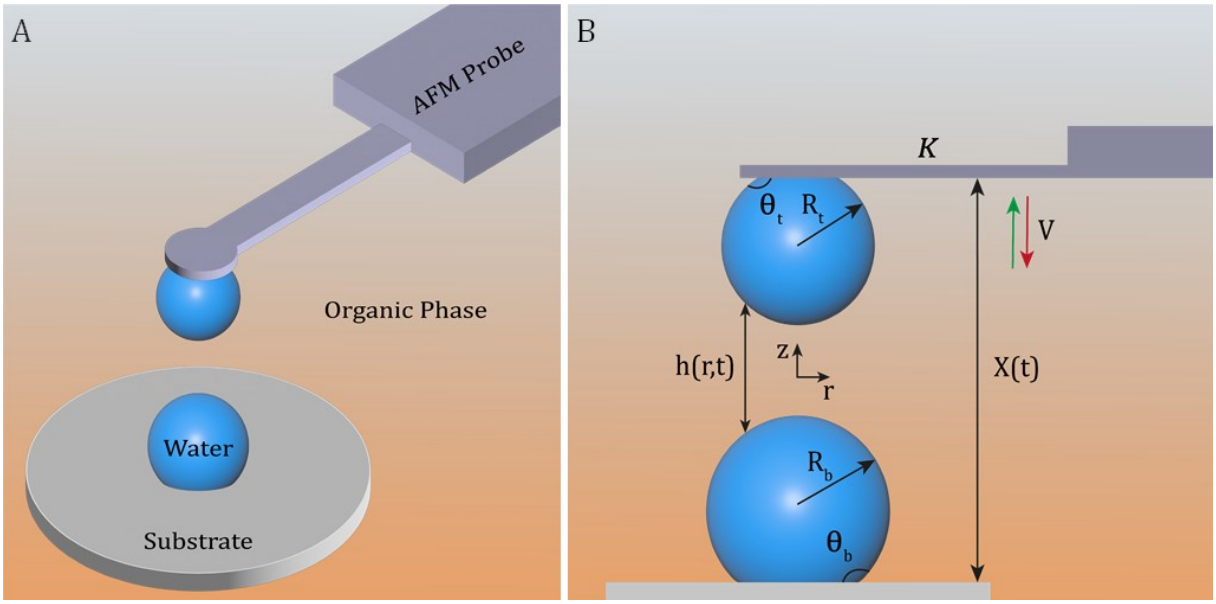

Figure 2.1 Schematic representation of two interacting water droplets within an organic phase. (A) Three-dimensional configuration of the AFM probe for measuring the dynamic force between the droplets. (B) Side-view illustration of the setup along with the necessary geometrical parameters for the theoretical study.

due to their interaction. Herein, we present these equations for two interacting droplets and describe the circumstances to which they can be applied.

The Stokes–Reynolds thin film drainage model for an axisymmetric film and tangentially immobile interfaces is written using Reynolds lubrication theory as follows:[10,16,17,22]

$$\frac{\partial h}{\partial t} = \frac{1}{12\mu r}\frac{\partial}{\partial r}\left(rh^3\frac{\partial p}{\partial r}\right) \tag{2.1}$$

where $h(r,t)$ is the film thickness; t is the time; r is the radial coordinate in the film; μ is the dynamic viscosity of the film (e.g., aqueous or organic), which is assumed to be Newtonian, and $p(r,t)$ is the hydrodynamic pressure in the thin film confined between two surfaces relative to the bulk fluid. Equation (2.1) defines the connection between the thinning rate of the continuous film between the surfaces and the radial parabolic velocity profile or the Poiseuille flow, compelled by

the radial pressure gradient. The so-called no-slip boundary condition is inherently present in eq (2.1) and thus accommodated at all interfaces.[17,23,35,60,76,77] When a droplet moves with a drive velocity V, there is a hydrodynamic drag acting on the bulk of the droplet. The Reynolds lubrication approximation neglects this hydrodynamic drag outside the interaction zone (the interaction zone or inner region is the region in which the interaction force between droplets is significant).[76,77] This is owing to the fact that the Capillary number ($\mathrm{Ca} = \mu V/\sigma$, where V is the drive velocity of the droplet and σ is the interfacial tension), which demonstrates the ratio of viscous drag forces to surface tension forces, is very small and generally falls in the range of 10^{-8}–10^{-6}.[76,77]

The interaction force between droplets can readily alter their shape owing to their deformability. Therefore, the surface deformation of the droplet must also be considered in the governing equations. Here, the augmented Young–Laplace equation is exploited to simulate the quasi-equilibrium behavior of the interacting deformable droplets. Since $\partial h/\partial r \ll 1$ (the film thickness is very small compared to the droplet radius), the linearized form of this equation can be applied to the corresponding system with two interacting droplets, given as[17]

$$\frac{\sigma}{2r}\frac{\partial}{\partial r}\left(r\frac{\partial h}{\partial r}\right) = \frac{2\sigma}{R} - p - \Pi \tag{2.2}$$

in which σ is the interfacial tension between the droplet phase and the surrounding medium and R is the unperturbed harmonic mean radius of the two interacting droplets, $R^{-1} = (R_{\mathrm{t}}^{-1} + R_{\mathrm{b}}^{-1})/2$, where subscripts t and b stand for "top" and "bottom", respectively. In addition, $\Pi\big(h(r,t)\big)$ is the disjoining pressure in the film, which in general stems from intermolecular and surface forces, such as vdW and EDL interactions. Since the density difference between the two phases $\Delta\rho_{\mathrm{f}}$ is

small and the radii of the drops are not large, the Bond number ($\mathrm{Bo} = \Delta\rho_{\mathrm{f}}\, gR^2/\sigma$) is well below unity; therefore, the role of gravity g is neglected in eq (2.2).

As mentioned earlier, the deformation of droplets takes place in a quasi-equilibrium manner.[77] In other words, the interacting droplets or bubbles instantaneously respond to the changes in the hydrodynamic and disjoining pressures and immediately adapt to the new condition. This is a feasible assumption because the surfaces of the droplets and bubbles are flexible and deform rapidly. Furthermore, in order to be able to utilize the SRYL model, the $R \gg r_{\mathrm{f}} \gg h$ condition must hold for the system, where r_{f} is the radial length of the film.[17] Also, the characteristic fluid velocities must be within the regime in which the Stokes–Reynolds equation is applicable.[17]

The overall instantaneous interaction force $F(t)$ between two surfaces, which has contributions from hydrodynamic and disjoining pressures, can be determined using Derjaguin's approximation, written as[17,29]

$$F(t) = 2\pi \int_0^\infty \left[p(r,t) + \Pi\big(h(r,t)\big)\right] r\mathrm{d}r = 2\pi\sigma G(t) \tag{2.3}$$

where $G(t)$ is a characteristic length associated with the interaction force $F(t)$ and will be utilized in the forthcoming equations and numerical computations.[17,78] The use of Derjaguin's approximation for force calculation using the hydrodynamic pressure and disjoining pressure due to the surface forces is well established in the literature, and many researchers have implemented eq (2.3) to calculate the interaction force between different surfaces.[16–18,34,63,68,75,77,79–81] In eq (2.3), it is assumed that the range of hydrodynamic forces is very small compared to the radii of the droplets or bubbles. As a result, the surfaces of interacting droplets or bubbles are almost flat and parallel.[17] The result of this assumption can be exploited in the formulae for disjoining pressures due to the surface forces.

The so-called SRYL model is a system of coupled non-linear partial differential equations (PDEs), which was first numerically solved by Lin and Slattery in 1982.[82] This model requires an initial condition and four boundary conditions. For this purpose, the appropriate radial domain, $0 < r < r_{\max}$, must be selected, where $r_{\max}$ is sufficiently large that an increase in its magnitude does not affect the results of the numerical approach. To put it differently, $r_{\max}$ is a point that is positioned outside the interaction zone and produces results that are independent of its position. The magnitude of $r_{\max}$ can be roughly approximated by $r_{\max}^2 \approx Rh$.[77]

The initial condition at $t = t_0$, which demonstrates the initial separation or film thickness between the interfaces of two interacting droplets, can be taken to be[17,29,74,77]

$$h(r, t_0) = h(0, t_0) + \frac{r^2}{R} \tag{2.4}$$

in which $h(0, t_0)$ or h_{i} is the initial apex separation or film thickness at $r = 0$ (at $r = 0$, $h(0, t) = h_0$ is the minimum separation or film thickness between two spherical droplets at all times) and R is the unperturbed mean radius of the droplets. Equation (2.4) assumes that each droplet possesses an undeformed spherical shape at large separations because of the zero film pressure.[23] For further information on the derivation and inherent assumptions of eq (2.4), see the Appendix, Section A.1. Axisymmetric considerations of the droplets' interaction lead to the formation of two boundary conditions, where at $r = 0$, the film thickness and pressure do not vary with the radial coordinate. These boundary conditions are

$$\left.\frac{\partial h}{\partial r}\right|_{r=0} = \left.\frac{\partial p}{\partial r}\right|_{r=0} = 0 \tag{2.5}$$

Outside the interaction zone, the hydrodynamic pressure p decays as r^{-4}. Consequently, at $r = r_{\max}$, the asymptotic form of the hydrodynamic pressure is exploited as[83]

$$\frac{\partial p}{\partial r} + \frac{4p}{r} = 0 \qquad \text{at } r = r_{\max} \tag{2.6}$$

When the radial domain r becomes greater than $r_{\max}$, the local film thickness $h(r,t)$ reaches a large value (> 100 nm) such that the magnitude of disjoining pressure becomes insignificant, which means $\Pi\big(h(r > r_{\max}, t)\big) \ll 2\sigma/R$.[17] Hence, the overall instantaneous interaction force from eq (2.3) can be expressed as

$$F(t) \cong 2\pi \int_0^{r_{\max}} \big[p(r,t) + \Pi\big(h(r,t)\big)\big]\, r\mathrm{d}r + 2\pi \int_{r_{\max}}^{\infty} p(r,t)\, r\mathrm{d}r \tag{2.7}$$

i.e., in the second integral of eq (2.7), the disjoining pressure parameter $\Pi\big(h(r,t)\big)$ has been ignored. Furthermore, because the second integral falls beyond the interaction zone, its magnitude is significantly smaller than the value of the first integral. Thus, the calculation of the overall force is typically done by solely considering the first integral of eq (2.7).

In AFM probes, the two droplets interact in a way that they maintain their constant volume during the whole interaction period. The reason that the constant volume boundary condition was introduced is that the surfaces of the droplets outside the interaction zone tend to move at a different velocity than they move inside the interaction zone (thus, a constant velocity boundary condition cannot be used). The constant volume boundary condition was first introduced by Carnie et al.[77,78] This boundary condition for two droplets with the same properties is defined as[17,74,84]

$$\begin{aligned} \frac{\partial h(r_{\max}, t)}{\partial t} &= \frac{\mathrm{d}X(t)}{\mathrm{d}t} - \frac{\mathrm{d}G(t)}{\mathrm{d}t}\left[-\frac{2\pi\sigma}{K} + 2\ln\left(\frac{r_{\max}}{2\sqrt{R_{\mathrm{t}}R_{\mathrm{b}}}}\right) + B(\theta_{\mathrm{t}}) + B(\theta_{\mathrm{b}})\right] \\ &= \frac{\mathrm{d}X(t)}{\mathrm{d}t} - \alpha\frac{\mathrm{d}G(t)}{\mathrm{d}t} \end{aligned} \tag{2.8}$$

The constant terms inside the bracket are denoted α for the sake of simplification. In eq (2.8), $X(t)$ is the displacement function of the cantilever with time and K is the spring constant of the

cantilever. In most cases, the cantilever-adhered droplet moves with a constant drive velocity, and thus, $\mathrm{d}X(t)/\mathrm{d}t$ is a constant number, i.e., $\pm V$, where negative and positive values demonstrate the approach and retraction of the cantilever-adhered droplet, respectively. It is worth mentioning that $\alpha \mathrm{d}G(t)/\mathrm{d}t$ accounts for the events occurring because of droplet deformations outside the interaction zone.[17] In eq (2.8), θ is the contact angle of the droplet on a surface, where subscripts t and b stand for "top" (cantilever) and "bottom" (substrate), respectively. Also, the constant B is dependent on the behavior that the three-phase contact line of the droplet exhibits during its deformation. For the purposes of this work, the three-phase contact line is considered to be *pinned* to the cantilever or the substrate, and the B terms are given by[17,67,74]

$$B(\theta) = 1 + \frac{1}{2}\ln\left(\frac{1+\cos\theta}{1-\cos\theta}\right) \tag{2.9}$$

Deriving a formula for the shear stress on the droplet–liquid interface and its investigation are interesting means to understand the flow behavior within the draining film during the interaction between droplets or between droplets and surfaces. Considering the immobile interface assumption mentioned earlier, the velocity profile of the draining film confined between two droplets is parabolic and for an axisymmetric film (relative to vertical plane $r = 0$, shown in Figure 1.1B) is given by[23]

$$u_{\mathrm{f}} = -\frac{1}{2\mu}\frac{\partial p}{\partial r}\left(z^2 - \left(\frac{h}{2}\right)^2\right) \tag{2.10}$$

The shear stress formula at the droplet–liquid interface ($z = h/2$) can be derived by taking the derivative of u_{f} in eq (2.10) relative to z and multiplying it by the dynamic viscosity of the film μ as[23,77]

$$\tau_{\mathrm{f}} = \mu \frac{\mathrm{d}u_{\mathrm{f}}}{\mathrm{d}z} = -\frac{h}{2}\frac{\partial p}{\partial r} \tag{2.11}$$

2.2.3 Disjoining Pressure

In general, the disjoining pressure Π originates from the intermolecular and surface forces. When the disjoining pressure is positive, the interaction between the interfaces is repulsive (i.e., film thickening), whereas a negative disjoining pressure describes an attractive interaction (i.e., film thinning). With the assumption of the parallel and flat surfaces at small separations that was mentioned previously,[17] the vdW and EDL disjoining pressures for two flat and parallel surfaces can be exploited. These assumptions have proven to work favorably for the prediction or fitting of disjoining pressures between two droplets or bubbles.[17] The disjoining pressure due to the vdW interaction is given by[85,86]

$$\Pi_{\mathrm{vdW}} = -\frac{A_{\mathrm{H}}}{6\pi h^3} \tag{2.12}$$

where A_{H} is the nonretarded Hamaker constant, which can be calculated using Lifshitz theory.[87,88] Furthermore, the disjoining pressure due to the EDL interaction for symmetric systems where the electrolyte ions have the same valency (e.g., NaCl) is defined as[7,13,86]

$$\Pi_{\mathrm{EDL}} = 64 k_{\mathrm{B}} T \rho_{\infty} \tanh^2\left(\frac{Ze\psi_0}{4k_{\mathrm{B}}T}\right) \exp(-\kappa h) \tag{2.13}$$

Here, k_{B} is the Boltzmann constant ($k_{\mathrm{B}} = 1.3806 \times 10^{-23}$ J/K), T is the absolute temperature, and ρ_{∞} is the number density of each type of electrolyte ion, i.e., salt ions (Na^+ or Cl^-) and water ions (H^+ or OH^-) in the aqueous solution far from the surface (i.e., ∞), Ze is the charge of the ions in which Z is the valency and e is the elementary charge ($e = 1.602 \times 10^{-19}$ C). Moreover, ψ_0 denotes the surface potential and κ^{-1} is the Debye length. It should be noted that in eq (2.13), the

number densities of each type of salt ion and water ion are the same because they have the same number of moles. Moreover, the contributions from both ion species of the electrolyte have already been considered in the coefficient "64" during the derivation of eq (2.13), and consequently, we do not need to multiply ρ_∞ by 2.[13]

2.3 Proposed New Force in Water-in-Oil Systems: Charge–Dipole (CD) Interaction

Herein, we propose a new interaction force between water droplets immersed in organic phases and derive a suitable equation for its calculation. As mentioned earlier, an unknown attractive force has been observed recently between two water droplets inside an organic phase.[37] While there are experimental studies on the interaction between water droplets in organic phases, these studies lack a theoretical foundation for computing the interaction force.[37,38] The current governing equations that work well for oil-in-water systems no longer produce accurate and dependable outcomes for water-in-oil systems, and some modifications are required. As mentioned earlier, many investigations have shown the presence of charges on the interface of water.[40–42,45] We hypothesized that the observed extra attractive force between two water droplets in a surrounding organic phase can be attributed to the interaction of surface charges on one droplet with the bulk dipoles in the second droplet, a fixed-surface-charge–bulk-dipole interaction, or charge–dipole (CD) interaction for short. Below, the detailed derivation steps of the CD interaction between two bodies are described.

As previously stated, at small separation distances ($\sim$100 nm), the interfaces of the droplets can be considered as almost flat and parallel.[17] Hence, the CD interaction can be derived for two identical, parallel, and flat plates, similar to the assumption that was made for vdW and EDL

interactions in eqs (2.10) and (2.11). The interaction free energy between a single charge and a single dipole $w(\rho)$ is given by[13]

$$w(\rho) = -\frac{Q^2 u^2}{6(4\pi\varepsilon_0\varepsilon_r)^2 k_B T \rho^4} \tag{2.14}$$

where Q is the electric charge (i.e., equivalent to e); u is the electric dipole moment; ε_0 and ε_r are the dielectric permittivity of the free space ($\varepsilon_0 = 8.854 \times 10^{-12}$ F/m) and relative permittivity of the medium, respectively; k_B is the Boltzmann constant; T is the absolute temperature; and ρ is the distance between the interacting species (i.e., charge and dipole). It is noteworthy that the CD interaction is proportional to ρ^{-4}. Thus, it acts at longer ranges when compared to dipole–dipole interactions (i.e., vdW interactions), which are proportional to ρ^{-6}. Equation (2.14) can be simply written as

$$w(\rho) = -\frac{\lambda_{CD}}{\rho^4} \tag{2.15}$$

where λ_{CD}, which we call the charge–dipole constant, is equal to $Q^2u^2/6(4\pi\varepsilon_0\varepsilon_r)^2k_BT$ (J m^4).

In order to determine the interaction energy, interaction force, and disjoining pressure between surface charges of one plate and bulk dipoles of another plate, a single point-like charge is considered at point P separated by a distance h from an infinitely large plate with a thickness l and number density or molecular density N (m^{-3}),[89] as shown in Figure 2.2A. The potential energy of the single charge at point P is calculated by integrating the interaction energy in eq (2.15) between the single charge and a ring of radius a with volume $2\pi a da dz$ over the entire volume of the plate (Figure 2.2A). The total number of molecules in this ring is $N \times 2\pi a da dz$. Therefore, the potential energy at point P, E_P, can be calculated by integration as follows[89]

$$E_{\mathrm{p}} = \int_{z=h}^{h+l} \int_{a=0}^{\infty} w(\rho)\, N\, 2\pi a \, \mathrm{d}a \, \mathrm{d}z \tag{2.16}$$

By substituting $w(\rho)$ from eq (2.15) into eq (2.16) and knowing that $\rho = \sqrt{a^2 + z^2}$

$$\begin{aligned} E_{\mathrm{p}} &= \int_{z=h}^{h+l} \int_{a=0}^{\infty} -\frac{\lambda_{\mathrm{CD}}}{(a^2+z^2)^2}\, N\, 2\pi a \, \mathrm{d}a \, \mathrm{d}z \\ &= 2\pi N \lambda_{\mathrm{CD}} \int_{z=h}^{h+l} \mathrm{d}z \int_{a=0}^{\infty} -\frac{a}{(a^2+z^2)^2} \, \mathrm{d}a \end{aligned} \tag{2.17}$$

The integral over a on the right-hand side of eq (2.17) can be named as

$$S = \int_{a=0}^{\infty} -\frac{a}{(a^2+z^2)^2} \, \mathrm{d}a \tag{2.18}$$

where it can be readily calculated as

$$\begin{aligned} S &= \frac{1}{2} \frac{1}{a^2+z^2} \Big|_{a=0}^{\infty} \\ &= \frac{1}{2}\left[0 - \frac{1}{z^2}\right] = -\frac{1}{2z^2} \end{aligned} \tag{2.19}$$

By substituting eq (2.19) as the result of the integral S in eq (2.17), one can write

$$E_{\mathrm{p}} = 2\pi N \lambda_{\mathrm{CD}} \int_{z=h}^{h+l} -\frac{1}{2z^2} \mathrm{d}z \tag{2.20}$$

The integral in eq (2.20) is calculated as

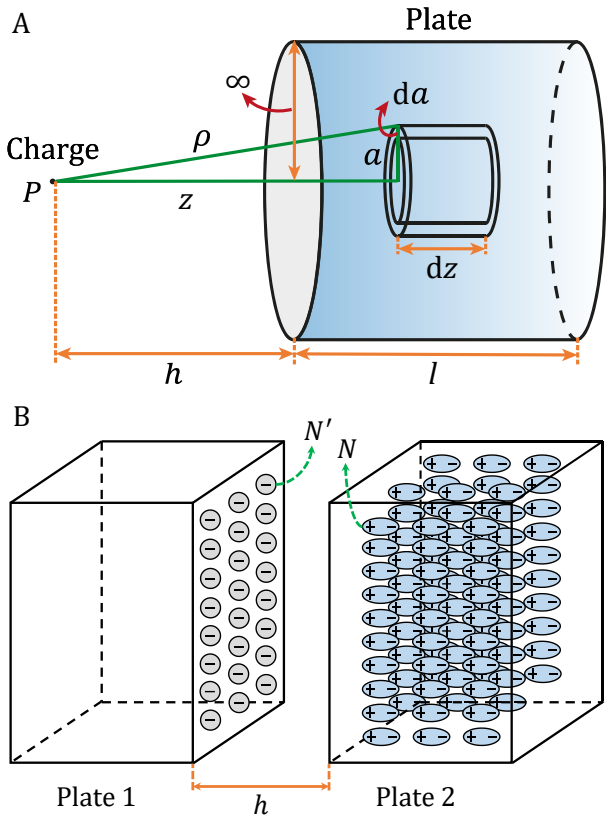

Figure 2.2 Schematic of the essential steps for the derivation of the equation for the charge–dipole interaction between two plates. (A) Interaction between a point charge at P and a plate. (B) Interaction between N' surface charges of plate 1 and N bulk dipoles of plate 2. The same interaction also exists between the surface charges of plate 2 and bulk dipoles of plate 1. The surface charges in (B) are arbitrarily chosen as negative for schematic representation only.

$$E_{\mathrm{p}} = 2\pi N\lambda_{\mathrm{CD}}\left[\frac{1}{2z}\right]\Bigg|_{z=h}^{h+l} = \pi N\lambda_{\mathrm{CD}}\left[\frac{1}{h+l} - \frac{1}{h}\right] \tag{2.21}$$

In particular, as $l \to \infty$, eq (2.21) becomes

$$E_{\mathrm{p}} = -\frac{\pi N\lambda_{\mathrm{CD}}}{h} \tag{2.22}$$

which is the derived interaction energy between a single charge and bulk dipoles of an infinitely thick plate at a distance h from the charge. According to Figure 2.2B, the interaction energy per unit area ($\mathrm{J/m^2}$) between all charges on the surface of plate 1 and the dipoles of plate 2 is found by multiplying eq (2.22) for a single charge by the number of surface charges per unit area N' ($\mathrm{m^{-2}}$) (Figure 2.2B), giving the overall interaction energy per unit area

$$E = -\frac{\pi N N' \lambda_{\mathrm{CD}}}{h} \tag{2.23}$$

Knowing that $F = -\mathrm{d}E/\mathrm{d}h$, the force per unit area ($\mathrm{N/m^2}$) is found by taking the derivative of eq (2.23) with respect to h, as follows

$$F = -\frac{\pi N N' \lambda_{\mathrm{CD}}}{h^2} \tag{2.24}$$

For the interaction between two droplets with identical interfaces and bulk fluids, we need to consider the interaction of surface charges of both droplets interacting with the bulk dipoles of the other droplet by multiplying the interaction energy and force per unit area by 2 giving

$$E_{\mathrm{CD}} = -\frac{2\pi N N' \lambda_{\mathrm{CD}}}{h} \tag{2.25}$$

$$F_{\mathrm{CD}} = -\frac{2\pi N N' \lambda_{\mathrm{CD}}}{h^2} \tag{2.26}$$

As a result, eqs (2.25) and (2.26) describe the fixed-surface-charge–bulk-dipole (CD) interaction energy and force per unit surface area between two identical thick plates separated by a distance h, respectively. The disjoining pressure due to the CD interaction is simply the interaction force per unit area (i.e., eq (2.26)), given by

$$\Pi_{\mathrm{CD}} = -\frac{2\pi N N' \lambda_{\mathrm{CD}}}{h^2} \tag{2.27}$$

Equation (2.27) may then be added to other disjoining pressures in the augmented Young–Laplace equation, eq (2.2), to determine the contribution of surface forces in droplet–droplet interactions. Equation (2.27) shows that the disjoining pressure due to the CD interaction is proportional to h^{-2}, whereas according to eq (2.12), vdW disjoining pressure is proportional to h^{-3}. Hence, we can conclude that the CD interactions act at longer ranges than vdW interactions.

2.4 Methods

2.4.1 General Methods

Details of the computational methods are given in the Appendix, Section A.2.[23,90,91] In summary, first, the capability of our numerical approach to solve eq (A.21) from the Appendix, Section A.2, and calculate the results of oil-in-water experimental cases using conventionally included forces (vdW, EDL, and hydrodynamic forces) is assessed. It is worth mentioning that the inclusion of vdW and EDL forces results in the conventional Derjaguin–Landau–Verwey–Overbeek (DLVO) theory.[92–94] This step assures the accuracy of the implemented computational approach and its potential application for other types of systems. Then, theoretical fittings with the number of surface charges per unit area N' as the only adjustable parameter are made for the interaction force between two water droplets in an organic phase by including vdW and hydrodynamic forces and adding the new CD disjoining pressure to the system. We fit experimental results from the literature for which theoretical study has not been done previously. Finally, the viscous shear stress at the water-droplet–liquid-oil interface will be discussed in detail.

Here, we summarize the reasons why the above-mentioned surface forces were considered in each system. In aqueous solutions, ions are dispersed in the medium and cause the existence of EDL interactions, while in organic media, these ions are absent and result in zero EDL forces.[18,92,95] In both oil-in-water and water-in-oil systems, the interaction between dipoles within the bulk of one droplet and bulk dipoles of another droplet (i.e., vdW forces) is one of the dominant forces.[89] As introduced in this work, in water-in-oil systems, the presence of charges on the surface of the droplets leads to the emergence of an attraction between the fixed surface charges of one water droplet and dipoles within the bulk of another water droplet (i.e., fixed-surface-charge–bulk-dipole attraction). Furthermore, we assume that because the organic phase is pure, the droplet interfaces are free of interfacially active species, and thus, that steric effects are absent.[96] We also assume that no hydrophobic interaction is present between the droplets.

2.4.2 Computational Approach Validation for Oil-in-Water Systems

In order to validate our numerical approach, an oil-in-water system in which two oil droplets interact with each other in an aqueous continuous phase is selected. Oil-in-water systems have been broadly investigated in the literature, and the SRYL model has proven to work well for them. As a result, the fundamentals and physics of the interactions have been well established. In this regard, the experimental data from the study of Shi et al. for two oil droplets in an aqueous solution are considered.[11,34] The oil phase is pure toluene immersed in a 1 mM NaCl solution with a pH value of 5.6 as reported in the study. One of the oil droplets is adhered to the AFM cantilever and approaches the second one, which has been anchored to the substrate. The valencies of Na^+ and Cl^- ions are unity. We calculated the number density of ions ρ_∞ for a 1 mM NaCl solution with a pH value of 5.6. The concentration of ions in the solution has a contribution from the added salt

(i.e., NaCl) and pH of the solution. The concentration of ions due to the pH is $10^{-5.6}$ mol/L, which can be summed with the concentration of ions due to the added salt (10^{-3} mol/L) and multiplied by Avogadro's number ($N_A = 6.022 \times 10^{23}$ mol^{-1}) to get $\rho_\infty = 6.037 \times 10^{23}$ m^{-3}. As mentioned before, in eq (2.13), the contributions from both ion species of water (H^+ and OH^-) and salt (Na^+ and Cl^-) have already been considered in the coefficient "64", and thus, we do not need to multiply ρ_∞ by 2.[13] The experimental input parameters and system properties required to calculate the interaction between the droplets are summarized in the Appendix, Section A.3, Table A.1.[11,17,34,97,98]

For the oil-in-water system, the magnitude of the surface potential in the experiments by Shi et al. is unavailable and consequently needs to be fitted. It is noteworthy that the zeta potential has been provided in Shi et al.'s article, and therefore, after the fitting for the surface potential in our numerical study, the surface potential magnitude can be compared with the zeta potential to assure the correctness and feasibility of our fit (generally, surface potential is larger than zeta potential). Furthermore, our fitting can be compared with the fitting done by Shi et al. in the same article to further confirm our results.[11,34] The initial apex separation h_i is also unknown and is required to be adjusted based on the fit value for the surface potential and experimental force-versus-time data. The least squared error method can be implemented to find the best fit with the lowest root mean sum of squared errors (RMSE). In this regard, the experimental force-versus-time data were extracted from Shi et al.'s paper and fitted for the surface potential and initial apex separation based on the lowest RMSE.

2.4.3 Theoretical Analysis for Water-in-Oil Droplet Interactions Incorporating the Proposed New Charge–Dipole (CD) Interactions

In this chapter, a novel surface force, namely a fixed-surface-charge–bulk-dipole interaction, or charge–dipole (CD) interaction for short, has been introduced for describing the interaction between water drops immersed in a surrounding organic phase. In order to thoroughly understand the role of the CD contributions to the disjoining pressure, two distinct experimental studies that investigate the behavior of water droplets in pure toluene[11,37] or pentol (i.e., the mixture of pentane and toluene at a volume ratio of 1:1)[38] are considered. These previous studies lack theoretical predictions or fittings and will be used here to evaluate the new theory developed in this work.

In order to theoretically evaluate the interaction mechanism between water drops in pure organic phases, the input parameters and system properties are required. The temperatures of both systems are assumed to be $25\,°C$. The dynamic viscosity of toluene is approximately $0.56\,\text{mPa s}$.[99,100] Moreover, the dynamic viscosity of pentol is reported to be $0.39\,\text{mPa s}$ in the literature.[101] A very close value can also be found for the viscosity of pentol via mixing rules. For more information, see the Appendix, Section A.4.[99–108] For water droplets suspended in toluene, the contact angle of the water droplet on the substrate θ_b is $90°$, and the contact angle of the cantilever-adhered droplet θ_t is $45°$.[38] Because of the lack of information on the contact angle of water droplets on the substrate and cantilever in the pentol case, the same contact angles as the ones in the toluene case are assumed. Besides the fluid-related parameters, several surface-force-related parameters are also required for the computation. The relative permittivity of pure toluene ε_r is 2.38 at $25\,°C$.[109] Using the Bruggeman mixing rule for the homogeneous mixing[110] of toluene and pentane with relative permittivities of 2.38 [109] and 1.82 [111] (at $25\,°C$), respectively, the relative permittivity of pentol is calculated to be 2.09. For detailed information on the calculation, see the

Appendix, Section A.5.[109–112] The number density or molecular density of water N is found to be $33.3291 \times 10^{27}\ \mathrm{m}^{-3}$ using the density of water ($997.04\ \mathrm{kg/m^3}$) [113] at 25 ℃, its molar mass ($18.015\ \mathrm{g/mol}$),[114,115] and Avogadro's number (using $N = \rho_\mathrm{f}\, N_\mathrm{A}/M$, where ρ_f is the density, M is the molar mass, and N_A is Avogadro's number). The nonretarded Hamaker constant for water–toluene–water is reported to be 9.72×10^{-21} J by Shi et al.[37] We calculated the Hamaker constant for water–pentol–water based on Lifshitz theory to be 5.20×10^{-21} J. The detailed steps of the calculation of the water–pentol–water Hamaker constant are provided in the Appendix, Section A.6.[13,87,88,102,104,116,117] The experimental input parameters and system properties required to calculate the interaction between the droplets are summarized in the Appendix, Section A.7, Table A.2 [11,34,37,99,100,109,113–115,118–120] and Table A.3 [11,37,38,101–107,109–111,113–120] for toluene and pentol, respectively. It should be noted that according to Xie et al.,[38] the radii of the water droplets submerged in pentol in various experiments are 50–70 μm (see the Appendix, Section A.7, Table A.3). In this study, because of the lack of information on the exact value of the sizes of the droplets (i.e., a single number rather than a range), we carried out the simulations and fittings based on radii of 60 μm as mentioned in the Appendix, Section A.7, Table A.3. However, as a sensitivity analysis, we also checked the results with the minimum possible radii suggested in the experimental work of 50 μm since the interaction force is more sensitive to the radii of the drops than other input parameters. Moreover, the magnitude of the cantilever spring constant K is reported to be 300–400 mN/m in both Shi et al.'s (toluene)[11,37] and Xie et al.'s (pentol)[38] papers. Although we chose the magnitude of the cantilever spring constant to be 350 mN/m, we also performed numerical simulations using $K = 300$ mN/m and $K = 400$ mN/m for both toluene (Shi et al.) and pentol (Xie et al.) cases in order to realize the effect of the cantilever spring constant on the calculated force and the resulting fit value for the number of surface charges per unit area.

For the water-in-oil systems being studied in this work, the number of surface charges per unit area N' on the interface of the droplets is the only fitting parameter in the fitting process of the force curves and is found by either (i) fitting to all the experimental data by minimizing the RMSE between the fit and all the data or (ii) fitting to only the last point (i.e., at the smallest piezo-displacement, ΔX).

2.5 Results and Discussion

2.5.1 Computational Approach Validation for Oil-in-Water Systems

Figure 2.3A shows the measured temporal force values of the study carried out by Shi et al.[11,34] (red squares) and our fits (black line) during the approach of the two pure toluene droplets. When

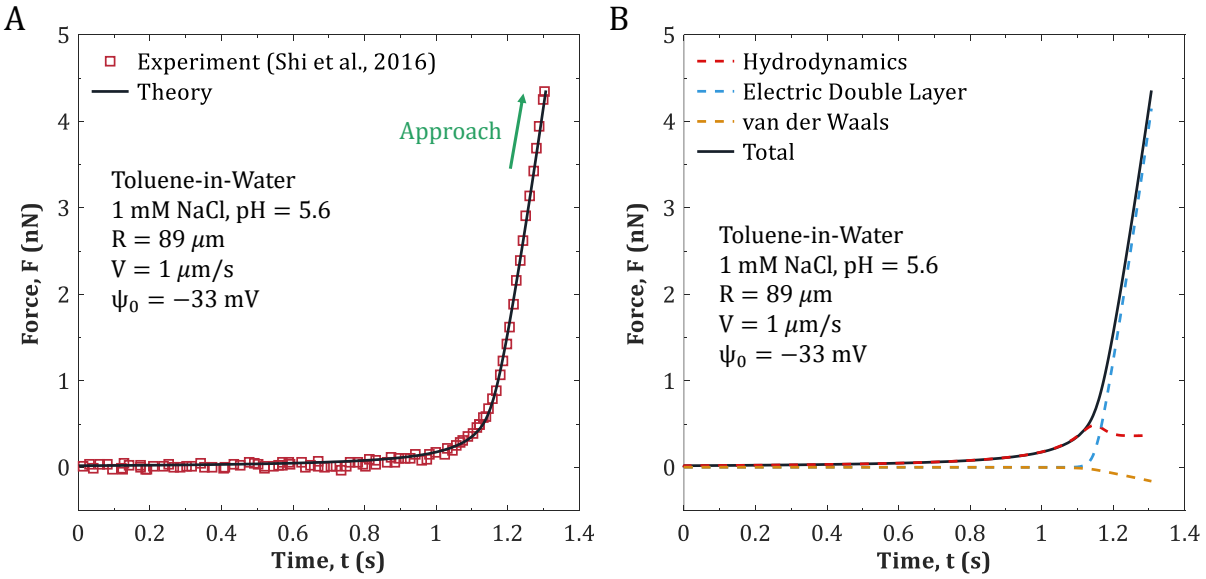

Figure 2.3 Interaction force between two pure toluene droplets suspended in an aqueous solution plotted vs time. (A) Comparison between the theoretical total force curves fit using the numerical approach of this study (black solid line) and the measured data points (red squares) of Shi et al.[34] (B) Contributions of different forces to the fit shown in (A).

the cantilever-adhered droplet approaches the fixed droplet on the substrate, the overall interaction force increases gradually until a separation distance below which the film thickness becomes very small and the resultant force from hydrodynamic and surface forces grows strong; consequently, the force curve shoots up. In both experimental and fitted cases, the magnitude of the overall force is repulsive (positive value) owing to the dominance of the EDL force. The maximum overall force in the fitting was found to be 4.36 nN during the approach. The comparisons in Figure 2.3A show that the fits are in excellent agreement with the experimental results.

In order to calculate the EDL force, the magnitude of the surface potential is required in eq (2.13), which is unknown. Hence, its value must be fitted. Using the least squared error method, the best fit for the surface potential was found to be -33 mV. Shi et al. reported a measured value of the zeta potential for the oil drops of -30 ± 3 mV for the same case as in the experiments.[11,34] Since, in general, the magnitude of surface potential is close to and larger than the zeta potential, our fitting value is reasonable. In addition, Shi et al. reported that the magnitude of their fit value for the surface potential was -35 ± 5 mV.[11,34] The comparisons show that our fitting number is consistent with the results of Shi et al. and falls within their proposed range. Also, adjusting the magnitude of the initial apex separation leads to a fit value of 1.18 μm.

Figure 2.3B shows the contributions of various forces, including hydrodynamic (red), vdW (orange), and EDL (blue) forces, in dashed lines. Hydrodynamics is the main origin of the repulsive force at relatively large distances, where the surface forces are negligible. The attractive vdW and repulsive EDL interactions begin to appear around 1.1 sec (i.e., below 90 nm) and become large, particularly the EDL force. From Figure 2.3B, one can also realize that the magnitude of the vdW force is small in contrast to that of the EDL force at very small separations. This is due to the fact that the 1 mM NaCl concentration cannot sufficiently screen ions around the droplet ($\kappa^{-1} =$

9.6 nm), and thus, at very small separations, the EDL force dominates the system and sustains the water film between the droplets, preventing the *jump-in* behavior and eventual coalescence of the droplets. At this point, the droplets' heads flatten, and the confined film between them nearly stabilizes. Hence, the hydrodynamic force tends to become almost constant above 1.2 sec, which was also observed in similar studies.[17] When the drops' heads become flattened, the radial change of the film thickness becomes equal to 0 ($\partial h/\partial r = 0$), and thus, the sum of the hydrodynamic and disjoining pressures is balanced by the Laplace pressure of the drops in that region. This behavior was found to occur at a minimum separation of around 30 nm, which was also reported in the numerical study by Shi et al.[11,34]

2.5.2 Theoretical Analysis for Water-in-Oil Droplet Interactions Incorporating the Proposed New Charge–Dipole (CD) Interaction

Figure 2.4 shows the experimental force measurements at different piezo-displacements ΔX and the corresponding theoretical fitting curves for two water droplets suspended in pure toluene or pure pentol when the cantilever-anchored droplet moves toward the substrate-adhered droplet at a drive velocity of 1 μm/s. In water-in-oil systems, the EDL interaction is absent, and because of that, the *jump-in* behavior is observed between the water drops, which brings about their coalescence due to the presence of attractive vdW and CD interactions. This behavior suggest that water-in-oil emulsions are generally unstable in the absence of stabilizers.[36] In Figure 2.4, the jump-in is indicated by a green arrow.

In Figure 2.4A,B, the results of the fitting are illustrated for toluene and pentol. The blue squares are the experimental measurements, and the red dashed–dotted lines and black solid lines

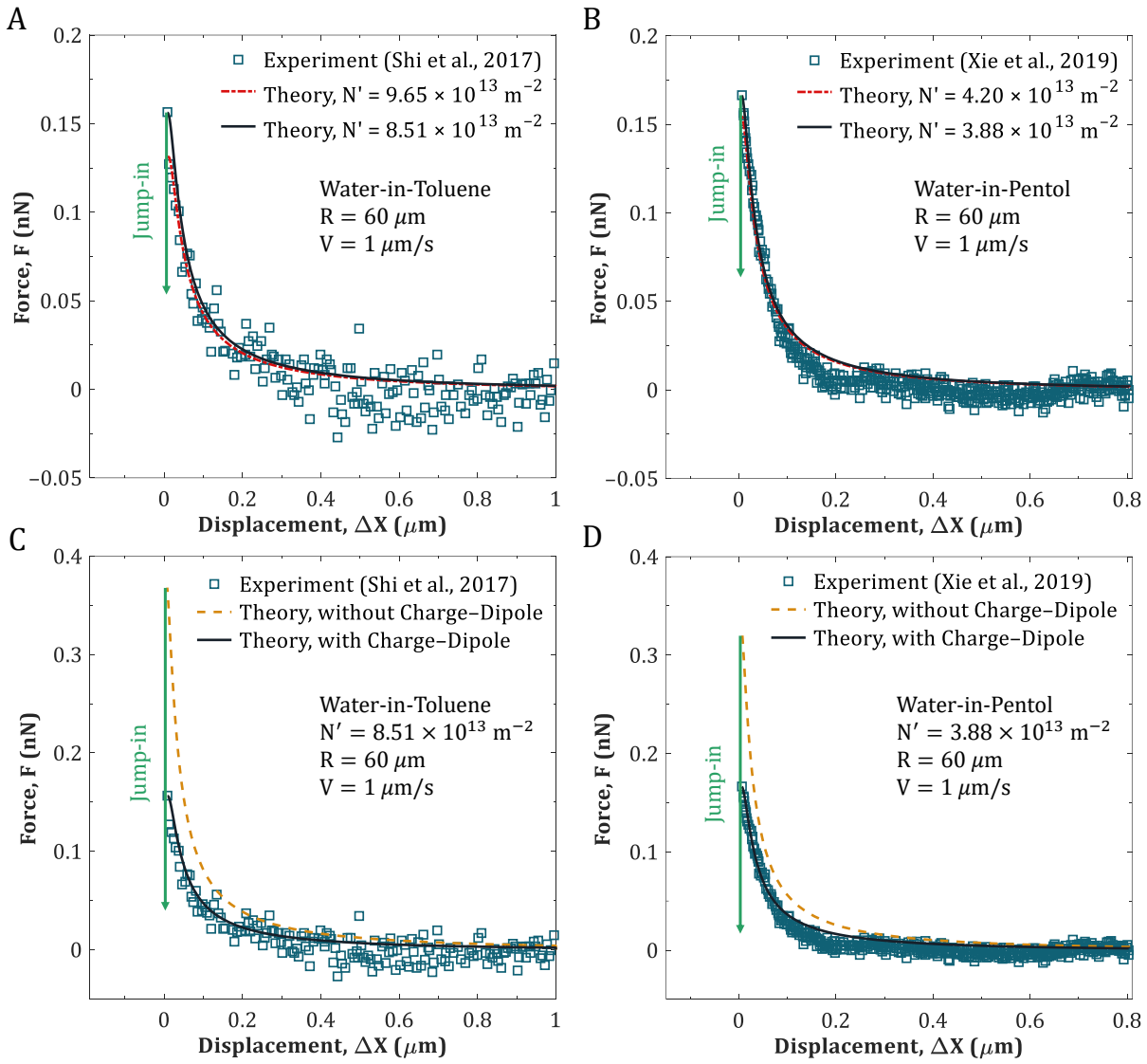

Figure 2.4 Measure interaction forces between two water droplets suspended in pure toluene (A,C) or pure pentol (B,D) vs piezo-displacement and the theoretical fits from this work. (A,B) Comparison between the force curves in the presence of CD interactions obtained using fitting to all data by the least squared error method (red dashed–dotted line) and fitting to only the smallest piezo-displacement (black solid line). (C,D) Comparison between the force curves in the absence (orange dashed line) and presence (black solid line) of CD interactions. The measured data points for the toluene and pentol cases are from the experimental studies (blue squares) conducted by Shi et al.[11,37] and Xie et al.,[38] respectively.

demonstrate the fitting to all the data by the lowest RMSE and fitting to only the last point, respectively. The measurements indicate that the overall interaction force between the droplets is slightly repulsive (positive quantity) during the approach of the drops. When the distance between

the drops becomes extremely small, and the force magnitude reaches a value of about 0.16 nN for toluene (Figure 2.4A) and 0.17 nN for pentol (Figure 2.4B), the vdW and CD interactions grow strong and induce the jump-in behavior and coalescence of the droplets. Table 2.1 summarizes the important outputs from our studies for the toluene and pentol cases. The fitting to all the data by the lowest RMSE predicts the jump-in at a force value of 0.13 and 0.15 nN for toluene and pentol cases, respectively. Obviously, this fitting method cannot accurately predict the actual jump-in because the lowest RMSE is attained at the expense of losing the accurate calculation of the last point (i.e., jump-in point). The alternative method that leads to the accurate computation of the original jump-in and the subsequent reliable results is the fitting to only the last point (smallest ΔX). This approach can accurately evaluate the jump-in point for both toluene and pentol, respectively, and leads to more reliable and correct results compared to the previous approach even though its RMSE value is slightly larger (Table 2.1). Since the jump-in point describes the location at which the attractive interactions can finally overcome the hydrodynamic interaction and initiate the droplets coalescence process, we are interested in the accurate calculation of its exact occurrence point. Fitting to all the data by the lowest RMSE cannot accurately describe this location and compute the magnitude of attractive surface forces and the hydrodynamic force, while fitting to only the last point is capable of capturing the real behavior observed in the experiments. In addition, the RMSE difference between the two methods is very small, and consequently, the minor difference can be omitted at the expense of acquiring more precise results, particularly computing the actual jump-in point. Therefore, fitting to only the last point has been chosen as the most important fitting method in our study. The numbers of surface charges per unit area for each method and each system are summarized in Table 2.1. Table 2.1 shows that the magnitude of the

Table 2.1 Important outputs from our studies for the toluene and pentol cases

Method of fitting	Output parameter	Value	
		Water-in-toluene	**Water-in-pentol**
All points (lowest RMSE)	Jump-in force, F	0.13 nN	0.15 nN
	Number of surface charges per unit area, N'	9.65×10^{13} m^{-2}	4.20×10^{13} m^{-2}
	RMSE	1.18×10^{-2} nN	7.52×10^{-3} nN
Last point (smallest ΔX)	Jump-in force, F	0.16 nN	0.17 nN
	Number of surface charges per unit area, N'	8.51×10^{13} m^{-2}	3.88×10^{13} m^{-2}
	RMSE	1.25×10^{-2} nN	7.77×10^{-3} nN

fitted number of surface charges per unit area for each case is within the range previously reported for a water phase in contact with various oil phases, which is 10^{13}–10^{14} m^{-2}.[42–45] This agreement lends strong support to our theory.

In Figure 2.4C,D, the results of force prediction in the absence of CD interactions (orange dashed line) and force fitting to only the last point in the presence of CD interactions (black solid line) are compared for toluene and pentol. This could be achieved by including or leaving out the contribution of disjoining pressure due to the CD interactions (eq (2.27)) in the augmented Young–Laplace equation (eq (2.2)). In the absence of the CD force, the attractive vdW force is not alone able to decrease the repulsive dominance of the long-ranged hydrodynamic effects, and as a result, the jump-in occurs at a much larger interaction force (0.37 nN for toluene and 0.33 nN for pentol). In the absence of the CD force, the force curve deviates from the real behavior. Thus, the attractive vdW force cannot alone be responsible for the jump-in behavior of the droplets and there must be another attractive surface force that leads to smaller overall repulsive interaction forces at small separations. Conversely, when the effects of the CD interactions with a number of surface charges

per unit area consistent with the known number of surface charges in the literature are incorporated into the computation, the theory can accurately describe the exact behavior of the droplets and can capture the actual jump-in point. As mentioned earlier, a sensitivity analysis was also carried out on the effects of choosing the minimum possible droplet radii of $50\ \mu$m (rather than the average of the radii suggested in the experimental work of $60\ \mu$m) in the pentol case. The results of force prediction in the absence of CD interactions and force fitting to only the last point in the presence of CD interactions are shown in the Appendix, Section A.8, Figure A.3. The results indicate that when the radii of the drops are taken to be $50\ \mu$m, the same conclusions are reached from the fitting results, i.e., that the experimental results cannot be explained in the absence of CD interactions, and that the fit number of surface charges per unit area is within the independently known range of surface charges. For more information, see the Appendix, Section A.8.[42] Moreover, our calculations using cantilever spring constants of 300, 350, and 400 mN/m show that changing the magnitude of this parameter within the values reported by Shi et al. and Xie et al. does not alter the shape of the resulting force curves and has a negligible effect on the magnitudes of the jump-in force. As a result, it does not change the magnitude of the fit value for the number of surface charges per unit area in both toluene and pentol cases.

Figure 2.5 shows the magnitude of different forces versus piezo-displacement (Figure 2.5A,B) and versus time (Figure 2.5C,D) during the interaction of water droplets in pure toluene or pentol calculated using the theory. According to Figure 2.5A,B, the magnitude of the hydrodynamic force (red dashed line) is slightly larger than the sum of vdW (orange dashed line) and CD (blue dotted line) forces, and consequently, the overall force is slightly repulsive (black solid line). When the film between the droplets becomes very thin, the hydrodynamic force increases at a larger rate due

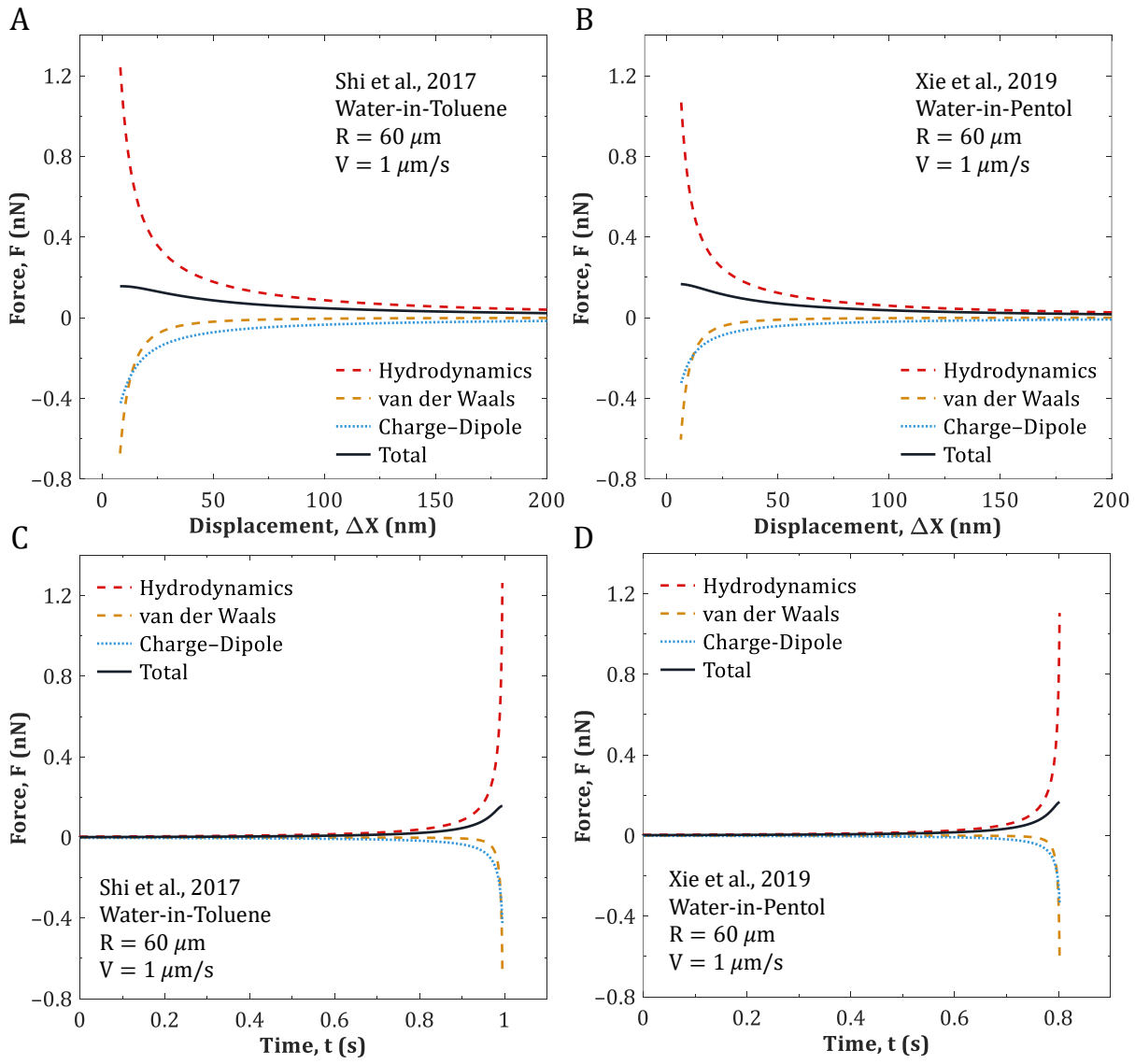

Figure 2.5 Contributions of different forces to the fits shown with black solid lines during the interaction between two water droplets submerged in pure toluene (A,C) or pure pentol (B,D). (A,B) The force curves vs piezo-displacement. (C,D) The force curves vs time.

to a rise in the hydrodynamic pressure of the thin film. As the separation distance decreases, the contribution of surface forces enhances, until a point at which the attractive vdW and CD interactions destabilize the thin film and lead to the jump-in. This phenomenon can be adequately described by the sudden growth in the magnitude of vdW and CD forces just before the jump-in

point. Figure 2.5A,B also shows the fact that the CD force acts at much longer ranges in comparison with the vdW force (around 200 nm). Furthermore, the magnitude of the CD force is comparable to the hydrodynamic force at intermediate distances (i.e., around 200 nm). These observations highlight the major role of the CD force in the destabilization of the thin film between drops during the interaction of water drops in pure organic media. Moreover, the behavior of these force versus time curves is described in Figure 2.5C,D. The initial apex separations between the water drops in toluene and pentol phases are 1 and 0.805 μm, respectively. Since the drive velocity is constant at 1 μm/s, it should take about 1 and 0.805 sec for the final coalescence of the droplets in the surrounding toluene and pentol, respectively. However, due to the existence of strong attractive surface forces, namely vdW (orange dashed line) and CD (blue dotted line) forces at very small distances, the droplets' interfaces are deformed, and the required time for the coalescence deviates slightly from the above-estimated values. These jump-in times are found to be 0.9951 and 0.8023 sec for droplets in toluene and pentol, respectively. Figure 2.5C,D also shows that the magnitude of all forces increases suddenly when the film thickness between the drops becomes very small. This behavior can be observed near times 1 and 0.8 sec for toluene and pentol, respectively.

In Figure 2.6 the computed droplet profiles, as well as the spatiotemporal profiles of the oil film confined between the water droplets for both toluene and pentol cases, are shown. In order to appreciate the effect of CD interactions on the two droplets profiles and film profiles, an interesting comparison is also carried out in their presence and absence. Figure 2.6A–D shows the droplet profiles in the presence (solid lines) and absence (dashed lines) of CD interactions at the beginning of the droplets' jump-in (Figure 2.6A,B) and at coalescence (Figure 2.6C,D) for toluene and pentol. The droplets' jump-in occurs at the critical film thickness, i.e., the critical separation (at $r = 0$),

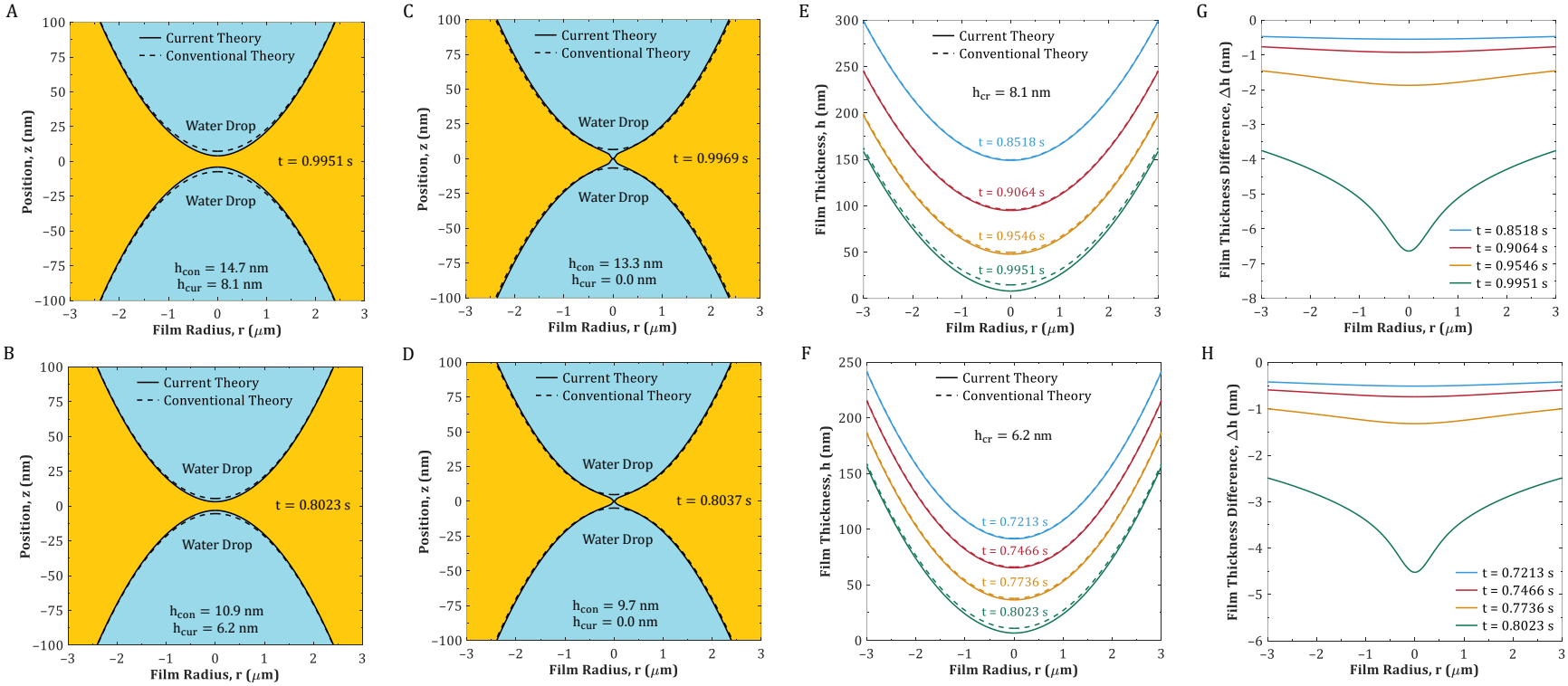

Figure 2.6 Theoretical water droplet profiles and spatiotemporal profiles of the thin film for two water droplets submerged in organic phases. (A–D) Comparison between the theoretical water droplet profiles in the presence (solid lines) and absence (dashed lines) of CD interactions for toluene (A,C) and pentol (B,D) at the critical film thickness (A,B) and at the beginning of the collision (C,D). (E,F) Spatiotemporal thicknesses of the thin oil film confined between two water droplets in the presence (solid lines) and absence (dashed lines) of CD interactions for toluene and pentol, respectively. (G,H) Temporal evolution of the film thickness difference between the theoretical calculations in the presence (solid lines) and absence (dashed lines) of CD interactions for toluene and pentol, respectively.

h_{cr}, where the attractive surface interactions overcome the repulsive hydrodynamic interaction and result in the jump-in. According to Figure 2.6A,B, at the beginning of the jump-in, in the presence of CD interactions, the critical film thicknesses are 8.1 and 6.2 nm for toluene and pentol, respectively. At the same instant of time (0.9951 sec for toluene and 0.8023 sec for pentol), these values for the case in which the CD interactions are absent are 14.7 and 10.9 nm, respectively. In the presence of CD interactions, an additional attractive force pulls the droplets toward each other, which facilitates the droplets' jump-in and results in a smaller film thickness as opposed to the case in which the CD interactions are absent and the drops are less attracted to each other. The necessary step to induce the coalescence of the droplets is that first, the disjoining pressure due to the attractive interactions must overcome the hydrodynamic pressure, and then, at the jump-in, it exceeds the Laplace pressure of the droplets.[63] The disjoining pressure initially becomes larger than the hydrodynamic pressure at 0.9877 sec and a minimum separation of 16.5 nm for toluene ($\Pi = -187.64$ Pa, $p = 180.30$ Pa at minimum separation h_0) and at 0.7973 sec and a minimum separation of 11.8 nm for pentol ($\Pi = -254.03$ Pa, $p = 243.32$ Pa at h_0). Therefore, the initial barrier toward the coalescence of the droplets is removed. The Laplace pressures of the water drops suspended in toluene and pentol are calculated to be 1183.33 and 1355 Pa, respectively. The corresponding attractive disjoining pressures associated with the critical film thicknesses (i.e., at the jump-in) for both cases are -1292.66 and -1434.87 Pa, which shows evidently that the attractive disjoining pressure overcomes the Laplace pressure at 0.9951 sec for toluene and 0.8023 sec for pentol.

When the jump-in takes place, the oil film instantaneously ruptures and induces the coalescence of the droplets.[63] As demonstrated in Figure 2.6C,D, at the beginning of the collision, the droplets' heads contact, and the film thickness at this location and around it becomes 0. Then,

the droplets merge and form a single drop. It is interesting to note that at the same time, in the absence of CD interactions, the vdW force alone cannot yet trigger the droplets' collision, and the film thicknesses are 13.3 and 9.7 nm for toluene and pentol, respectively. One must bear in mind that although in the absence of CD interactions the results deviate from the experimental observations, the vdW forces can eventually induce the collision of the droplets in the succeeding times, i.e., longer than 0.9969 and 0.8037 sec for toluene and pentol, respectively (orange dashed line in Figure 2.4C,D). This conclusion coincides with the observations made in previous studies where vdW forces are the only governing surface forces that induce the collision in systems containing droplets or bubbles.[34,60] Furthermore, Figure 2.6A–D shows that the droplets deform rapidly in response to external forces and coalesce in less than 2 ms starting from the jump-in point. All these observations in our study emphasize the fact that, unlike solid particles, droplets and bubbles can readily deform in response to external forces.[77,121,122]

The spatiotemporal thicknesses of the thin oil film confined between two water droplets are shown in Figure 2.6E,F. The solid lines represent the theoretical results in the presence of CD interactions, while the dashed lines represent the same results in their absence. As the cantilever-anchored droplet approaches the second droplet on the substrate, the film thickness decreases, and due to the existence of attractive surface forces, the profile becomes deformed near the center at small separations (i.e., 0.9951 sec for toluene and 0.8023 sec for pentol). The effect of the CD force on the film profiles, which begins approximately from $t = 0.8518$ sec and $t = 0.7213$ sec for toluene and pentol, respectively, can be noticed from the slight mismatch between the solid and dashed curves. In the absence of the CD force, the vdW force alone is not able to instantly cause the coalescence of the droplets, and thus, the dashed curves fall behind the solid curves

through time. The extra CD force pulls the drops more toward each other and initiates the jump-in at earlier times.

The evolution of the difference between the theoretical results of interfacial thin film profiles in the presence and absence of CD effects is shown in Figure 2.6G,H. As the upper drop approaches the lower drop, the film profile in the absence of CD interactions falls behind the one in their presence, and consequently, their difference increases through time. According to Figure 2.6G,H, although the initial difference between the film thicknesses is small, as the separation decreases, the CD effects become stronger, and their ability to pull the droplets together increases. As a result, the film thickness difference $\Delta h = h_{\text{current}} - h_{\text{conventional}}$ becomes larger. The maximum difference occurs at the center of the film profile at the jump-in ($t = 0.9951$ sec and $t = 0.8023$ sec for toluene and pentol, respectively), where the CD force is the strongest. This difference is found to be 6.6 and 4.7 nm for toluene and pentol, respectively.

Figure 2.7 shows the time evolution of the hydrodynamic and disjoining pressures along the radial coordinate for both toluene and pentol cases until the jump-in. As can be seen in Figure 2.7A,B, when the separation between the droplets is relatively large (blue curve with $h_0 = 207.6$ nm and $h_0 = 182.5$ nm for toluene and pentol, respectively), the hydrodynamic pressure $p(r, t)$ is nearly 0 along the radial coordinate ($t = 0.7929$ sec and $t = 0.6229$ sec for toluene and pentol, respectively). As the upper drop proceeds toward the lower drop, the separation becomes small, and the hydrodynamic pressure develops within the confined thin film between the drops. Moreover, for a particular time, the hydrodynamic effect reduces along the radial coordinate because of the increase in the film thickness. The maximum hydrodynamic pressures (purple curve) at the critical film thicknesses for toluene and pentol are 959.39 and 1073.85 Pa, respectively.

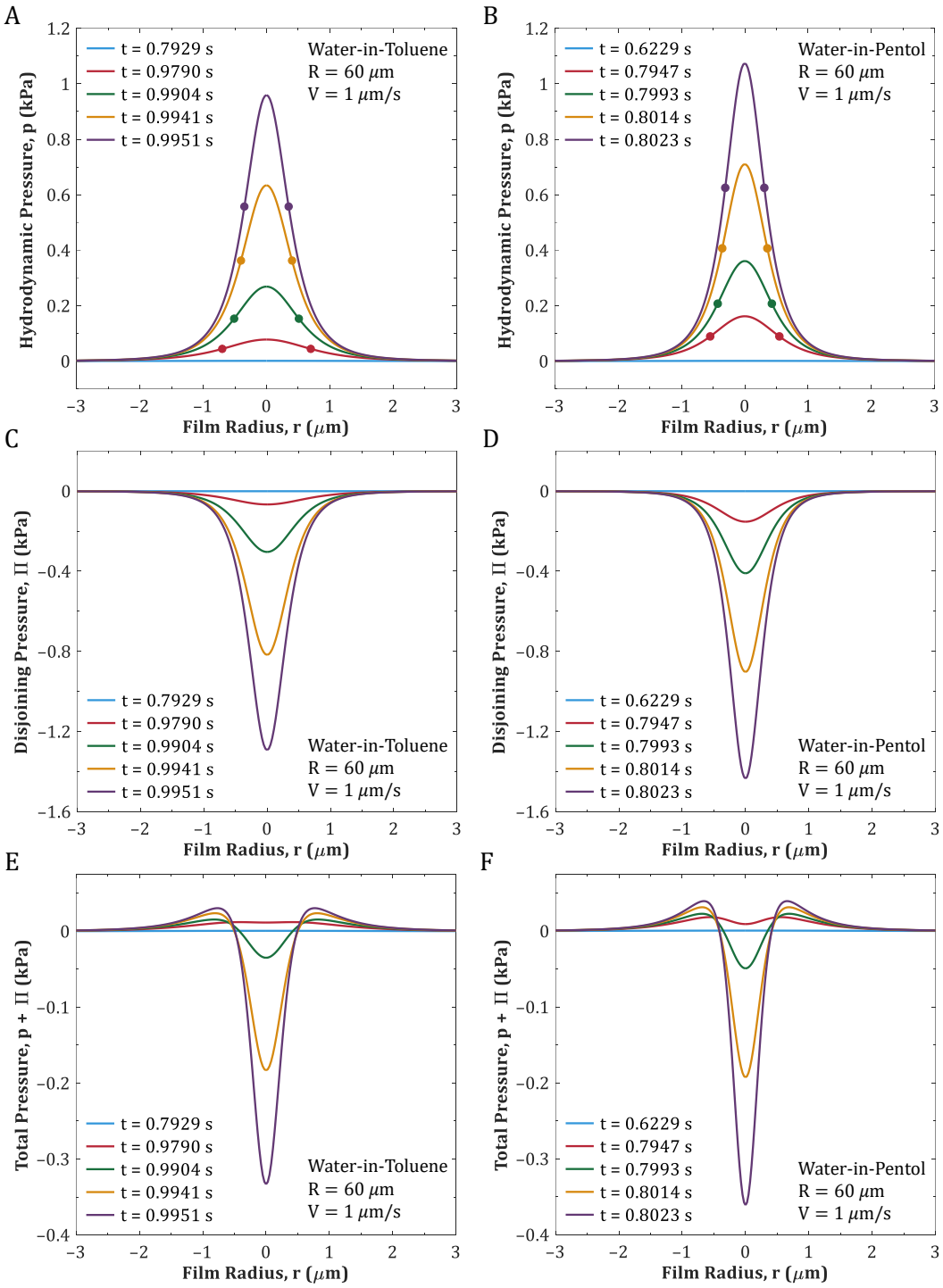

Figure 2.7 Temporal evolution of pressure profiles for the interaction between water droplets immersed in pure toluene (A,C,E) or pure pentol (B,D,F) along the radial coordinate. (A,B) Hydrodynamic pressure profiles in the draining oil film. The filled circles indicate the inflection points of the curves. (C,D) Disjoining pressure profiles due to the attractive surface forces (vdW and CD interactions here). (E,F) Total dynamic pressure profile in the film.

Furthermore, the behavior of the disjoining pressure, $\Pi(r,t)$, including vdW and CD forces along the radial coordinate is shown in Figure 2.7C,D. As mentioned earlier, the surface forces act at small distances. Therefore, at relatively large separations, the disjoining pressure is 0 along the radial coordinate (blue curve, for the same times and separations as in Figure 2.7A,B). As the separation reduces, the attractive disjoining pressures due to the surface forces come into play and increase the pulling effect between the drops. As a consequence, the pressure curves move toward larger negative regions over time. Also, the disjoining pressure decays along the radial coordinate since the film thickness enlarges, and the interfaces of the droplets become farther from each other. The maximum disjoining pressures (purple curve) at the critical film thicknesses for toluene and pentol are -1292.66 and -1434.87 Pa, respectively.

An interesting outcome of this study, which is shown in Figure 2.7E,F, is the total dynamic pressure $p + \Pi$. At small separations and small radial coordinates (near the drops' heads), the droplets' interfaces are close to each other. Hence, as the separation lessens, the disjoining pressure due to the surface forces begins to prevail over the hydrodynamic pressure and results in negative total pressures (i.e., attractive). Thus, the initial barrier against the collision of the droplets is removed. The magnitude of this total dynamic pressure increases as the heads of the droplets are brought closer together. It is worth noting that the total pressure becomes positive (i.e., repulsive) at intermediate radial coordinates (around 500 nm). The film thickness enlarges along the radial coordinate, and both hydrodynamic and disjoining pressures reduce in size. However, the surface forces are more sensitive to separation change in contrast to the hydrodynamic effects. Thus, the disjoining pressure decays more rapidly along the radial coordinate compared to the hydrodynamic pressure, which leads to positive total pressures. The maximum total dynamic pressures at the critical film thickness (purple curves) for toluene and pentol are -333.27 and -361.02 Pa,

respectively. The numerical calculations for hydrodynamic, disjoining, and total dynamic pressures were also compared to previous studies with droplets and bubbles, and the same trends were identified.[16,77,80,84]

The computed hydrodynamic and disjoining pressure profiles along with the total dynamic pressure are plotted versus the minimum separation h_0 until the jump-in for both toluene and pentol in the Appendix, Section A.9, Figure A.3. In order to observe the jump-in, the attractive disjoining pressure must initially overcome the hydrodynamic pressure and then, become larger than the Laplace pressure of the drop. For more information, see the Appendix, Section A.9.

2.5.3 Shear Stress at the Droplet–Liquid Interface in Water-in-Oil

One of the best ways to gain insight into the flow behavior of the draining liquid between the drops is to determine the exerted shear stress at the droplet–liquid interface. Viscous shear stress can accurately capture the incidents occurring within the draining film during the interaction of droplets. In the Appendix, Section A.10, Figure A.4, the time evolutions of viscous shear stress profiles at the droplet–liquid interface are shown for both toluene and pentol until the jump-in. It should be noted that the filled circles in Figure 2.7A,B are inflection points of the hydrodynamic pressure profiles, which correspond to the shear stress maxima in the Appendix, Section A.10, Figure A.4. The shear stress calculations here have similar trends with the results of previous studies on droplets or bubbles that had vdW forces as the only attractive force;[16,84] however, the results of our calculations differ numerically since we included CD attraction. For more information, see the Appendix, Section A.10.

2.6 Conclusions

In this study, the fundamental behaviors of water droplets interacting through oil phases were quantitatively investigated, and for the first time, a novel theory based on the charge–dipole (CD) interaction between the water droplets was developed. An unexplained attractive interaction between water droplets suspended in pure organic phases had been observed experimentally and reported in the literature. We hypothesized that this interaction could be attributed to the presence of charges on the surface of the droplets, which gives rise to an attractive interaction between surface charges of one droplet and bulk dipoles of the second droplet, i.e., a fixed-surface-charge–bulk-dipole interaction, or charge–dipole (CD) interaction for short. An equation for the disjoining pressure due to the CD interaction was developed and then incorporated into the SRYL model. First, the computational approach was validated with an oil-in-water system where two pure toluene droplets interact in an aqueous solution. Then, two distinct AFM experimental studies that investigate the behavior of water droplets in pure toluene and pentol (i.e., a 1:1 mixture of pentane and toluene by volume) were considered, and the effect of the CD interaction on the behavior of the droplets was examined. The results indicated that in the absence of CD interactions, the numerical net force curves deviated from the experimental data, which demonstrates the fact that vdW forces are not the only surface forces that govern the interaction. Conversely, when the CD interaction with number of surface charges per unit area as the only fitting parameter was added to the model, the numerical force curve followed the experimental data and showed an excellent match. Importantly, the fit values of the number of surface charges per unit area so obtained were in agreement with independent measurements and calculations of their value in the literature. The contributions of different forces, the droplet and film thickness profiles, the contribution of hydrodynamic and disjoining pressures, and the imparted shear stresses to the surfaces of the

droplets were also investigated. It is worth mentioning that in this study, in situations where the properties of the phases in the experiments are not provided in the literature, the properties of pure water and pure oil are utilized to make calculations. The slight solubility of water in oil only alters the properties of the oil, not the equations, and could be considered in future work. Our findings provide useful insight into the interaction mechanisms of water droplets submerged in organic phases with practical implications to the behavior and stability of water droplets in a variety of applications.

Chapter 3

Application of the Developed Theory of Charge–Dipole Interaction to Additional Water-in-Oil Systems

In this chapter, the developed theory of fixed-surface-charge–bulk-dipole interaction, or charge–dipole (CD) interaction for short, is applied to two additional water-in-oil systems in which two water droplets interact in a pure oil medium, either n-dodecane (a different oil than those in Chapter 2) or toluene (larger droplet radii than those in Chapter 2). The experiments that we will analyze for water drops inside n-dodecane and toluene were performed by Mao et al.[31] and Sun et al.,[39] respectively. First, in the Methods section (Section 3.1), the detailed steps of simulation are described and the required physical parameters are presented. Then, the results of the theoretical simulations for the two aforementioned systems are introduced in the Results and Discussion section (Section 3.2).

3.1 Methods

In order to perform the theoretical simulations for the two new systems, namely water-in-n-dodecane and water-in-toluene with larger drops, we used the Stokes–Reynolds–Young–Laplace (SRYL) model presented in Chapter 2 along with the computational methods outlined in the Appendix, Section A.2. Because the oil media are nonpolar and do not contain any ions, the electric double layer (EDL) interaction is absent; hence, attractive van der Waals (vdW) and charge–dipole (CD) interactions are the only surface forces present in the simulations. Like Chapter 2, the number of surface charges per unit area N' is the only adjustable parameter (i.e., fitting parameter) for calculating the interaction force between two water droplets in an organic phase. We again fit experimental results from the literature for which theoretical study has not been carried out previously. These experimental data are for two distinct studies in which water drops interact in pure n-dodecane or pure toluene. It is worth mentioning that we performed the fitting for another water-in-toluene system in Chapter 2 as well, and the analysis of this new water-in-toluene system in this chapter allows us to compare the fit value for the number of surface charges for this new system with the fit value for the other system found in Chapter 2. Also, we need to compare the fit value of the new systems with independent measurements and calculations in the literature. Our reviews of the literature in Chapter 2, showed that the number of surface charges per unit area for water droplets immersed in oil phases (i.e., non-polar) are approximately 10^{13}–10^{14} m^{-2}.[42,43,45]

Herein, we present the input parameters and system properties required to evaluate the interaction between water droplets in pure organic phases, namely n-dodecane and toluene. The temperature of the water-in-n-dodecane[31] and water-in-toluene[39] systems are 21.5 and 20 ℃, respectively. The interfacial tension of water–toluene in water-in-toluene system is calculated using[123]

$$\sigma = 0.03663 \frac{10000 - T_c^2}{10526 - T_c^2} \tag{3.1}$$

where T_c is the temperature in ℃. The interfacial tension of water–toluene is calculated to be $34.73\ \mathrm{mN/m}$. The contact angles of cantilever-anchored water drops and water drops on substrates are assumed to be 45 and 90°, respectively, the same as the ones in the water-in-toluene system analyzed in Chapter 2.[11,37] It is worth mentioning that according to Sun et al.,[39] the radii of the water droplets immersed in toluene in various experiments are $120–130\ \mu\mathrm{m}$. In our simulations, because of the lack of information on the exact value of the sizes of the droplets (i.e., a single number rather than a range), we carried out the fittings based on radii of $125\ \mu\mathrm{m}$. The magnitude of the cantilever spring constant K is assumed to be $350\ \mathrm{mN/m}$ based on the reported values of Shi et al.[11,37] and Xie et al.[38] According to Sedrez et al.,[124] the relative permittivity of n-dodecane can be calculated using

$$\varepsilon_r = 0.817886 + \frac{1.00289}{T} + 1.47205 \times 10^{-3}\rho_f + \frac{4.18223 \times 10^{-2}\rho_f}{T} \tag{3.2}$$

where T is the absolute temperature in K and ρ_f is the density of the liquid (i.e., n-dodecane here) in $\mathrm{kg/m^3}$. The relative permittivity of n-dodecane is found to be 2.0287 using a temperature of 294.65 K (i.e., 21.5 ℃) and the density of n-dodecane ($748.074\ \mathrm{kg/m^3}$)[125] at 21.5 ℃. The number densities or molecular densities of water N are found to be $33.3576 \times 10^{27}\ \mathrm{m^{-3}}$ (at 21.5 ℃) and $33.3684 \times 10^{27}\ \mathrm{m^{-3}}$ (at 20 ℃) using the densities of water (997.880 at 21.5 ℃ and $997.203\ \mathrm{kg/m^3}$ at 20 ℃),[113] its molar mass ($18.015\ \mathrm{g/mol}$),[114,115] and Avogadro's number $6.02214 \times 10^{23}\ \mathrm{mol^{-1}}$ (using $N = \rho_f N_A / M$, where ρ_f is the density, M is the molar mass, and N_A is Avogadro's number). We calculated the nonretarded Hamaker constant for water–n-dodecane–water based on Lifshitz theory (using eq (A.26) and values in Table 3.1; see the

Appendix, Section A.6 for more information) to be 4.863×10^{-21} J. Moreover, the nonretarded Hamaker constant for water–toluene–water is reported to be 9.72×10^{-21} J by Sun et al.[39] It is worth mentioning that the temperature of the water-in-toluene system was not reported by Sun et al.,[39] and only the value of Hamaker constant (9.72×10^{-21} J) was mentioned in the paper. As a result, we used the values of parameters in Table 3.2 at different temperatures to find the temperature of the water-in-toluene system. Our calculations show that the reported Hamaker constant by Sun et al. belongs to the temperature of 20 ℃. We used this temperature to collect the input parameters and physical properties of the water-in-toluene system. The experimental input parameters and system properties required to calculate the interaction between water droplets within pure organic phases are summarized in Table 3.1 and Table 3.2.

For both water-in-oil systems being studied here, we only fit for the number of charges per unit area N' at the interface of water drops with oil phases and find the force curves by fitting to only the last point (i.e., at the smallest piezo-displacement, ΔX). In Chapter 2, we described our reasons why fitting to only the last point was chosen as the main fitting method in our study.

3.2 Results and Discussion

Herein, we extend our research on the role of CD interaction during the interaction of two water droplets within a pure organic phase to two new cases by fitting for the number of surface charges per unit area N' using the total interaction force in the experiments carried out by Mao et al.[31] and Sun et al.[39] Figure 3.1 shows the force measurements in the experiments at different piezo-displacements ΔX and the corresponding theoretical curves fitted for the number of charges per unit area at the interface as well as the contributions of different forces to the overall interaction

Table 3.1 Various input parameters used in modeling the interaction of water droplets in pure n-dodecane at 21.5 ℃ for the theoretical fitting.

Type	Physical parameter	Value	Literature source	Notes
Fluid	Viscosity of n-dodecane, μ	1.457 mPa s	[125]	Interpolated linearly between the values at 288.15 and 298.19 K for 21.5 ℃
	Interfacial tension, σ	52.774 mN/m	[126]	Interpolated linearly between the values at 20 and 25 ℃ for 21.5 ℃
	Capillary number, Ca	2.76×10^{-8}	-	$\mathrm{Ca} = \mu V/\sigma$; calculated for this work from other values in this table
	Density of water, ρ_f	997.88 kg/m^3	[113]	Value at 21.5 ℃
	Density of n-dodecane, ρ_f	748.074 kg/m^3	[125]	Interpolated linearly between the values at 288.15 and 298.19 K for 21.5 ℃
	Molar mass of water, M	18.015 g/mol	[114,115]	-
	Radius of curvature of the droplets, R	75 μm	[31]	-
	Droplet contact angle on the cantilever, θ_t	45°	[11,37]	Assumed in this work; the same as the exploited number in the referenced water-in-oil study
	Droplet contact angle on the substrate, θ_b	90°	[11,37]	Assumed in this work; the same as the exploited number in the referenced water-in-oil study
Surface force	Dipole moment of water, u	2.651 D	[127]	Interpolated linearly between the values at 290 and 298 K for 21.5 ℃

	Relative permittivity of water, ε_r	79.5633	[117]	Interpolated linearly between the values at 20 and 25 ℃ for 21.5 ℃
	Relative permittivity of n-dodecane, ε_r	2.0287	[124]	Calculated using eq (3.2) and density of n-dodecane at 21.5 ℃
	Number density of water, N	$33.3576 \times 10^{27}\ \mathrm{m}^{-3}$	-	Calculated for this work from other values in this table; see Section 3.1 for more information
	Refractive index of water, n	1.3332	[128]	Interpolated linearly between the values at 20 and 25 ℃ for 21.5 ℃ at the wavelength of 589 nm
	Refractive index of n-dodecane, n	1.4215	[129,130]	Interpolated linearly between the values at 293.15 and 303.15 K for 21.5 ℃ at the wavelength of 589.3 nm
	Electronic absorption frequency in the ultraviolet (UV) region, ν_e	$3 \times 10^{15}\ \mathrm{s}^{-1}$	[13]	-
	Nonretarded Hamaker constant (water–n-dodecane–water), A_H	4.863×10^{-21} J	-	Calculated for this work from other values in this table using eq (A.26); see Sections A.6 and 3.1 for more information
AFM	Cantilever spring constant, K	350 mN/m	[11]	300–400 mN/m in the literature reference; assumed to be 350 mN/m in this work
	Initial apex separation of droplets, h_i	3 μm	[31]	-
	Drive velocity, V	1 μm/s	[31]	-

Table 3.2 Various input parameters used in modeling the interaction of water droplets in pure toluene at 20 ℃ for the theoretical fitting.

Type	Physical parameter	Value	Literature source	Notes
Fluid	Viscosity of toluene, μ	0.589 mPa s	[100]	Interpolated linearly between the values at 290 and 295 K for 20 ℃
	Interfacial tension, σ	34.73 mN/m	[123]	Calculated using eq (3.1) at 20 ℃
	Capillary number, Ca	1.70×10^{-8}	-	$\mathrm{Ca} = \mu V/\sigma$; calculated for this work from other values in this table
	Density of water, ρ_f	998.203 kg/m^3	[113]	Value at 20 ℃
	Molar mass of water, M	18.015 g/mol	[114,115]	-
	Radius of curvature of the droplets, R	125 μm	[39]	120–130 μm in the literature reference; assumed to be 125 μm in this work
	Droplet contact angle on the cantilever, θ_t	45°	[11,37]	Assumed in this work; the same as the exploited number in the referenced water-in-oil study
	Droplet contact angle on the substrate, θ_b	90°	[11,37]	Assumed in this work; the same as the exploited number in the referenced water-in-oil study
Surface force	Dipole moment of water, u	2.656 D	[127]	Interpolated linearly between the values at 290 and 298 K for 20 ℃

	Relative permittivity of water, ε_r	80.1030	[117]	Value at 20 ℃
	Relative permittivity of toluene, ε_r	2.3925	[109]	Interpolated linearly between the values at 15 and 25 ℃ for 20 ℃
	Number density of water, N	$33.3684 \times 10^{27}\ \mathrm{m}^{-3}$	-	Calculated for this work from other values in this table; see Section 3.1 for more information
	Refractive index of water, n	1.3334	[128]	Value at 20 ℃
	Refractive index of toluene, n	1.4971	[102]	Extrapolated linearly using the values at 25 and 30 ℃ for 20 ℃ at the wavelength of 589 nm
	Electronic absorption frequency in the ultraviolet (UV) region, ν_e	$3 \times 10^{15}\ \mathrm{s}^{-1}$	[13]	-
	Nonretarded Hamaker constant (water–toluene–water), A_H	$9.72 \times 10^{-21}\ \mathrm{J}$	[39]	Calculation made in the literature reference. Used to find the temperature of the system using values of the parameters in Lifshitz theory at 20 ℃ (values of the parameters at 20 ℃ result in this value)

AFM	Cantilever spring constant, K	$350\ \mathrm{mN/m}$	[11]	$300–400\ \mathrm{mN/m}$ in the literature reference; assumed to be $350\ \mathrm{mN/m}$ in this work
	Initial apex separation of droplets, h_i	$2.2\ \mu\mathrm{m}$	[39]	-
	Drive velocity, V	$1\ \mu\mathrm{m/s}$	[39]	-

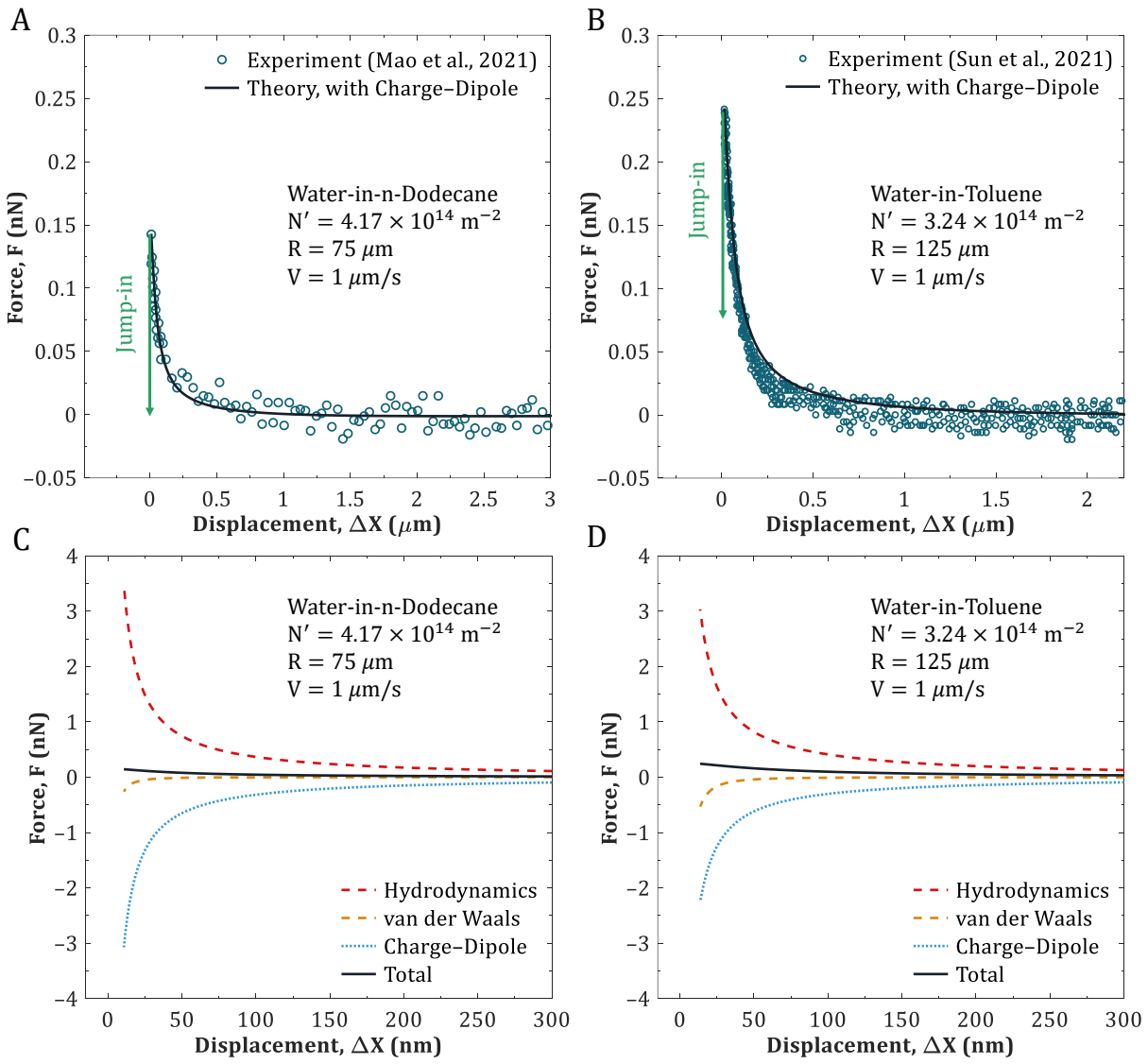

Figure 3.1 (A,B) Measured interaction forces (blue circles) and the theoretical fits from this work (black lines) for interaction of two water droplets suspended in pure n-dodecane (A) or pure toluene (B) vs piezo-displacement. The measured data points for the n-dodecane and toluene cases are from the experimental studies conducted by Mao et al.[31] and Sun et al.,[39] respectively. (C,D) Contributions of different forces to the fits shown with black solid lines during the interaction between two water droplets submerged in pure n-dodecane (C) or pure toluene (D).

force for two water droplets suspended in pure n-dodecane or pure toluene when the cantilever-adhered drop moves toward the second drop on the substrate at a drive velocity of $1\,\mu\mathrm{m/s}$. According to Figure 3.1, the so-called *jump-in* behavior occurs at very small nanometer

separations, and then, the drops coalesce. This is due to the fact that the repulsive EDL interaction is zero, and thus, attractive vdW and CD interactions induce the collision of the droplets. The jump-in is indicated by a green arrow in Figure 3.1.

In Figure 3.1A,B, the results of force fitting to the last point in the presence of CD interactions are shown. The blue circles represent the experimental measurements, and the black solid lines are the fittings to only the last point. We only report the results of fittings in the presence of CD interactions since in Chapter 2, we clearly proved that this additional attractive force (i.e., CD interaction) is required to sufficiently explain the behavior of water droplets during their interaction in a pure oil phase. According to Figure 3.1A,B, the experimental measurements show that the overall interaction force is repulsive (a positive value), and jump-in takes place when the separation between the droplets reaches an extremely small quantity, called critical separation h_{cr} (for more information see Chapter 2, Section 2.5). At this separation, the overall interaction forces are 0.14 and 0.24 nN for water-in-n-dodecane and water-in-toluene cases, respectively. At relatively large separations, the magnitude of hydrodynamic forces dominates over the attractive surface forces (which are almost negligible), and hence, the overall force is repulsive. However, when the separation between the interfaces of the droplets reaches the critical separation, attractive vdW and CD interactions grow strong and induce the jump-in and subsequent coalescence of the drops. Table 3.3 summarizes the important outputs from our studies for the n-dodecane and toluene cases. According to Table 3.3, the number of surface charges per unit area are 4.17×10^{14} and 3.24×10^{14} m^{-2} for n-dodecane and toluene cases, respectively. The magnitude of the fit value for the number of surface charges per unit area for each case is very close to the range previously reported for a water phase in contact with various oil phases, which is 10^{13}–10^{14} m^{-2}.[42–45] Also,

Table 3.3 Important outputs from our studies for the toluene and pentol cases

Method of fitting	Output parameter	Value	
		Water-in-n-dodecane	**Water-in-toluene**
Last point (smallest ΔX)	Jump-in force, F	0.14 nN	0.24 nN
	Number of surface charges per unit area, N'	4.17×10^{14} m^{-2}	3.24×10^{14} m^{-2}

our comparisons for the fit value of the number of surface charges per unit area for the water-in-toluene case found here (3.24×10^{14} m^{-2}) with the fit value for the other water-in-toluene case in Chapter 2 (8.51×10^{13} m^{-2}) show that the number of surface charges per unit area are very close, which lends strong support to our theory.

In Figure 3.1C,D, the contributions of various forces, including hydrodynamic, vdW, and CD forces, versus piezo-displacement for the interaction of water droplets in pure n-dodecane and pure toluene computed using the theory are shown. According to Figure 3.1C,D, hydrodynamic forces (red dashed line) are dominant at intermediate and larger separations because as the film thickness between the droplets decreases, the hydrodynamic pressure increases. As the droplets reach small separations, the magnitudes of attractive vdW (orange dashed line) and CD (blue dotted line) forces start to grow, and their sum becomes comparable to the magnitude of the hydrodynamic forces. When the sum of vdW and CD disjoining pressures (i.e., a negative value) prevails over the Laplace pressure of the drop, the thin film between the droplets becomes destabilized, and jump-in happens (i.e., at the critical separation or critical film thickness). In Figure 3.1C,D, this phenomenon can be observed by the sudden growths of vdW and CD forces near the jump-in point. Moreover, it should be noted that the CD force acts at much longer ranges in comparison with the vdW force, and that here, the magnitude of the CD force is larger than the vdW force before the jump-in point at all separations. Figure 3.1C,D sufficiently describes the role of the CD force and

sheds light on the fact that CD interaction is required to completely explain the actual physics of water droplet interaction within organic phases.

3.3 Conclusions

In this chapter, our theory of fixed-surface-charge–bulk-dipole interaction or charge–dipole (CD) interaction for short developed in Chapter 2 was applied to two additional water-in-oil systems where two water droplets interact within a pure n-dodecane or pure toluene. The water-in-n-dodecane system contains a different oil than those in Chapter 2 that was not analyzed before, and the water-in-toluene considers the interactions of larger droplet radii than those in Chapter 2. We again fitted for the number of charges per unit at the interface of water with pure oil medium using experimental force versus piezo-displacement data and compared the numbers of surface charges per unit area with the independent measurements and calculations of their value made in the literature. The results of comparisons show that the fit values for the number of surface charges per unit area for water-in-n-dodecane and water-in-toluene systems are very close to the range previously reported for a water phase in contact with various oil phases. The results presented in this chapter for two additional water-in-oil systems support our theory of charge–dipole interaction and adequately describe the underlying physics of water drop interactions suspended in pure oil phases.

Chapter 4

Elaboration on the Absence of Electric Double Layer and Electrostatic Interactions

In this chapter, the reasons why the electric double layer (EDL) interactions are absent between two water drops within a pure oil phase, and why the surface electrostatic interaction is zero are presented from a mathematical perspective and by comparisons with experimental data. In Chapter 2 and Chapter 3, we had assumed that the EDL interaction is zero because there are no ions dispersed inside the oil phase. We developed our theory in Chapter 2 based on the inclusion of a fixed-surface-charge–bulk-dipole interaction and conducted the simulations by considering this charge–dipole (CD) interaction and van der Waals (vdW) interactions as the only surface forces. The results of our fittings for a single parameter, the number of surface charges per unit area at the oil–water interface, had excellent agreement with the experimental data, and the obtained values were either within, or very close to, the range of the numbers of surface charges that we collected from independent measurements and calculations in the literature, which lent strong support to our

theory. However, one might ask whether there are electrostatic interactions that arise from the presence of these charges at the oil–water interface. Herein, we mathematically prove that EDL and electrostatic interactions between two water droplets with surface charges within a pure oil phase (i.e., nonpolar) are zero from a mathematical viewpoint and by comparisons with experimental data and provide a discussion on the role of EDL and electrostatic interactions in such water-in-oil systems.

4.1 Poisson–Boltzmann Theory for Electric Double Layer Interaction between Two Identically Charged Plates

Here, we utilize Poisson–Boltzmann theory[13,95,131,132] to mathematically prove that the disjoining pressure due to the EDL interaction between two water droplets within a pure oil phase (i.e., nonpolar) is zero. Figure 4.1 illustrates two parallel flat plates with identical surface charges separated by h immersed within a nonpolar phase (i.e., oil here). The charges are distributed in space by the arrangement of water and oil molecules at the interface but their distribution is assumed to occupy a thickness less than the size of one water molecule, i.e., on the order of 1 Å, or a few Å. Thus, the potential decays to zero over a region out from the interface shown by δ in Figure 4.1. Outside this region, no charges or ions are present inside the oil medium. As a result, the medium is nonconductive, and electric fields that these two identically charged surfaces create in between cancel out. In other words, the net electric field between the surfaces is zero. The surface potentials of the plates are ψ_0, and the potential between the plates in the medium outside the region δ is zero. This means that the electric potential decreases from ψ_0 on the surface of a plate to 0 very quickly in the region δ and remains constant at zero until it increases again to ψ_0 on the second plate (Figure 4.1).

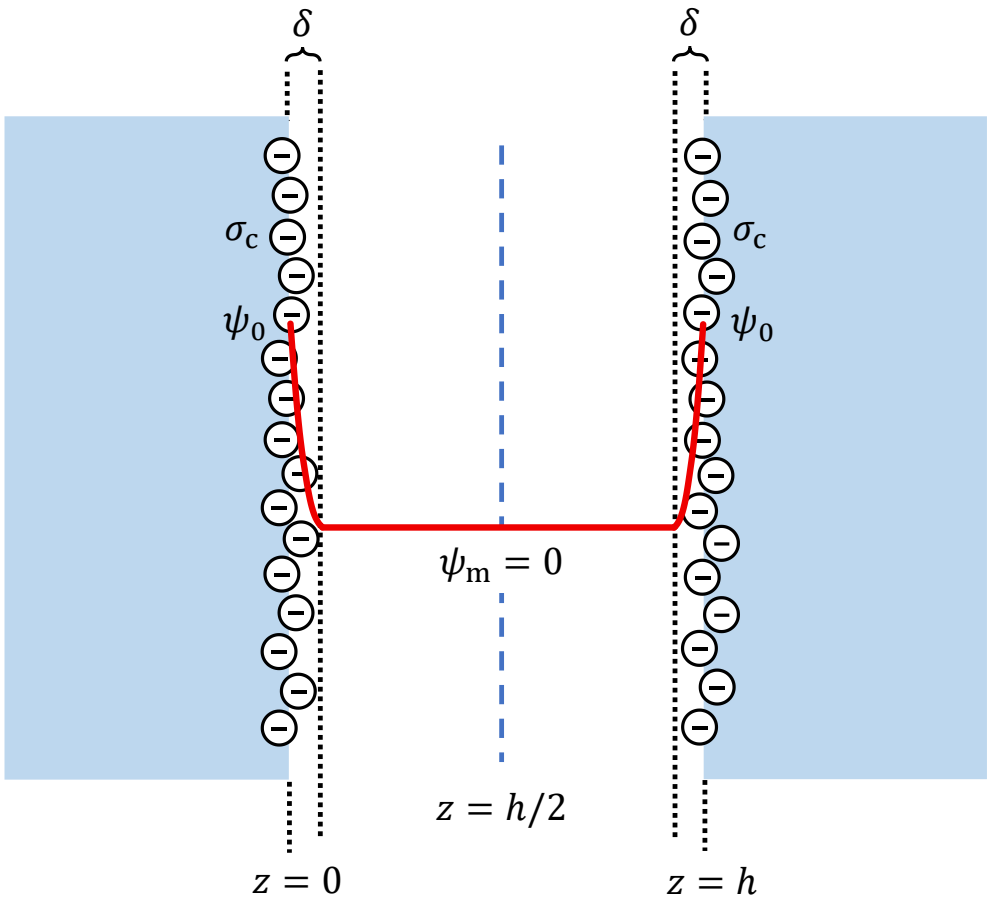

Figure 4.1 Two parallel flat plates with identical surface charges in contact with a nonpolar medium (e.g., oil). Surface charges are distributed at the surface and occupy the region δ. Electric potential decreases from ψ_0 at the surface of a plate to 0 very quickly in the region δ and remains constant at zero until it increases again to ψ_0 on the second plate. σ_c represents the surface charge density of the plates.

We use the symmetry of the system to derive the disjoining pressure due to the EDL interaction between the plates and show that its magnitude is zero. According to Figure 4.1, the potential at the midplane ψ_m is equal to zero because as mentioned earlier, there are no charges or ions within the nonpolar medium. The change in pressure Π at any point z on bringing two plates together from an infinite separation to a separation of h at constant temperature is given by[13,131,132]

$$\Pi_z(h) - \Pi_z(\infty) = -\frac{1}{2}\varepsilon_0\varepsilon_\mathrm{r}\left[\left(\frac{\mathrm{d}\psi}{\mathrm{d}z}\right)^2_{z(h)} - \left(\frac{\mathrm{d}\psi}{\mathrm{d}z}\right)^2_{z(\infty)}\right] + k_\mathrm{B}T[\rho_z(h) - \rho_z(\infty)] \tag{4.1}$$

where ε_0 and ε_r are the dielectric permittivity of the free space ($\varepsilon_0 = 8.854 \times 10^{-12}$ F/m) and relative permittivity of the medium, respectively; ψ is the electric potential; ρ_z is the concentration of charges (i.e., number density of charges); k_B is the Boltzmann constant ($k_\mathrm{B} = 1.3806 \times 10^{-23}$ J/K); and T is the absolute temperature. It is worth mentioning that the first two terms represent the contribution of the Maxwell stress tensor or the pressure that arises from the electric field and the third and fourth terms correspond to the osmotic pressure due to the charge concentration difference between the surfaces and midplane.[131,132] The effects of osmotic pressure is considered owing to the fact that the potential does not instantly become zero as we move away from the surface, and it happens over δ. For ρ_z we have

$$\rho_z = \rho_\mathrm{m} + \frac{\varepsilon_0\varepsilon_\mathrm{r}}{2k_\mathrm{B}T}\left(\frac{\mathrm{d}\psi}{\mathrm{d}z}\right)^2_z \tag{4.2}$$

in which the first term ρ_m is the charge concentration (i.e., number density of charges) at the midplane ($z = h/2$) and the second term represents the contribution of surface charges. Incorporating eq (4.2) into eq (4.1) yields

$$\begin{aligned}\Pi_z(h) - \Pi_z(\infty) &= -\frac{1}{2}\varepsilon_0\varepsilon_\mathrm{r}\left[\left(\frac{\mathrm{d}\psi}{\mathrm{d}z}\right)^2_{z(h)} - \left(\frac{\mathrm{d}\psi}{\mathrm{d}z}\right)^2_{z(\infty)}\right] \\ &+ k_\mathrm{B}T\left[\rho_\mathrm{m}(h) + \frac{\varepsilon_0\varepsilon_\mathrm{r}}{2k_\mathrm{B}T}\left(\frac{\mathrm{d}\psi}{\mathrm{d}z}\right)^2_{z(h)} - \rho_\mathrm{m}(\infty) - \frac{\varepsilon_0\varepsilon_\mathrm{r}}{2k_\mathrm{B}T}\left(\frac{\mathrm{d}\psi}{\mathrm{d}z}\right)^2_{z(\infty)}\right]\end{aligned} \tag{4.3}$$

where $\rho_{\mathrm{m}}(h)$ and $\rho_{\mathrm{m}}(\infty)$ are the midplane charge concentration when plates are positioned at separation $z = h$ and $z = \infty$ apart, respectively. Rearranging eq (4.3) and knowing that at $z = \infty$, the pressure $\Pi_z(\infty)$ is zero we have

$$\Pi_z(h) = k_{\mathrm{B}}T[\rho_{\mathrm{m}}(h) - \rho_{\mathrm{m}}(\infty)] \tag{4.4}$$

Equations (4.3) and (4.4) show that the electric field plays no role in the EDL disjoining pressure equation because the terms owing to the contribution of electrostatic pressure cancel out with the terms that are due to the osmotic pressure of charges in region δ in eq (4.3). Since there are no charges or ions inside the medium, the concentrations at the midplane ρ_{m} when the plates are separated by $z = h$ and $z = \infty$ are equal to zero ($\rho_{\mathrm{m}}(h) = \rho_{\mathrm{m}}(\infty) = 0$). As a result, the pressure due to the EDL becomes zero

$$\Pi_{\mathrm{EDL}} = \Pi_z(h) = 0 \tag{4.5}$$

Equations (4.1)–(4.5) evidently show that when two identical parallel plates with the same charges are immersed inside a nonpolar medium, the EDL interaction between the plates is zero. The results of the mathematical derivations in this section can be applied to two identical water droplets immersed within a surrounding oil phase (i.e., nonpolar).

4.2 Electrostatic Interaction between Two Identically Charged Plates

As mentioned previously, according to Figure 4.1, the decrease in potential from ψ_0 on the surface of a plate to zero inside the medium takes place in a region called δ, with a thickness on the order of 1 Å, or a few Å. In other words, the potential does not instantly become zero as we move away from the surface and it happens over δ. As a result, the effects of osmotic pressure must be considered in the calculation of the disjoining pressure due to the presence of surface charges.

However, here, we explore what would happen if we only considered the effects of electric field and use the electrostatic pressure due to the interactions of charges on two parallel flat plates with the same charge signs. The electrostatic pressure between two charged infinite parallel flat plates is given by[13,131,133]

$$\Pi_{\mathrm{CC}} = \frac{{\sigma_c}^2}{2\varepsilon_0\varepsilon_{\mathrm{r}}} \tag{4.6}$$

where σ_c is the surface charge density of the flat plates in $\mathrm{C/m^2}$ and ε_0 and ε_{r} are the dielectric permittivity of the free space ($\varepsilon_0 = 8.854 \times 10^{-12}$ F/m) and relative permittivity of the medium, respectively. Substituting $\sigma_c = QN'$, where Q is the elementary electric charge (i.e., equivalent to e) and N' is the number of surface charges per unit area into eq (4.6) yields

$$\Pi_{\mathrm{CC}} = \frac{Q^2 N'^2}{2\varepsilon_0\varepsilon_{\mathrm{r}}} \tag{4.7}$$

One might wonder if eq (4.7) should be used to calculate the electrostatic pressure between two water droplets submerged in a pure oil phase.

4.3 Results and Discussion

In Section 4.1, we showed that the EDL interaction between two water droplets within a pure oil phase (i.e., nonpolar) is zero (eq (4.5)). Hence, the disjoining pressure due to the EDL interaction Π_{EDL} is absent in the augmented Young–Laplace equation (eq (2.2)), which means that vdW and CD disjoining pressures are the only surface interactions between water droplets submerged in a surrounding pure oil medium. However, because one might wonder whether eq (4.7) should be used instead, the magnitude of the electrostatic disjoining pressure due to the surface-charge–surface-charge interaction shown by eq (4.7) needs to be examined.

Here, we show that the magnitude of the electrostatic disjoining pressure found by eq (4.7) is not in agreement with experiments, and thus, eq (4.7) cannot be correct for water droplets within a pure oil phase. We consider two different water-in-oil systems analyzed in Chapter 3, i.e., water-in-n-dodecane and water-in-toluene systems. According to eq (4.7), the electrostatic disjoining pressure is not a function of the distance between the droplets and thus is a constant value. In Table 4.1, the input parameters for eq (4.7) for water-in-n-dodecane and water-in-toluene systems are summarized. For the sake of understating the magnitude of the electrostatic disjoining pressure, we use the fit values of N' from Chapter 3. Also, as mentioned before, the electric charge Q is equivalent to the elementary charge e, having the magnitude of 1.602×10^{-19} C.

As shown in Table 4.1, the electrostatic disjoining pressures between two water drops in a pure oil phase for water-in-n-dodecane and water-in-toluene systems predicted by eq (4.7) are 124.23 and 63.59 Pa, respectively. These pressure values are constant at all separations and along all radial coordinates. Hence, according to Derjaguin's force approximation (eq (2.3)), this electrostatic disjoining pressure produces a huge repulsive force that does not allow the approach

Table 4.1 Input parameters for calculating the magnitude of electrostatic disjoining pressure between two water droplets immersed in either pure n-dodecane or toluene and the values of the disjoining pressure predicted by eq (4.7).

Water-in-oil system	**Number of surface charges, N'**	**Relative permittivity, ε_r**	**Electrostatic disjoining pressure, Π_{CC}**	**Electrostatic force, F_{cc}**
n-Dodecane	4.17×10^{14} m^{-2}	2.0287	124.23 Pa	56.90 nN
Toluene	3.24×10^{14} m^{-2}	2.3925	63.59 Pa	63.42 nN

of two droplets and prevents the coalescence of the drops, while the jump-in behavior and the subsequent coalescence of water drops have been observed in various pure oil phases in the experiments.[31,37–39] We calculated the electrostatic forces due to the presence of surface charges for water-in-n-dodecane and water-in-toluene systems to be 56.90 and 63.42 nN, respectively, using eq (2.3) for $r^*_{\max} = 12.5$ (a value that showed our computations are independent of the position of $r^*_{\max}$), which is used in our entire simulations in this thesis. For more information on the choice of $r^*_{\max}$, see the Appendix, Section A.2. According to Table 3.3, the values of the jump-in forces for water-in-n-dodecane and water-in-toluene systems are 0.14 and 0.24 nN, which are the maximum force values in Figure 3.1A,B. If we add the value of the constant repulsive electrostatic force found above in each case to the total interaction force calculated between the drops in each system (i.e., force curves in Figure 3.1A,B without the contributions of electrostatic forces), the force versus piezo-displacement results extensively deviate from experimental observations in the literature because the addition of electrostatic force shifts the total force curve to higher regions on force versus piezo-displacement graph.[31,37–39] The observations in the literature suggest that such huge repulsive force due to the electrostatic interaction is unrealistic and cannot be present between the drops in a pure oil medium. Our calculations using CD and vdW surface forces adequately describe the physics of water droplets interaction inside pure oil phases, and addition of electrostatic disjoining pressure to the force calculations causes a huge deviation of numerical force versus piezo-displacement curves from experimental data. As a result, the discussion made here proves the fact that neither EDL nor electrostatic forces are present between two water droplets immersed within a pure oil phase as suggested by experimental data.

4.4 Conclusions

In this chapter, we mathematically proved that electric double layer (EDL) interaction is absent between two water drops inside a pure oil phase, and that electrostatic interaction is zero. Although charges are present at the interface of water drops and pure organic phases, no EDL interaction is present. The pure oil acts as a nonconductive medium, and the electric fields that the surfaces of the charged water drops create in between are the same and thus cancel out. In other words, the net electric field between the surfaces of the droplets inside the oil phase is zero. Our derivations of the EDL disjoining pressure showed that the pressure that originates from the contribution of electric field cancels out with the terms related to osmotic pressure because of the presence of charges in the region δ near the surfaces. Moreover, our calculations of hypothetical pure electrostatic disjoining pressures for two water-in-n-dodecane and water-in-toluene systems showed that the magnitude of the resultant forces from these disjoining pressures are very large and unrealistic, whereas no such repulsive force has been detected in various water-in-oil experiments. Therefore, this electrostatic interaction cannot be present between two water droplets within a pure oil medium, and the contributions of osmotic pressure due to the presence of charges in the region δ must be taken into account. Our discussion in this chapter shows that neither EDL nor electrostatic forces are present between two water droplets immersed within a pure oil medium as suggested by experimental data.

Chapter 5

Conclusions

In this study, we developed a new theory based on fixed-surface-charge–bulk-dipole interaction, or charge–dipole (CD) interaction for short, to fully describe the unexplained behavior observed between water droplets immersed within a pure oil phase in various experiments. More specifically, Chapter 2 develops a fundamental understanding on the interactions of two water drops suspended in a pure oil medium. Our investigations indicated that most of these experimental studies lack a theoretical foundation and do not explain the physics of water drop interactions within oil media. Moreover, we realized that implementing the Stokes–Reynolds–Young–Laplace (SRYL) model with the conventional surface forces, i.e., only van der Waals (vdW) forces, does not explain the experimental observations in the literature, and there is a huge deviation between force calculations and the experimental force data; hence, a further relatively long-ranged attractive force is required to fully describe these experimental observations. In order to fill the research gap found in the literature, we hypothesized that the unexplained additional attractive

interaction between water droplets in oil pertains to the presence of charges at the interface of water drops with organic phases and proposed that fixed surface charges of one water droplet interact with dipoles within the bulk of another water droplet, i.e., a fixed-surface-charge–bulk-dipole interaction. It is worth mentioning that the same interaction exists between the surface charges of the second droplet and dipoles within the bulk of the first droplet. Since the SRYL model requires the disjoining pressure term, we developed an equation for the disjoining pressure of this CD interaction and incorporated it in the current SRYL model. This equation only requires a single fitting parameter, namely the number of charges per unit area at the interface of water with the pure oil phase. For further validation of our theory, we compared this fitting parameter with independent measurements and calculations of its value in the literature. In Chapter 2, we first validated our SRYL computational approach using an oil-in-water system where two micron-sized toluene drops interact within an aqueous solution. Then, two different oil-in-water systems, namely water-in-toluene and water-in-pentol systems in which two water droplets interact in a surrounding pure oil phase, were considered, and our theory was tested against their force versus piezo-displacement data. Next, we evaluated our new theory, the SRYL model with the added new CD interaction for water-in-oil systems. Our results showed that in the absence of the CD interactions, the numerical force versus piezo-displacement curves deviated from the experimental data, suggesting that an additional attractive force is required to fully explain the physics behind the interaction of the drops, and that vdW interaction is not the only surface force between the droplets. In contrast, when the CD interactions with number of surface charges per unit area as the only fitting parameter were included in the SRYL model, the numerical force curves followed the experimental data and showed an excellent agreement. The number of surface charges at the interface of water with various oil phases that we collected from independent measurements and

calculations in the literature were 10^{13}–10^{14} m^{-2}. Also, the fit values of the number of surface charges per unit area found for water-in-toluene and water-in-pentol systems were 8.51×10^{13} and 3.88×10^{13} m^{-2}. Hence, our calculations in Chapter 2 showed that the fit values of the number of surface charges per unit area so obtained for water-in-toluene and water-in-pentol systems lied within the range previously reported for a water phase in contact with various oil phases. The results and comparisons for the developed theory here adequately explain the experimental observations in the literature. Moreover, we studied the contributions of different forces to the total interaction force that indicated that the CD interactions act as relatively long-ranged forces compared to vdW forces, which can explain the observation that a relatively longed-ranged force is required to fully explain the physics of water drop interactions inside pure oil phases. We also investigated the droplet profiles during interaction at the jump-in and coalescence, the spatiotemporal film profile, the hydrodynamic and disjoining pressures profiles along the radial coordinate of the droplet, the shear stress applied to the interface of the droplets, and the droplets rim position at various instants of time. Finally, in an Appendix, some important details were provided, including the computational methods, the required properties, detailed steps for the calculations of the input parameters, and some important results.

Chapter 3 applied our theory of CD interaction developed in Chapter 2 to two additional water-in-oil systems in which two water drops interact within pure n-dodecane or pure toluene. The n-dodecane was a different oil phase than those investigated in Chapter 2, and the toluene was an oil phase that had already been studied in Chapter 2, but with larger water drops radii in Chapter 3 than those studied in Chapter 2. Again, we fitted for the number of surface charges per unit area as the only fitting parameter while calculating the total force curves for water-in-n-dodecane and water-in-toluene systems. Then, we compared the numbers of surface charges per unit area with

the independent measurements and calculations made in the literature. As mentioned earlier, the number of surface charges at the interface of water with various oil phases that we collected from independent measurements and calculations in the literature were 10^{13}–10^{14} m^{-2}. Our fittings for the number of surface charges per unit area for the two additional water-in-n-dodecane and water-in-toluene systems led to the values of 4.17×10^{14} and 3.24×10^{14} m^{-2}. The comparisons indicated that the numbers of surface charges per unit area found by fitting here were very close to the range previously reported for a water phase in contact with various oil phases. The contributions of various forces, including hydrodynamic, vdW, and CD interactions were also investigated, indicating that the CD interactions act as relatively long-ranged forces compared to the vdW forces. It is worth mentioning that the same conclusions were also made in our studies in Chapter 2. The results presented in Chapter 3 for two additional water-in-oil systems add further support that our theory of CD interaction when added to the SRYL model adequately describes the underlying physics of water drops interactions suspended in pure oil phases.

In Chapter 4, we presented the reasons why the electric double layer (EDL) interactions are absent between two water drops within a pure oil phase, and why the surface electrostatic interaction is zero from mathematical points of view and by comparing with experimental data. In Chapter 2 and Chapter 3, we assumed a priori that the EDL interaction is zero because there are no ions dispersed inside the oil phase. The results of our fittings for a single parameter, i.e., the number of surface charges per unit area at the oil–water interface, had excellent agreement with the experimental data, and the obtained values of the number of surface charges per unit area were either within, or very close to, the range of the numbers of surface charges that we collected from independent measurements and calculations in the literature. In Chapter 4, we mathematically proved that although charges are present at the interface of water droplets and pure oil phases, the

EDL interaction is absent. We used Poisson–Boltzmann theory to mathematically derive the EDL interaction between two identical parallel flat plates due to the presence of identical charges at their surfaces. The EDL disjoining pressure consisted of the terms that arise from the electric field and the terms corresponding to the osmotic pressure due to the charge concentration difference between the surfaces and midplane. Our derivations showed that the pressure that originates from the contribution of electric field cancels out with the terms related to osmotic pressure owing to the presence of charges in the region δ near the surface of the plates. Moreover, because there are no charges or ions inside the oil phase (since the oil phase is nonpolar), the osmotic pressure due to the presence of charges or ions inside the oil medium was zero. Therefore, the EDL interaction is zero between the water drops. To further investigate whether this was the correct interpretation, we also made calculations for the hypothetical pure electrostatic disjoining pressures between two water drops in the water-in-n-dodecane and water-in-toluene systems. The results showed that the magnitude of the resultant forces from these disjoining pressures are very large and unrealistic, whereas no such repulsive force has been detected in various water-in-oil experiments. Our discussion in Chapter 4 indicated that the contribution of electrostatic disjoining pressure cannot be considered alone since the charges in the small region δ also play an important role (i.e., osmotic pressure) in the EDL disjoining pressure calculations. In other words, the presence of these surface charges in the region δ cause the appearance of an osmotic pressure that cancels out the pressure because of the electrostatic pressure. As a result, the conclusion made in Chapter 4 that the EDL and surface electrostatic interactions between two water droplets suspended in a pure oil medium are zero as suggested by experimental data provides a strong support to our theory of CD interaction.

This thesis provides a strong theoretical foundation for the interactions of water droplets within organic systems and adequately explains the unexplored underlying physics behind such water-in-oil systems in various applications.

In summary, the main contributions of this work are as follows:

1) We hypothesized that the unexplained additional attractive interaction between water droplets in pure oil is related to the presence of charges at the interface of water drops with organic phases and proposed that fixed surface charges of one water droplet interact with dipoles within the bulk of another water droplet, i.e., a fixed-surface-charge–bulk-dipole interaction or charge–dipole (CD) interaction for short.
2) We derived a disjoining pressure equation for the CD interaction and incorporated the equation in the current Stokes–Reynolds–Young–Laplace (SRYL) model. Our resulting modified SRYL model requires only one fitting parameter, namely the number of charges per unit area at the interface of water droplets with a pure oil phase. The obtained fit values for four different water-in-oil systems, namely water-in-toluene with small droplet radii, water-in-pentol, water-in-n-dodecane, and water-in-toluene with relatively large droplet radii, were either within, or very close to, the range of the numbers of surface charges that we collected from independent measurements and calculations in the literature, which lent strong support to our theory.
3) Various useful input parameters and system properties, including dynamic viscosity, relative permittivity, and refractive index, were calculated for pentol (i.e., a mixture of pentane and toluene at a volume ratio of 1:1). Furthermore, we calculated the nonretarded Hamaker constant for the water–pentol–water system using Lifshitz theory since no values were provided in the literature.

4) Both in the presence and absence of CD interactions, spatiotemporal thicknesses of the thin oil film confined between two water droplets and also droplet profiles at nanometer separations were drawn and the droplet coalescence mechanisms were explained. These profiles extend our understanding of the mechanisms of thin oil film drainage between water droplets.
5) In the presence CD interactions, various pressure profiles, such as hydrodynamic, disjoining, and total dynamic pressures were drawn and analyzed along the droplet profile. The theoretical pressure profiles provide useful insight into the required disjoining pressure for observing the jump-in between the droplets.
6) We mathematically proved that neither electric double layer (EDL) nor surface electrostatic forces are present between two water droplets immersed within a pure oil medium and provided a discussion on our proof by comparisons with experimental data.

References

(1) He, L.; Lin, F.; Li, X.; Sui, H.; Xu, Z. Interfacial Sciences in Unconventional Petroleum Production: From Fundamentals to Applications. *Chem. Soc. Rev.* **2015**, *44*, 5446–5494.

(2) Zolfaghari, R.; Fakhru'l-Razi, A.; Abdullah, L. C.; Elnashaie, S. S. E. H.; Pendashteh, A. Demulsification Techniques of Water-in-Oil and Oil-in-Water Emulsions in Petroleum Industry. *Sep. Purif. Technol.* **2016**, *170*, 377–407.

(3) Wanzke, C.; Tena-Solsona, M.; Rieß, B.; Tebcharani, L.; Boekhoven, J. Active Droplets in a Hydrogel Release Drugs with a Constant and Tunable Rate. *Mater. Horizons* **2020**, *7*, 1397–1403.

(4) Danalou, S. Z.; Ding, X. F.; Zhu, N.; Emady, H. N.; Zhang, L. 4D Study of Liquid Binder Penetration Dynamics in Pharmaceutical Powders Using Synchrotron X-Ray Micro Computed Tomography. *Int. J. Pharm.* **2022**, *627*, 122192.

(5) Schroen, K.; Berton-Carabin, C.; Renard, D.; Marquis, M.; Boire, A.; Cochereau, R.; Amine, C.; Marze, S. Droplet Microfluidics for Food and Nutrition Applications. *Micromachines* **2021**, *12*, 863.

(6) Souza, E. M. C.; Ferreira, M. R. A.; Soares, L. A. L. Pickering Emulsions Stabilized by Zein Particles and Their Complexes and Possibilities of Use in the Food Industry: A Review. *Food Hydrocoll.* **2022**, *131*, 107781.

(7) Zhang, J.; Zeng, H. Intermolecular and Surface Interactions in Engineering Processes. *Engineering* **2021**, *7*, 63–83.

(8) Manica, R.; Xiang, B.; Bai, T.; Ashani, M. N.; Li, J.; Li, M.; Zhang, Z.; Liu, Q. Fundamentals of Secondary Process Aids in Oil Sands Extraction. *Can. J. Chem. Eng.* **2022**, *100*, 2682–2706.

(9) Yang, D.; Peng, X.; Peng, Q.; Wang, T.; Qiao, C.; Zhao, Z.; Gong, L.; Liu, Y.; Zhang, H.; Zeng, H. Probing the Interfacial Forces and Surface Interaction Mechanisms in Petroleum Production Processes. *Engineering* **2022**, *In press*.

(10) Lin, C. -Y; Slattery, J. C. Thinning of a Liquid Film as a Small Drop or Bubble Approaches a Fluid–Fluid Interface. *AIChE J.* **1982**, *28*, 786–792.

(11) Shi, C. Understanding Interaction Mechanism of Deformable Droplets in Oil Production, University of Alberta, 2016.

(12) Chen, J.-D. Effects of London—van Der Waals and Electric Double Layer Forces on the Thinning of a Dimpled Film between a Small Drop or Bubble and a Horizontal Solid Plane. *J. Colloid Interface Sci.* **1984**, *98*, 329–341.

(13) Jacob N. Israelachvili. *Intermolecular and Surface Forces*, 3rd ed.; Academic Press, 2011.

(14) Derjaguin, B. V.; Obuchov, E. Anomalien Dünner Flussigkeitsschichten. III. Ultramikrometrische Untersuchungen Der Solvathüllen Und Des "Elementaren" Quellungsaktes. *Acta Physicochim. U.R.S.S.* **1936**, *5*, 1–22.

(15) Derjaguin, B. V.; Churaev, N. V. Structural Component of Disjoining Pressure. *J. Colloid Interface Sci.* **1974**, *49*, 249–255.

(16) Manica, R.; Connor, J. N.; Carnie, S. L.; Horn, R. G.; Chan, D. Y. C. Dynamics of

Interactions Involving Deformable Drops: Hydrodynamic Dimpling under Attractive and Repulsive Electrical Double Layer Interactions. *Langmuir* **2007**, *23*, 626–637.

(17) Manica, R.; Connor, J. N.; Dagastine, R. R.; Carnie, S. L.; Horn, R. G.; Chan, D. Y. C. Hydrodynamic Forces Involving Deformable Interfaces at Nanometer Separations. *Phys. Fluids* **2008**, *20*, 032101.

(18) Ivanova, N. O.; Manica, R.; Liu, Q.; Xu, Z. Effect of Velocity, Solid Wettability, and Temperature on Drainage Dynamics of C5PeC11-in-Toluene Liquid Films between Silica and Water Droplet. *Energy & Fuels* **2020**, *34*, 6834–6843.

(19) Bai, T.; Manica, R.; Liu, B.; Klaseboer, E.; Xu, Z.; Liu, Q. Water Film Drainage between a Very Viscous Oil Drop and a Mica Surface. *Phys. Rev. Lett.* **2021**, *127*, 124503.

(20) Nespolo, S. A.; Chan, D. Y. C.; Grieser, F.; Hartley, P. G.; Stevens, G. W. Forces between a Rigid Probe Particle and a Liquid Interface: Comparison between Experiment and Theory. *Langmuir* **2003**, *19*, 2124–2133.

(21) Feng, L.; Manica, R.; Lu, Y.; Liu, B.; Lu, H.; Liu, Q. Effect of Sodium Citrate on Asphaltene Film at the Oil–Water Interface. *J. Colloid Interface Sci.* **2022**, *625*, 24–32.

(22) Reynolds, O. IV. On the Theory of Lubrication and Its Application to Mr. Beauchamp Tower's Experiments, Including an Experimental Determination of the Viscosity of Olive Oil. *Philos. Trans. R. Soc. London* **1886**, *177*, 157–234.

(23) Klaseboer, E.; Chevaillier, J. P.; Gourdon, C.; Masbernat, O. Film Drainage between Colliding Drops at Constant Approach Velocity: Experiments and Modeling. *J. Colloid*

Interface Sci. **2000**, *229*, 274–285.

(24) Young, T. III. An Essay on the Cohesion of Fluids. *Philos. Trans. R. Soc. London* **1805**, *95*, 65–87.

(25) Laplace, P. S. *Mécanique Céleste, Supplement to the Tenth Edition*; Courier, Paris, 1806.

(26) Gauss, C. F. *Principia Generalia Theoriae Figurae Fluidorum in Statu Aequilibrii*; Dieterichs, 1830.

(27) Stefan, J. Versuche Über Die Scheinbare Adhäsion. *sitzungsber, Abt.II, Osterr.Akad.Wiss., Math-Naturwiss.kl.* **1874**, *69*, 713–735.

(28) Ivanov, I. B.; Dimitrov, D. S.; Somasundaran, P.; Jain, R. K. Thinning of Films with Deformable Surfaces: Diffusion-Controlled Surfactant Transfer. *Chem. Eng. Sci.* **1985**, *40*, 137–150.

(29) Xie, L.; Shi, C.; Cui, X.; Zeng, H. Surface Forces and Interaction Mechanisms of Emulsion Drops and Gas Bubbles in Complex Fluids. *Langmuir* **2017**, *33*, 3911–3925.

(30) Manor, O.; Chau, T. T.; Stevens, G. W.; Chan, D. Y. C.; Grieser, F.; Dagastine, R. R. Polymeric Stabilized Emulsions: Steric Effects and Deformation in Soft Systems. *Langmuir* **2012**, *28*, 4599–4604.

(31) Mao, X.; Yang, D.; Xie, L.; Liu, Q.; Tang, T.; Zhang, H.; Zeng, H. Probing the Interactions between Pickering Emulsion Droplets Stabilized with PH-Responsive Nanoparticles. *J. Phys. Chem. B* **2021**, *125*, 7320–7331.

(32) Kuznicki, N. P.; Harbottle, D.; Masliyah, J.; Xu, Z. Dynamic Interactions between a Silica

Sphere and Deformable Interfaces in Organic Solvents Studied by Atomic Force Microscopy. *Langmuir* **2016**, *32*, 9797–9806.

(33) Pan, M.; Gong, L.; Xiang, L.; Yang, W.; Wang, W.; Zhang, L.; Hu, W.; Han, L.; Zeng, H. Modulating Surface Interactions for Regenerable Separation of Oil-in-Water Emulsions. *J. Memb. Sci.* **2021**, *625*, 119140.

(34) Shi, C.; Zhang, L.; Xie, L.; Lu, X.; Liu, Q.; Mantilla, C. A.; Van Den Berg, F. G. A.; Zeng, H. Interaction Mechanism of Oil-in-Water Emulsions with Asphaltenes Determined Using Droplet Probe AFM. *Langmuir* **2016**, *32*, 2302–2310.

(35) Shi, C.; Xie, L.; Zhang, L.; Lu, X.; Zeng, H. Probing the Interaction Mechanism between Oil Droplets with Asphaltenes and Solid Surfaces Using AFM. *J. Colloid Interface Sci.* **2019**, *558*, 173–181.

(36) Vakarelski, I. U.; Li, E. Q.; Thoroddsen, S. T. Soft Colloidal Probes for AFM Force Measurements between Water Droplets in Oil. *Colloids Surfaces A Physicochem. Eng. Asp.* **2014**, *462*, 259–263.

(37) Shi, C.; Zhang, L.; Xie, L.; Lu, X.; Liu, Q.; He, J.; Mantilla, C. A.; Van Den Berg, F. G. A.; Zeng, H. Surface Interaction of Water-in-Oil Emulsion Droplets with Interfacially Active Asphaltenes. *Langmuir* **2017**, *33*, 1265–1274.

(38) Xie, L.; Lu, Q.; Tan, X.; Liu, Q.; Tang, T.; Zeng, H. Interfacial Behavior and Interaction Mechanism of Pentol/Water Interface Stabilized with Asphaltenes. *J. Colloid Interface Sci.* **2019**, *553*, 341–349.

(39) Sun, X.; Yang, D.; Zhang, H.; Zeng, H.; Tang, T. Unraveling the Interaction of Water-in-Oil Emulsion Droplets via Molecular Simulations and Surface Force Measurements. *J. Phys. Chem. B* **2021**, *125*, 7556–7567.

(40) Tammet, H.; Hõrrak, U.; Kulmala, M. Negatively Charged Nanoparticles Produced by Splashing of Water. *Atmos. Chem. Phys.* **2009**, *9*, 357–367.

(41) Chaplin, M. Theory vs Experiment: What Is the Surface Charge of Water? *Water* **2009**, *1*, 1–28.

(42) Schoeler, A. M.; Josephides, D. N.; Sajjadi, S.; Lorenz, C. D.; Mesquida, P. Charge of Water Droplets in Non-Polar Oils. *J. Appl. Phys.* **2013**, *114*, 144903.

(43) Leunissen, M. E.; Zwanikken, J.; van Roij, R.; Chaikin, P. M.; van Blaaderen, A. Ion Partitioning at the Oil–Water Interface as a Source of Tunable Electrostatic Effects in Emulsions with Colloids. *Phys. Chem. Chem. Phys.* **2007**, *9*, 6405–6414.

(44) Zwanikken, J.; van Roij, R. Charged Colloidal Particles and Small Mobile Ions near the Oil-Water Interface: Destruction of Colloidal Double Layer and Ionic Charge Separation. *Phys. Rev. Lett.* **2007**, *99*, 178301.

(45) de Graaf, J.; Zwanikken, J.; Bier, M.; Baarsma, A.; Oloumi, Y.; Spelt, M.; van Roij, R. Spontaneous Charging and Crystallization of Water Droplets in Oil. *J. Chem. Phys.* **2008**, *129*, 194701.

(46) Baki, G.; Alexander, K. S. *Introduction to Cosmetic Formulation and Technology*; Wiley, 2015.

(47) Ashaolu, T. J. Nanoemulsions for Health, Food, and Cosmetics: A Review. *Environ. Chem. Lett.* **2021**, *19*, 3381–3395.

(48) Akiyama, Y.; Shinose, M.; Watanabe, H.; Yamada, S.; Kanda, Y. Cryoprotectant-Free Cryopreservation of Mammalian Cells by Superflash Freezing. *Proc. Natl. Acad. Sci. U. S. A.* **2019**, *116*, 7738–7743.

(49) Fan, X.; Dong, X.; Karacakol, A. C.; Xie, H.; Sitti, M. Reconfigurable Multifunctional Ferrofluid Droplet Robots. *Proc. Natl. Acad. Sci. U. S. A.* **2020**, *117*, 27916–27926.

(50) McClements, D. J. Edible Nanoemulsions: Fabrication, Properties, and Functional Performance. *Soft Matter* **2011**, *7*, 2297–2316.

(51) Tan, C.; McClements, D. J. Application of Advanced Emulsion Technology in the Food Industry: A Review and Critical Evaluation. *Foods* **2021**, *10*, 812.

(52) Wang, D.; Yang, D.; Huang, C.; Huang, Y.; Yang, D.; Zhang, H.; Liu, Q.; Tang, T.; Gamal El-Din, M.; Kemppi, T.; Perdicakis, B.; Zeng, H. Stabilization Mechanism and Chemical Demulsification of Water-in-Oil and Oil-in-Water Emulsions in Petroleum Industry: A Review. *Fuel* **2021**, *286*, 119390.

(53) Li, R.; Lou, Y.; Xu, Y.; Ma, G.; Liao, B. Q.; Shen, L.; Lin, H. Effects of Surface Morphology on Alginate Adhesion: Molecular Insights into Membrane Fouling Based on XDLVO and DFT Analysis. *Chemosphere* **2019**, *233*, 373–380.

(54) Riechers, B.; Maes, F.; Akoury, E.; Semin, B.; Gruner, P.; Baret, J. C. Surfactant Adsorption Kinetics in Microfluidics. *Proc. Natl. Acad. Sci. U. S. A.* **2016**, *113*, 11465–11470.

(55) Chan, D. Y. C.; Dagastine, R. R.; White, L. R. Forces between a Rigid Probe Particle and a Liquid Interface. I. The Repulsive Case. *J. Colloid Interface Sci.* **2001**, *236*, 141–154.

(56) Connor, J. N.; Horn, R. G. The Influence of Surface Forces on Thin Film Drainage between a Fluid Drop and a Flat Solid. *Faraday Discuss.* **2003**, *123*, 193–206.

(57) Kubochkin, N.; Gambaryan-Roisman, T. Surface Force-Mediated Dynamics of Droplets Spreading over Wetting Films. *Phys. Fluids* **2021**, *33*, 122107.

(58) Zhang, Y.; Xing, Y.; Ding, S.; Cao, Y.; Gui, X. New Method to Measure Interaction Force between Particle and Air Bubble/Water Droplet Using a Micro-Newton Mechanics Testing Instrument. *Powder Technol.* **2020**, *373*, 142–146.

(59) Butt, H.-J. A Technique for Measuring the Force between a Colloidal Particle in Water and a Bubble. *Colloid Interface Sci.* **1994**, *166*, 109–117.

(60) Vakarelski, I. U.; Manica, R.; Tang, X.; O'Shea, S. J.; Stevens, G. W.; Grieser, F.; Dagastine, R. R.; Chan, D. Y. C. Dynamic Interactions between Microbubbles in Water. *Proc. Natl. Acad. Sci. U. S. A.* **2010**, *107*, 11177–11182.

(61) Liu, B.; Manica, R.; Zhang, X.; Bussonnière, A.; Xu, Z.; Xie, G.; Liu, Q. Dynamic Interaction between a Millimeter-Sized Bubble and Surface Microbubbles in Water. *Langmuir* **2018**, *34*, 11667–11675.

(62) Liu, B.; Manica, R.; Liu, Q.; Klaseboer, E.; Xu, Z.; Xie, G. Coalescence of Bubbles with Mobile Interfaces in Water. *Phys. Rev. Lett.* **2019**, *122*, 194501.

(63) Shi, C.; Cui, X.; Xie, L.; Liu, Q.; Chan, D. Y. C.; Israelachvili, J. N.; Zeng, H. Measuring

Forces and Spatiotemporal Evolution of Thin Water Films between an Air Bubble and Solid Surfaces of Different Hydrophobicity. *ACS Nano* **2015**, *9*, 95–104.

(64) Zhang, X.; Tchoukov, P.; Manica, R.; Wang, L.; Liu, Q.; Xu, Z. Simultaneous Measurement of Dynamic Force and Spatial Thin Film Thickness between Deformable and Solid Surfaces by Integrated Thin Liquid Film Force Apparatus. *Soft Matter* **2016**, *12*, 9105–9114.

(65) Zhang, L.; Xie, L.; Shi, C.; Huang, J.; Liu, Q.; Zeng, H. Mechanistic Understanding of Asphaltene Surface Interactions in Aqueous Media. *Energy & Fuels* **2017**, *31*, 3348–3357.

(66) Aston, D. E.; Berg, J. C. Quantitative Analysis of Fluid Interface-Atomic Force Microscopy. *J. Colloid Interface Sci.* **2001**, *235*, 162–169.

(67) Bardos, D. C. Contact Angle Dependence of Solid Probe–Liquid Drop Forces in AFM Measurements. *Surf. Sci.* **2002**, *517*, 157–176.

(68) Horn, R. G.; Asadullah, M.; Connor, J. N. Thin Film Drainage: Hydrodynamic and Disjoining Pressures Determined from Experimental Measurements of the Shape of a Fluid Drop Approaching a Solid Wall. *Langmuir* **2006**, *22*, 2610–2619.

(69) Feng, L.; Manica, R.; Grundy, J. S.; Liu, Q. Unraveling Interaction Mechanisms between Molybdenite and a Dodecane Oil Droplet Using Atomic Force Microscopy. *Langmuir* **2019**, *35*, 6024–6031.

(70) Tabor, R. F.; Lockie, H.; Mair, D.; Manica, R.; Chan, D. Y. C.; Grieser, F.; Dagastine, R. R. Combined AFM–Confocal Microscopy of Oil Droplets: Absolute Separations and Forces in Nanofilms. *J. Phys. Chem. Lett.* **2011**, *2*, 961–965.

(71) Jamieson, E. J.; Fewkes, C. J.; Berry, J. D.; Dagastine, R. R. Forces between Oil Drops in Polymer-Surfactant Systems: Linking Direct Force Measurements to Microfluidic Observations. *J. Colloid Interface Sci.* **2019**, *544*, 130–143.

(72) Kuznicki, N. P.; Harbottle, D.; Masliyah, J. H.; Xu, Z. Probing Mechanical Properties of Water–Crude Oil Interfaces and Colloidal Interactions of Petroleum Emulsions Using Atomic Force Microscopy. *Energy & Fuels* **2017**, *31*, 3445–3453.

(73) Mettu, S.; Wu, C.; Dagastine, R. R. Dynamic Forces between Emulsified Water Drops Coated with Poly-Glycerol-Poly-Ricinoleate (PGPR) in Canola Oil. *J. Colloid Interface Sci.* **2018**, *517*, 166–175.

(74) Chan, D. Y. C.; Klaseboer, E.; Manica, R. Film Drainage and Coalescence between Deformable Drops and Bubbles. *Soft Matter* **2011**, *7*, 2235–2264.

(75) Tabor, R. F.; Wu, C.; Grieser, F.; Dagastine, R. R.; Chan, D. Y. C. Measurement of the Hydrophobic Force in a Soft Matter System. *J. Phys. Chem. Lett.* **2013**, *4*, 3872–3877.

(76) Dagastine, R. R.; Manica, R.; Carnie, S. L.; Chan, D. Y. C.; Geoffrey W. Stevens; Franz Grieser. Dynamic Forces between Two Deformable Oil Droplets in Water. *Science (80-.).* **2006**, *313*, 210–213.

(77) Carnie, S. L.; Chan, D. Y. C.; Lewis, C.; Manica, R.; Dagastine, R. R. Measurement of Dynamical Forces between Deformable Drops Using the Atomic Force Microscope. I. Theory. *Langmuir* **2005**, *21*, 2912–2922.

(78) Carnie, S. L.; Chan, D. Y. C.; Manica, R. Modelling Drop-Drop Interactions in an Atomic

Force Microscope. *ANZIAM J.* **2004**, *46*, C805–C819.

(79) Yang, D.; Xie, L.; Mao, X.; Gong, L.; Peng, X.; Peng, Q.; Wang, T.; Liu, Q.; Zeng, H.; Zhang, H. Probing Hydrophobic Interactions between Polymer Surfaces and Air Bubbles or Oil Droplets: Effects of Molecular Weight and Surfactants. *Langmuir* **2021**, *38*, 5257–5268.

(80) Manor, O.; Vakarelski, I. U.; Stevens, G. W.; Grieser, F.; Dagastine, R. R.; Chan, D. Y. C. Dynamic Forces between Bubbles and Surfaces and Hydrodynamic Boundary Conditions. *Langmuir* **2008**, *24*, 11533–11543.

(81) Xie, L.; Shi, C.; Wang, J.; Huang, J.; Lu, Q.; Liu, Q.; Zeng, H. Probing the Interaction between Air Bubble and Sphalerite Mineral Surface Using Atomic Force Microscope. *Langmuir* **2015**, *31*, 2438–2446.

(82) Lin, C. -Y; Slattery, J. C. Thinning of a Liquid Film as a Small Drop or Bubble Approaches a Solid Plane. *AIChE J.* **1982**, *28*, 147–156.

(83) Yiantsios, S. G.; Davis, R. H. On the Buoyancy-Driven Motion of a Drop towards a Rigid Surface or a Deformable Interface. *J. Fluid Mech.* **1990**, *217*, 547–573.

(84) Zhang, X.; Manica, R.; Tchoukov, P.; Liu, Q.; Xu, Z. Effect of Approach Velocity on Thin Liquid Film Drainage between an Air Bubble and a Flat Solid Surface. *J. Phys. Chem. C* **2017**, *121*, 5573–5584.

(85) Hamaker, H. C. The London—van Der Waals Attraction between Spherical Particles. *Physica* **1937**, *4*, 1058–1072.

(86) van Oss, C. J.; Chaudhury, M. K.; Good, R. J. Interfacial Lifshitz—van Der Waals and Polar Interactions in Macroscopic Systems. *Chem. Rev.* **1988**, *88*, 927–941.

(87) Lifshitz, E. M. The Theory of Molecular Attractive Forces between Solids. *Zhurnal Eksp. Teor. Fiz.* **1955**, *29*, 94–110.

(88) Lifshitz, E. M.; Hamermesh, M. The Theory of Molecular Attractive Forces between Solids. In *Perspectives in Theoretical Physics*; Pergamon Press plc, 1992; pp 329–349.

(89) Ohshima, H. Interaction of Colloidal Particles. In *Colloid and Interface Science in Pharmaceutical Research and Development*; Elsevier B.V., 2014; pp 1–28.

(90) Atkinson, K. E. *An Introduction to Numerical Analysis*, 2nd ed.; John Wiley & Sons, 1991.

(91) Jin, H.; Wang, W.; Liu, F.; Yu, Z.; Chang, H.; Li, K.; Gong, J. Roles of Interfacial Dynamics in the Interaction Behaviours between Deformable Oil Droplets. *Int. J. Multiph. Flow* **2017**, *94*, 44–52.

(92) Verwey, E. J. W. Theory of the Stability of Lyophobic Colloids. *J. Phys. Chem.* **1947**, *51*, 631–636.

(93) Verwey, E. J. W.; Overbeek, J. T. G.; Van Nes, K. *Theory of the Stability of Lyophobic Colloids*; Elsevier Publishing Company, 1948.

(94) Derjaguin, B.; Landau, L. Theory of the Stability of Strongly Charged Lyophobic Sols and of the Adhesion of Strongly Charged Particles in Solutions of Electrolytes. *Prog. Surf. Sci.* **1993**, *43*, 30–59.

(95) Butt, H.-J.; Kappl, M. *Surface and Interfacial Forces*, 2nd ed.; Wiley-VCH, 2018.

(96) Zhang, S.; Zhang, L.; Lu, X.; Shi, C.; Tang, T.; Wang, X.; Huang, Q.; Zeng, H. Adsorption Kinetics of Asphaltenes at Oil/Water Interface: Effects of Concentration and Temperature. *Fuel* **2018**, *212*, 387–394.

(97) Kestin, J.; Khalifa, H. E.; Correia, R. J. Tables of the Dynamic and Kinematic Viscosity of Aqueous NaCl Solutions in the Temperature Range 20–150 °C and the Pressure Range 0.1–35 MPa. *J. Phys. Chem. Ref. Data* **1981**, *10*, 71–88.

(98) Aleksandrov, A. A.; Dzhuraeva, E. V.; Utenkov, V. F. Viscosity of Aqueous Solutions of Sodium Chloride. *High Temp.* **2012**, *50*, 354–358.

(99) Krall, A. H.; Sengers, J. V.; Kestin, J. Viscosity of Liquid Toluene at Temperatures from 25 to 150°C and at Pressures up to 30 MPa. *J. Chem. Eng. Data* **1992**, *37*, 349–355.

(100) Santos, F. J. V.; Nieto de Castro, C. A.; Dymond, J. H.; Dalaouti, N. K.; Assael, M. J.; Nagashima, A. Standard Reference Data for the Viscosity of Toluene. *J. Phys. Chem. Ref. Data* **2006**, *35*, 1–8.

(101) Zahabi, A. Flocculation of Silica Particles in a Model Oil Solution: Effect of Adsorbed Asphaltene, University of Alberta, 2011.

(102) Katz, M.; Lobo, P. W.; Miñano, A. S.; Sólimo, H. Viscosities, Densities, and Refractive Indices of Binary Liquid Mixtures. *Can. J. Chem.* **1971**, *49*, 2605–2609.

(103) Asfour, A. F. A.; Dullien, F. A. L. Viscosities and Densities of Four Binary Liquid Systems at 25.00 °C. *J. Chem. Eng. Data* **1981**, *26*, 312–316.

(104) Aucejo, A.; Part, E.; Medina, P.; Sancho-Tello, M. Viscosity of Some N-Alkane/1-

Chloroalkane Binary Liquid Mixtures. *J. Chem. Eng. Data* **1986**, *31*, 143–145.

(105) Avgeri, S.; Assael, M. J.; Huber, M. L.; Perkins, R. A. Reference Correlation of the Viscosity of Toluene from the Triple Point to 675 K and up to 500 MPa. *J. Phys. Chem. Ref. Data* **2015**, *44*, 033101.

(106) PubChem. *National Center for Biotechnology Information (2022). PubChem Compound Summary for CID 1140, Toluene.* https://pubchem.ncbi.nlm.nih.gov/compound/Toluene (accessed 2022-04-13).

(107) PubChem. *National Center for Biotechnology Information (2022). PubChem Compound Summary for CID 8003, Pentane.* https://pubchem.ncbi.nlm.nih.gov/compound/Pentane (accessed 2022-04-13).

(108) Das, A.; Frenkel, M.; Gadalla, N.; Marsh, K.; Wilhoit, R. C. *TRC Thermodynamic Tables*; Thermodynamic Research Center, Texas A&M University: College Station, TX., 1994.

(109) Ritzoulis, G.; Papadopoulos, N.; Jannakoudakis, D. Densities, Viscosities, and Dielectric Constants of Acetonitrile + Toluene at 15, 25, and 35 °C. *J. Chem. Eng. Data* **1986**, *31*, 146–148.

(110) Gric, T.; Hess, O. Electromagnetics of Metamaterials. In *Phenomena of Optical Metamaterials, Micro and Nano Technologies*; 2019; pp 41–73.

(111) Sastry, N. V.; Valand, M. K. Densities, Viscosities, and Relative Permittivities for Pentane + 1-Alcohols (C1 to C12) at 298.15 K. *J. Chem. Eng. Data* **1998**, *43*, 152–157.

(112) D. A. G. Bruggeman. Berechnung Verschiedener Physikalischer Konstanten von

Heterogenen Substanzen. I. Dielektrizitätskonstanten Und Leitfähigkeiten Der Mischkörper Aus Isotropen Substanzen. *Ann. Phys.* **1935**, *416*, 636–664.

(113) Spieweck, F.; Bettin, H. Review: Solid and Liquid Density Determination / Übersicht: Bestimmung Der Dichte von Festkörpern Und Flüssigkeiten. *tm - Tech. Mess.* **1992**, *59*, 285–292.

(114) Cohen, E. R.; Cvitaš, T.; Frey, J. G.; Holmstrőm, B.; Kuchitzu, K.; Marquardt, R.; Mills, I.; Pavese, F.; Quack, M.; Stohner, J.; Strauss, H. L.; Takami, M.; Thor, A. J. *Quantities, Units and Symbols in Physical Chemistry*, 3rd ed.; International Union of Pure and Applied Chemistry, The Royal Society of Chemistry, 2007.

(115) PubChem. *National Center for Biotechnology Information (2022). PubChem Compound Summary for CID 962, Water.* https://pubchem.ncbi.nlm.nih.gov/compound/962 (accessed 2022-04-13).

(116) Hale, G. M.; Querry, M. R. Optical Constants of Water in the 200-Nm to 200-Mm Wavelength Region. *Appl. Opt.* **1973**, *12*, 555–563.

(117) Malmberg, C. G.; Maryott, A. A. Dielectric Constant of Water from 0° to 100°C. *J. Res. Natl. Inst. Stand. Technol.* **1956**, *56*, 1–8.

(118) Bai, C.; Kale, S.; Herzfeld, J. Chemistry with Semi-Classical Electrons: Reaction Trajectories Auto-Generated by Sub-Atomistic Force Fields. *Chem. Sci.* **2017**, *8*, 4203–4210.

(119) Bakó, I.; Csókás, D.; Mayer, I.; Pothoczki, S.; Pusztai, L. The Influence of Cations on the

Dipole Moments of Neighboring Polar Molecules. *Int. J. Quantum Chem.* **2021**, *122*, e26758.

(120) Gregory, J. K.; Clary, D. C.; Liu, K.; Brown, M. G.; Saykally, R. J. The Water Dipole Moment in Water Clusters. *Science (80-.).* **1997**, *275*, 814–817.

(121) Gao, Y.; Jung, S.; Pan, L. Interaction Forces between Water Droplets and Solid Surfaces across Air Films. *ACS Omega* **2019**, *4*, 16674–16682.

(122) Wang, Z.; Zhao, M.; Jiang, J.; Zhang, L.; Zhuang, S.; Zhao, Y.; Huang, Y.; Zheng, Y. Measurement of Interaction between Water Droplets and Curved Super-Hydrophobic Substrates in the Air. *AIP Adv.* **2018**, *8*, 045009.

(123) Teleszewski, T.; Gajewski, A. Measurement Approach of Interfacial Tension on Example of Water-Toluene. *Int. Commun. Heat Mass Transf.* **2020**, *118*, 104817.

(124) Sedrez, P. C.; Sanchez, C. J. N.; da Silva, M. J.; Barbosa, J. R. Dielectric Constant of Mixtures of Carbon Dioxide and N-Dodecane Between 283 K and 343 K. *Int. J. Thermophys.* **2020**, *41*, 1–16.

(125) Dymond, J. H.; Young, K. J. Transport Properties of Nonelectrolyte Liquid Mixtures—I. Viscosity Coefficients for n-Alkane Mixtures at Saturation Pressure from 283 to 378 K. *Int. J. Thermophys.* **1980**, *1*, 331–344.

(126) Zeppieri, S.; Rodríguez, J.; López De Ramos, A. L. Interfacial Tension of Alkane + Water Systems. *J. Chem. Eng. Data* **2001**, *46*, 1086–1088.

(127) Rick, S. W. Simulations of Ice and Liquid Water over a Range of Temperatures Using the

Fluctuating Charge Model. *J. Chem. Phys.* **2001**, *114*, 2276–2283.

(128) Bashkatov, A. N.; Genina, E. A. Water Refractive Index in Dependence on Temperature and Wavelength: A Simple Approximation. In *Proc. SPIE 5068, Saratov Fall Meeting 2002: Optical Technologies in Biophysics and Medicine IV*; 2003; pp 393–395.

(129) Paredes, M. L. L.; Reis, R. A.; Silva, A. A.; Santos, R. N. G.; Ribeiro, M. H. A.; Ayres, P. F. Thermodynamic Modeling and Experimental Speeds of Sound, Densities, and Refractive Indexes of (Tetralin + n-Dodecane). *J. Chem. Thermodyn.* **2012**, *54*, 377–384.

(130) Wohlfarth, C. Refractive Index of Dodecane. In *Optical Constants*; Springer Berlin Heidelberg: Berlin, Heidelberg, 2017; Vol. III, p 388.

(131) Donaldson, E. C.; Alam, W. Surface Forces. In *Wettability*; Elsevier, 2008; pp 57–119.

(132) Ohshima, H. Interaction of Electrical Bouble Layers. In *Electrical Phenomena at Interfaces*; Routledge, 2018; pp 57–85.

(133) Gallot-Lavallée, O. *Dielectric Materials and Electrostatics*; John Wiley & Sons, Inc.: Hoboken, NJ USA, 2013.

Appendix

Supplementary Information for Chapter 2

A.1 Initial Condition between Two Interacting Droplets

Here, we describe the different steps toward deriving the initial condition. The initial condition represents the initial vertical separation between the interfaces of the droplets at different locations on the interface, which requires a number of assumptions. Droplets possess an undeformed profile at large separation distances because of the zero film pressure, where they can maintain their spherical shape.[A1,A2]

First, we assume that the geometry of two drops with unperturbed harmonic mean radius of R can be approximated by considering two equal drops, each of radius R. Suppose two droplets each of radius R are positioned at an initial apex separation of h_{i} (i.e., $h(0,t_0)$) as shown in Figure A.1. Every location on the interface of one droplet has a distinct separation with the mirrored position on the interface of the second droplet. Parameter ϕ is the angle between the line that connects an arbitrary point on the interface (point B) to the center of the droplet (point O) and the vertical line that passes this center. Because the interaction between the droplets occurs in a relatively small region, i.e., the interaction zone or inner region,[A2] the magnitude of ϕ is small. Parameter r, i.e., the radial coordinate in the film, is the length of the line that connects point B to the vertical line AC that passes the center of the droplet O and is a small length according to the small magnitude of ϕ. Also, d is a small length on AC, which indicates the unknown portion of $h(r,t_0)$ and needs to be found based on other known parameters. From Figure A.1, the magnitude of $h(r,t_0)$ is the sum of $h(0,t_0)$ and $2d$,

$$h(r,t_0) = h(0,t_0) + 2d \tag{A.1}$$

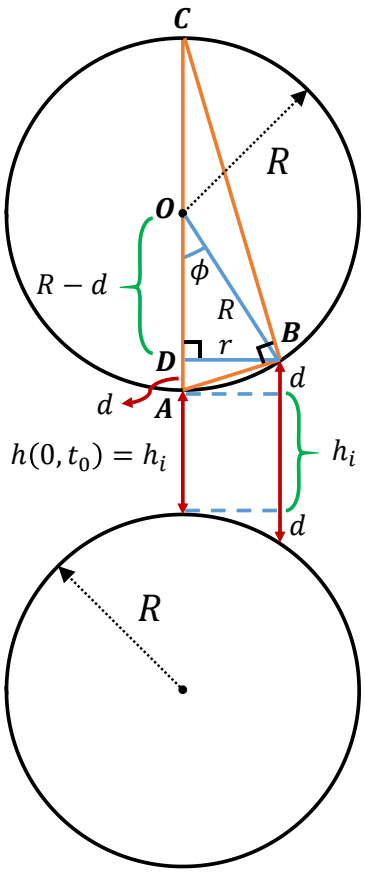

Figure A.1 Two interacting drops each of radius R (representing two drops with an unperturbed harmonic mean radius of R) positioned at a minimum separation of h_{i}.

For triangle BOD, one can write

$$R^2 = r^2 + (R-d)^2 \tag{A.2}$$

Rearranging eq (A.2) for r^2 results in

$$\begin{aligned} r^2 &= R^2 - (R-d)^2 \\ &= R^2 - (R^2 - 2Rd + d^2) \\ &= R^2 - R^2 + 2Rd - d^2 \end{aligned} \tag{A.3}$$

$$= 2Rd - d^2$$

Because d is a small value, its square d^2 is very small and can be neglected from eq (A.3). Thus, eq (A.3) can be approximated

$$r^2 \approx 2Rd \tag{A.4}$$

Rearranging eq (A.4) for d gives

$$d = \frac{r^2}{2R} \tag{A.5}$$

Substituting eq (A.5) into eq (A.1) leads to

$$h(r, t_0) = h(0, t_0) + \frac{r^2}{R} \tag{A.6}$$

Equation (A.6) can be used as the initial condition for the interaction between two droplets with a mean radius of R.

A.2 Computational Methods

In this section, the selected approach to solving the governing equations is described in detail. Non-dimensionalization of the equations simplifies the numerical simulation procedure and reduces the computation time; consequently, the equations are transformed to their dimensionless form. The capillary number $\mathrm{Ca} = \mu V/\sigma$ is exploited to describe the scaling factors for the non-dimensionalization process, where V is the drive velocity of the cantilever-adhered droplet, μ is the dynamic viscosity of the film, and σ is the interfacial tension. The scaling factors were first proposed by Klaseboer et al. and are written as[A1]

$$h_c = R\mathrm{Ca}^{1/2}$$

$$r_c = R\mathrm{Ca}^{1/4}$$

$$p_c = \sigma/R \tag{A.7}$$

$$t_c = \mu\mathrm{Ca}^{-1/2}/p_c$$

The dimensionless forms of the parameters (with asterisks) are given by $h^* = h/h_c$, $r^* = r/r_c$, $p^* = p/p_c$, and $t^* = t/t_c$, which links them to the original dimensional variables. Substituting the relationships in eq (A.7) in the dimensionless forms of the parameters (h^*, r^*, p^*, and t^*) gives

$$h = h^* R\mathrm{Ca}^{1/2}$$

$$r = r^* R\mathrm{Ca}^{1/4}$$

$$p = p^* \sigma/R \tag{A.8}$$

$$t = t^* \mu\mathrm{Ca}^{-1/2}/\sigma$$

The dimensional variables in eqs (2.1)–(2.13) and eq (2.27) from Chapter 2 are replaced by the relations shown in eq (A.8) to establish their dimensionless form. This process for eqs (2.1)–(2.3) from Chapter 2 yields

$$\frac{\partial h^*}{\partial t^*} = \frac{1}{12r^*}\frac{\partial}{\partial r^*}\left(r^* h^{*3}\frac{\partial p^*}{\partial r^*}\right) \tag{A.9}$$

$$\frac{1}{2r^*}\frac{\partial}{\partial r^*}\left(r^*\frac{\partial h^*}{\partial r^*}\right) = 2 - p^* - \Pi^* \tag{A.10}$$

$$F^*(t^*) = 2\pi\int_0^\infty \left[p^*(r^*, t^*) + \Pi^*\left(h^*(r^*, t^*)\right)\right] r^* \mathrm{d}r^* = 2\pi G^*(t^*) \tag{A.11}$$

where $F^* = F\mathrm{Ca}^{-1/2}/R\sigma$ and $G^* = G\mathrm{Ca}^{-1/2}/R$. The dimensionless forms of the initial and boundary conditions in eqs (2.4)–(2.6) and eq (2.8) from Chapter 2 are

$$h^*(r^*, t_0^*) = \frac{h^*(0, t_0^*)\mathrm{Ca}^{-1/2}}{R} + r^{*2} \tag{A.12}$$

$$\left.\frac{\partial h^*}{\partial r^*}\right|_{r^*=0} = \left.\frac{\partial p^*}{\partial r^*}\right|_{r^*=0} = 0 \tag{A.13}$$

$$\frac{\partial p^*}{\partial r^*} + \frac{4p^*}{r^*} = 0 \qquad \text{at } r^* = r_{\max}^* \tag{A.14}$$

$$\frac{\partial h^*(r_{\max}^*, t^*)}{\partial t^*} + \alpha \frac{\mathrm{d}G^*(t^*)}{\mathrm{d}t^*} = \pm 1 \tag{A.15}$$

where

$$\alpha = -\frac{2\pi\sigma}{K} + 2\ln\left(\frac{r_{\max}^* R\mathrm{Ca}^{1/4}}{2\sqrt{R_\mathrm{t}R_\mathrm{b}}}\right) + B(\theta_\mathrm{t}) + B(\theta_\mathrm{b}) \tag{A.16}$$

In eq (A.15), the negative and positive values of unity are associated with the approach and retraction of the upper droplet, respectively. For shear stress at the droplet–liquid interface, in eq (2.11) from Chapter 2 we have

$$\tau_\mathrm{f}^* = -\frac{h^*}{2}\frac{\partial p^*}{\partial r^*} \tag{A.17}$$

where $\tau_\mathrm{f}^* = \tau_\mathrm{f}\, 2R\mathrm{Ca}^{-1/4}/\sigma$. Similarly, the disjoining pressures in eqs (2.12), (2.13), and (2.27) from Chapter 2 are non-dimensionalized to give

$$\Pi_\mathrm{vdW}^* = -\frac{A_\mathrm{H}\mathrm{Ca}^{-3/2}}{6\pi R^2 \sigma {h^*}^3} \tag{A.18}$$

$$\Pi_\mathrm{EDL}^* = \frac{64 k_\mathrm{B} T \rho_\infty R}{\sigma} \tanh^2\left(\frac{ze\psi_0}{4k_\mathrm{B}T}\right) \exp\left(-\kappa R\mathrm{Ca}^{1/2} h^*\right) \tag{A.19}$$

$$\Pi^*_{\mathrm{CD}} = -\frac{2\pi N N' \lambda_{\mathrm{CD}}}{R\sigma \mathrm{Ca} h^{*2}} \tag{A.20}$$

where $\Pi^* = R\Pi/\sigma$. In order to solve eqs (A.9)–(A.20), the method of lines is utilized to discretize eqs (A.9) and (A.10) with the central differencing scheme in r^* for the points $j = 2, 3, \ldots, N-1$. Also, forward differencing applies to the boundary conditions in eq (A.13) for the initial point $j = 1$ and backward differencing to boundary conditions in eqs (A.14) and (A.15) for the last point $j = N$. These difference approximations of the derivatives in r^* are second-order (i.e., truncation error of order 2 ($O(r^{*2})$)), increasing the precision of the numerical solution. Simpson's rule is applied to eq (A.11) to approximate the integral value.[A3] All these procedures convert the initial system of partial differential equations (PDEs) to differential-algebraic equations (DAEs) of index 1.

Conversion of PDEs to DAEs of index 1 generates a linearly semi-explicit problem here, which needs to be solved for $\mathrm{d}h^*/\mathrm{d}t^*$, $\mathrm{d}G^*/\mathrm{d}t^*$, and $\mathrm{d}p^*/\mathrm{d}t^*$. In other words, the equations need to be written in the form $\dot{y} = \mathrm{d}y/\mathrm{d}t = k(t, y, z)$, where time-dependent variables $\dot{h}^*$, $\dot{G}^*$, and $\dot{p}^*$ are positioned on one side of the equation and the terms from discretization on the other side (for equations related to p^*, $\mathrm{d}p^*/\mathrm{d}t^*$ is zero). Furthermore, the mass matrix needs to be produced based on these equations. As a result, using this method, the final system of equations becomes

$$\begin{pmatrix} 0 & 0 & \cdots & \cdots & \cdots & \cdots & \cdots & 0 \\ 0 & 1 & 0 & \cdots & \cdots & \cdots & 0 & 0 \\ \vdots & \ddots & \ddots & \vdots & \vdots & \vdots & \vdots & \vdots \\ 0 & 0 & \ddots & 1 & \alpha & 0 & \cdots & 0 \\ 0 & 0 & \ddots & \ddots & 0 & 0 & \cdots & 0 \\ 0 & 0 & \ddots & \ddots & 0 & 0 & 0 & 0 \\ \vdots & \vdots & \ddots & \ddots & \ddots & \vdots & \ddots & \vdots \\ 0 & 0 & 0 & 0 & 0 & 0 & \cdots & 0 \end{pmatrix} \begin{pmatrix} \dot{h}^*_1 \\ \dot{h}^*_2 \\ \vdots \\ \dot{h}^*_{\mathrm{N}} \\ \dot{G}^* \\ \dot{p}^*_1 \\ \vdots \\ \dot{p}^*_{\mathrm{N}} \end{pmatrix} = \begin{pmatrix} H^*_1 \\ H^*_2 \\ \vdots \\ \pm 1 \\ G^* - I \\ P^*_1 \\ \vdots \\ P^*_{\mathrm{N}} \end{pmatrix} \tag{A.21}$$

in matrix form where H_i^* and P_i^* are the contributions from the discretization of eqs (A.9) and (A.10), respectively, and α is a constant value described in eq (A.16). Moreover, using Simpson's rule, I which is the integral in eq (A.11) can be written as $\sum_{j=1}^{N} \omega_j \left(p_j^* + \Pi_j^*\right) r_j$, where ω_j is the coefficient of each node in Simpson's rule. In this study, composite Simpson's rule is employed to evaluate the value of I.

In order to solve the DAEs outlined in eq (A.21), the grid in r^* is chosen to be uniform with $\Delta r^* = 0.04$ and $r_{\max}^* = 12.5$. The choice of $r_{\max}^*$ in our study satisfies the condition $r_{\max} < R$ required for employing the SRYL model.[A4] Furthermore, the quantity of $r_{\max}^*$ was closely examined to guarantee that the results, such as the values of forces, are independent of its magnitude. The overall interaction forces, including hydrodynamic and surface forces between two droplets, have shown to vary rapidly at small distances. This behavior is called stiffness, and as a result, the selected approach to solving the DAEs in eq (A.21) must consider very small step sizes in time t^* when the numerical approach tends to become unstable. MATLAB® provides a variety of ODE solvers for stiff differential equations and DEAs. Among them, ode15s, which demonstrates a great ability to solve eq (A.21), was implemented in our study.

A.3 Values of Parameters Used in Oil-in-Water Simulations

In this section, the experimental input parameters and system properties required to calculate the interaction between two pure toluene droplets within an aqueous solution are summarized in Table A.1.

Table A.1 Various input parameters used in modeling the interaction of pure toluene droplets in the aqueous solution for validating the numerical approach.

Type	Physical parameter	Value	Literature source	Notes
Fluid	Viscosity of the aqueous solution, μ	0.97 mPa s	A5,A6	Value at 25 ℃
	Interfacial tension, σ	35.5 mN/m	A7,A8	Reported by the literature references
	Radius of curvature of the droplets, R	89 μm	A7,A8	-
	Droplet contact angle on the cantilever, θ_{t}	90°	A7	-
	Droplet contact angle on the substrate, θ_{b}	50°	A9	Assumed in this work; same as the exploited number in the referenced oil-in-water study
Surface force	Electrolyte concentration (i.e., NaCl), [NaCl]	1 mM	A7,A8	-
	Solution pH	5.6	A7,A8	-
	Valency, Z	1	-	Deduced for this work from the valency of Na^{+} and Cl^{-} ions in an NaCl solution
	Number density of ions, ρ_{∞}	6.037×10^{23} m^{-3}	-	Calculated for this work from other values in this table; see Section 2.4 for more information
	Nonretarded Hamaker constant (toluene–water–toluene), A_{H}	9.80×10^{-21} J	A7,A8	Calculation made in the literature references
	Debye length, κ^{-1}	9.6 nm	A7,A8	Calculation made in the literature references
AFM	Cantilever spring constant, K	350 mN/m	A7	300–400 mN/m in the literature reference; assumed to be 350 mN/m in this work
	Drive velocity, V	1 μm/s	A7,A8	-

A.4 Calculation of the Viscosity of Pentol

The dynamic viscosity of a mixture, such as pentol, can be found using mixing rules. Here, we implement a simple mixing rule in which densities and molar masses of both toluene and pentane are utilized to calculate their mole fractions and then find the dynamic viscosity of pentol using these mole fractions and the dynamic viscosities of toluene and pentane. First, the volume of each liquid (with a volume ratio of 1:1) is converted to mass using their densities ($m = \rho_f \forall$, where m is the mass, ρ_f is the density, and $\forall$ is the volume). Then, the number of moles of each liquid is found using their masses and molar masses ($mol = m/M$, where m and M are the mass and molar mass of each component, respectively). As a result, the mole fraction of each component x can be simply computed using their numbers of moles

$$x_1 = mol_1/(mol_1 + mol_2) \tag{A.22}$$

$$x_2 = mol_2/(mol_1 + mol_2) \tag{A.23}$$

Finally, the dynamic viscosity of pentol can be found using

$$\mu_{\text{pentol}} = x_{\text{toluene}}\mu_{\text{toluene}} + x_{\text{pentane}}\mu_{\text{pentane}} \tag{A.24}$$

where μ is the dynamic viscosity and x is the mole fraction. The densities of toluene and pentane are $862.1\ \text{kg/m}^3$ [A10–A12] and $621\ \text{kg/m}^3$,[A12] respectively at $25\ ℃$. Also, their molar masses are $92.14\ \text{g/mol}$ [A13,A14] and $72.15\ \text{g/mol}$,[A15] respectively. After finding the masses of toluene and pentane, they can be used with their molar masses to calculate the numbers of moles. In this study, using the calculated number of moles for each component, the mole fractions from eqs (A.22) and (A.23) are found to be 0.5209 and 0.4791 for toluene and pentane, respectively. The dynamic viscosities of toluene and pentane are $0.56\ \text{mPa s}$ [A16,A17] and $0.212\ \text{mPa s}$,[A18] respectively at

25 ℃. From eq (A.24) using the dynamic viscosities and computed mole fractions of toluene and pentane, the dynamic viscosity of pentol is found to be 0.393 mPa s, which is very close to the reported value of 0.39 mPa s [A19] used in Chapter 2.

A.5 Calculation of the Permittivity of Pentol

The Bruggeman mixing rule can be utilized to calculate the effective permittivity of a mixture consisting of two components.[A20,A21] The mixing occurs homogenously and the components are not distinguishable in the solution after mixing. The basic form of the Bruggeman mixing rule can be written as[A20,A21]

$$(1-f)\frac{\varepsilon_{\mathrm{e}}-\varepsilon_{\mathrm{eff}}}{\varepsilon_{\mathrm{e}}+2\varepsilon_{\mathrm{eff}}}+f\frac{\varepsilon_{\mathrm{i}}-\varepsilon_{\mathrm{eff}}}{\varepsilon_{\mathrm{i}}+2\varepsilon_{\mathrm{eff}}}=0 \qquad \text{(A.25)}$$

where f is the volume fraction of one component, $\varepsilon_{\mathrm{eff}}$ is the permittivity of the mixture, and ε_{e} and ε_{i} are the permittivities of the two components. The relative permittivities, ε_{r}, of toluene and pentane are 2.38 [A22] and 1.82 [A23] at 25 ℃, respectively. In this study, pentol is a 1:1 mixture of toluene and pentane by volume; hence, the volume fraction f is 0.5. Substituting these numbers into eq (A.25) gives the value of 2.09 for the relative permittivity of pentol.

A.6 Calculation of the Water–Pentol–Water Hamaker Constant

The Hamaker constant for a particular system can be calculated by Lifshitz theory.[A24,A25] The non-retarded Hamaker constant (only the first two terms of an infinite series) for two macroscopic phases 1 and 2 interacting across medium 3 is given by[A26]

$$A_{132} = \frac{3}{4}k_{\mathrm{B}}T\left(\frac{\varepsilon_1 - \varepsilon_3}{\varepsilon_1 + \varepsilon_3}\right)\left(\frac{\varepsilon_2 - \varepsilon_3}{\varepsilon_2 + \varepsilon_3}\right) + \frac{3v_{\mathrm{e}}(2\pi\hbar)}{8\sqrt{2}}\frac{(n_1^2 - n_3^2)(n_2^2 - n_3^2)}{(n_1^2 + n_3^2)^{1/2}(n_2^2 + n_3^2)^{1/2}[(n_1^2 + n_3^2)^{1/2} + (n_2^2 + n_3^2)^{1/2}]} \quad \text{(A.26)}$$

where ε_1, ε_2, and ε_3 are the permittivities of the three components, n_1, n_2, and n_3 are the refractive indices of the three components, k_{B} is the Boltzmann constant ($k_{\mathrm{B}} = 1.3806 \times 10^{-23}$ J/K), T is the absolute temperature, $\hbar$ is the reduced Planck's constant ($\hbar = 6.626/2\pi \times 10^{-34}$ J s), v_{e} is the main electronic absorption frequency in the ultraviolet (UV) region, which is reported to be approximately 3×10^{15} s^{-1}.[A26]

In order to calculate the nonretarded Hamaker constant for water–pentol–water, the relative permittivities and refractive indices of both pentol and water are required. However, the refractive index of pentol is unknown and can be calculated via mixing rules. Here, we implement a simple mixing rule like the one that was described in Section A.4 in which density and molar masses of both toluene and pentane are utilized to calculate their mole fractions and then find the refractive index of pentol using these mole fractions and the refractive indices of toluene and pentane. The refractive index of pentol can be written as

$$n_{\mathrm{pentol}} = x_{\mathrm{toluene}}n_{\mathrm{toluene}} + x_{\mathrm{pentane}}n_{\mathrm{pentane}} \quad \text{(A.27)}$$

where n is the refractive index and x is the mole fraction. The refractive indices of toluene and pentane are 1.4943 [A10] and 1.3547,[A12] respectively at 25 ℃. From eq (A.27) with the values of $x_{\mathrm{toluene}} = 0.5209$ and $x_{\mathrm{pentane}} = 0.4791$ computed in Section A.4, the refractive index of pentol is calculated to be 1.4274. Furthermore, the refractive index of water is 1.3325 at 25 ℃.[A27] From Section A.5, the relative permittivity of pentol is calculated to be 2.09. Also, the relative permittivity of water is 78.3 at 25 ℃.[A28] Substituting the relative permittivities and refractive

indices of pentol and water into eq (A.26) leads to a value of 5.20×10^{-21} J for the Hamaker constant of water–pentol–water system. For other combinations of systems, the same procedure can be implemented.

A.7 Values of Parameter Used in Water-in-Oil Simulations

The experimental input parameters and system properties for the interaction of two water droplets inside pure toluene and pentol (1:1 mixture of toluene and pentane by volume) can be found in Table A.2 and Figure A.3, respectively.

A.8 Sensitivity Analysis on the Effect of Droplet Size on the Overall Interaction Force between Water Droplets Suspended in Pentol

In Figure A.2, the results of force prediction in the absence of CD interactions (orange dashed line) and force fitting to only the last point in the presence of CD interactions (black solid line) are compared for two droplets with radii of 50 μm interacting in pure pentol. Fifty micrometers is the outside value given in the literature used, whereas, in the main text a value of 60 μm that is in the middle of the literature range was used. In the absence of the CD force, the attractive vdW force cannot alone reduce the repulsive dominance of the long-ranged hydrodynamic effects, and consequently, the jump-in occurs at a larger interaction force, which is 0.22 nN. The results indicate that in the absence of the CD force, the overall force curve deviates from the experiments, and there must still be another attractive surface force present, leading to the behavior observed in the experiments. On the other hand, when the CD interactions with a number of surface charges per unit area consistent with known number of surface charges in the literature are incorporated

Table A.2 Various input parameters used in modeling the interaction of water droplets in toluene for the theoretical fitting

Type	Physical parameter	Value	Literature source	Notes
Fluid	Viscosity of toluene, μ	0.56 mPa s	A16,A17	Around 0.55–0.56 mPa s at 25 ℃ in the literature; taken as 0.56 mPa s in this work
	Interfacial tension, σ	35.5 mN/m	A7,A8	Reported by the literature references
	Capillary number, Ca	1.58×10^{-8}	-	$\mathrm{Ca} = \mu V/\sigma$; calculated for this work from other values in this table
	Density of water, ρ_f	997.04 kg/m^3	A29	Value at 25 ℃
	Molar mass of water, M	18.015 g/mol	A30,A31	-
	Radius of curvature of the droplets, R	60 μm	A7,A32	-
	Droplet contact angle on the cantilever, θ_t	45°	A7,A32	-
	Droplet contact angle on the substrate, θ_b	90°	A7,A32	-
Surface force	Dipole moment of water, u	2.6 D	A33–A35	In a recent study, it was reported to be 2.6 D.[A34] Some references propose a range; the overall range from the references is 2.4–2.9 D
	Relative permittivity of toluene, ε_r	2.38	A22	Value at 25 ℃
	Number density of water, N	33.3291×10^{27} m^{-3}	-	Calculated for this work from other values in this table; see Section 2.4 for more information

	Nonretarded Hamaker constant (water–toluene–water), A_{H}	9.72×10^{-21} J	A7,A32	Calculation made in the literature references
AFM	Cantilever spring constant, K	350 mN/m	A7	300–400 mN/m in the literature reference; assumed to be 350 mN/m in this work
	Initial apex separation of droplets, h_{i}	1 μm	A7,A32	-
	Drive velocity, V	1 μm/s	A7,A32	-

Table A.3 Various input parameters used in modeling the interaction of water droplets in pure pentol for the theoretical fitting

Type	Physical parameter	Value	Literature source	Notes
Fluid	Viscosity of pentol, μ	0.39 mPa s	A19	Reported by the literature reference; see Section A.4 for more information
	Interfacial tension, σ	40.65 mN/m	A36	-
	Capillary number, Ca	9.59×10^{-9}	-	$\mathrm{Ca} = \mu V/\sigma$; calculated for this work from other values in this table
	Density of water, ρ_{f}	997.04 kg/m^3	A29	Value at 25 °C
	Density of toluene, ρ_{f}	862.1 kg/m^3	A10–A12	Value at 25 °C
	Density of pentane, ρ_{f}	621 kg/m^3	A12	Value at 25 °C
	Molar mass of water, M	18.015 g/mol	A30,A31	-
	Molar mass of toluene, M	92.14 g/mol	A13,A14	-
	Molar mass of pentane, M	72.15 g/mol	A15	-

	Mole fraction of toluene, x	0.5209	-	Calculated for this work from other values in this table; see Section A.4 for more information
	Mole fraction of pentane, x	0.4791	-	Calculated for this work from other values in this table; see Section A.4 for more information
	Radius of curvature of the droplets, R	60 μm	A36	50–70 μm in the literature reference; assumed to be 60 μm in this work
	Droplet contact angle on cantilever, θ_t	45°	A7,A32	Assumed in this work; same as the exploited number in the referenced water-in-oil studies
	Droplet contact angle on substrate, θ_b	90°	A7,A32	Assumed in this work; same as the exploited number in the referenced water-in-oil studies
Surface force	Dipole moment of water, u	2.6 D	A33–A35	In a recent study, it was reported to be 2.6 D.[A34] Some references propose a range; the overall range from the references is 2.4–2.9 D
	Relative permittivity of water, ε_r	78.3	A28	Value at 25 °C
	Relative permittivity of toluene, ε_r	2.38	A22	Value at 25 °C
	Relative permittivity of pentane, ε_r	1.82	A21,A23	Value at 25 °C
	Relative permittivity of pentol, ε_r	2.09	-	Calculated for this work from other values in this table; see Sections 2.4 and A.5 for more information
	Number density of water, N	33.3291×10^{27} m^{-3}	-	Calculated for this work from other values in this table; see Section 2.4 for more information
	Refractive index of water, n	1.3325	A27	Value at 25 °C
	Refractive index of toluene, n	1.4943	A10	Value at 25 °C

	Refractive index of pentane, n	1.3547	A12	Value at 25 °C
	Refractive index of pentol, n	1.4274	-	Calculated for this work from other values in this table; see Section A.6 for more information
	Electronic absorption frequency in the ultraviolet (UV) region, ν_e	3×10^{15} s^{-1}	A26	-
	Nonretarded Hamaker constant (water–pentol–water), A_H	5.20×10^{-21} J	-	Calculated for this work from other values in this table; see Section A.6 for more information
AFM	Cantilever spring constant, K	350 mN/m	A7	300–400 mN/m in the literature reference; assumed to be 350 mN/m in this work
	Initial apex separation of droplets, h_i	0.805 μm	A36	-
	Drive velocity, V	1 μm/s	A36	-

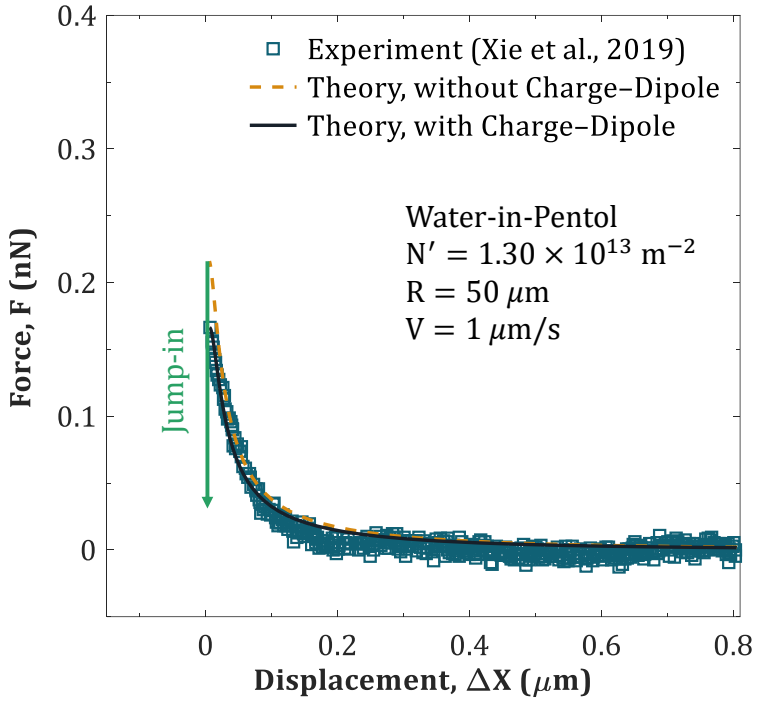

Figure A.2 Comparison between the force curves in the absence (orange dashed line) and presence (black solid line) of CD interactions for water-in-pentol droplets with radii of 50 μm for the sensitivity analysis. The measured data points are from the experimental studies (blue squares) conducted by Xie et al.[A36]

into the computation, the theory can accurately describe the behavior of the droplets and can capture the actual jump-in point. The number of surface charges per unit area is found to be 1.30×10^{13} m^{-2}, which resides in the reported range (10^{13}–10^{14} m^{-2}).[A37–A40] The results indicate that when the radii of the drops are taken to be the minimum reasonable size of 50 μm, the same conclusions can be deduced from the fitting results as when a value of 60 μm had been used, which suggests that our proposed new force is applicable.

A.9 Hydrodynamic and Disjoining Pressures versus Minimum Separation

Figure A.3 shows the computed hydrodynamic and disjoining pressure profiles along with the total dynamic pressure versus the minimum separation, i.e., the separation between the droplets' heads (h_0) until the jump-in for both toluene (Figure A.3A) and pentol (Figure A.3B). It is evident that the magnitude of the pressures is large at the jump-in (i.e., at critical separation h_{cr}) and they decay gradually as the separation between the droplets' heads increases. The magnitude of the attractive disjoining pressure (green dashed–dotted line) at small separations grows large and destabilizes the film. This phenomenon gives rise to the jump-in and initiates the collision. In other words, the attractive disjoining pressure due to the surface forces initially prevails over the hydrodynamic pressure (see the total pressure, black solid line), and then, when the magnitude of this disjoining

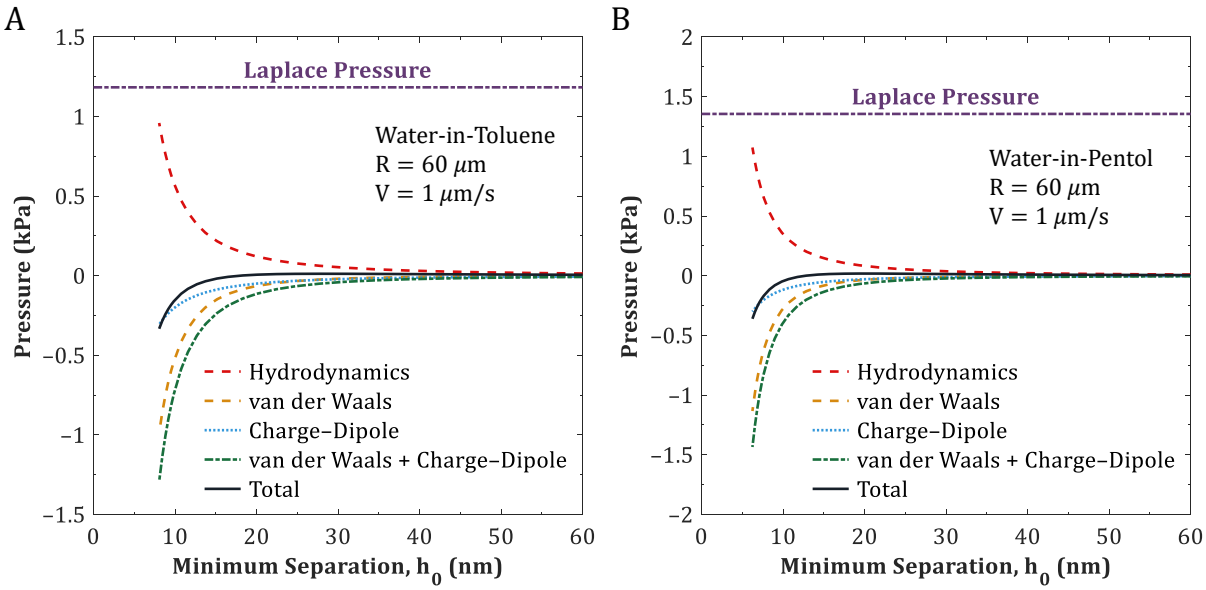

Figure A.3 Theoretical curves of different pressure contributions for the interaction between two water droplets submerged in pure toluene (A) and pure pentol (B) vs minimum separation h_0.

pressure becomes larger than the Laplace pressure (purple dashed–dotted line), the jump-in occurs.[A41]

A.10 Shear Stress at the Droplet–Liquid Interface in Water-in-Oil Systems

The reason that a maximum point (i.e., the droplet's rim) is observed along the shear stress profile can be explained by eq (2.11) from Chapter 2. The shear stress formula is proportional to the change of the hydrodynamic pressure along the radial coordinate ($\tau_f \propto \partial p/\partial r$). From the mathematical viewpoint, there are two inflection points on each hydrodynamic pressure profile (marked by circles in Figure 2.7A,B in Chapter 2) at which the curvature sign alters (due to $\partial^2 p/\partial r^2 = 0$). In other words, at these points, the slope of the shear stress curve becomes zero ($\partial \tau_f/\partial r = \partial^2 p/\partial r^2 = 0$) and two extremum values appear on its profile. These maximum points are demonstrated by circles in Figure A.4 as well (one on each side of the droplet). Before the inflection point, the curvature of the hydrodynamic pressure profile is concave downward, while it is concave upward after passing this point (evident in Figure 2.7A,B in Chapter 2). This point is also known as the *rim* of the droplet.[A1,A42]

Since, in this study, droplets eventually coalesce, the thin liquid film between the droplets experience huge alterations. As the upper droplet approaches the lower one, the film thickness reduces, and the interface of the droplets becomes more prone to deformation due to the existence of strong hydrodynamic effects and large attractive surface forces (i.e., vdW and CD). The attractive surface forces tend to rupture the film and lead to the coalescence of the drops. Therefore, the attractive surface forces drastically alter the behavior of the draining film and affect the shear stress profiles. As can be seen from Figure A.4, the shear stress curves move toward the upper

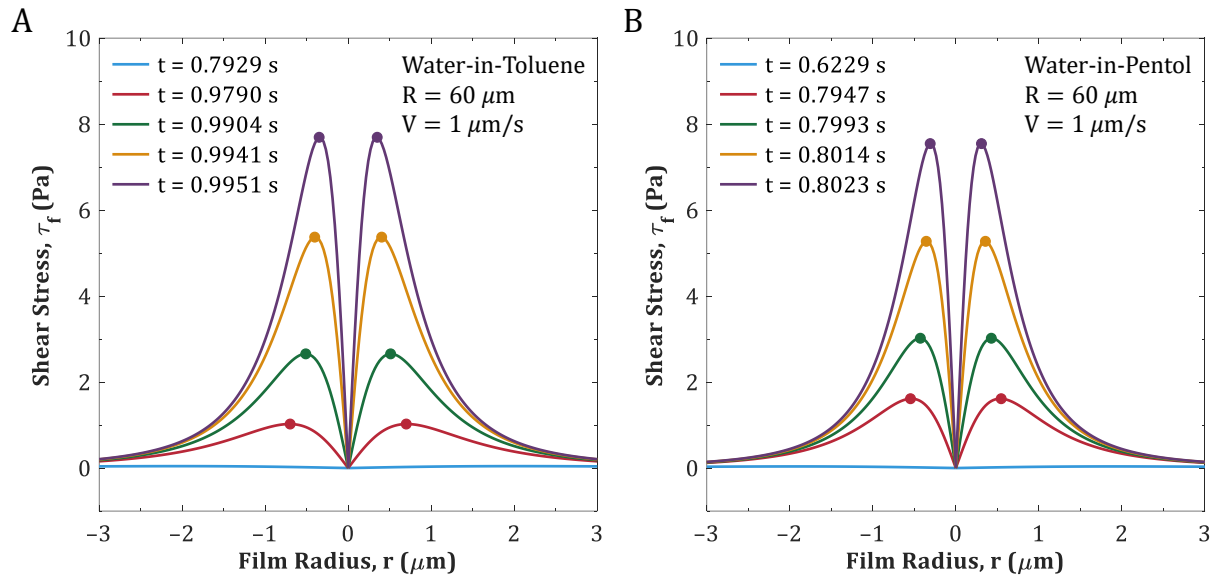

Figure A.4 Temporal evolution of shear stress at the water droplet and oil interface for pure toluene (A) and pure pentol (B). The filled circles at the peaks of the profiles indicate the corresponding inflection points on the hydrodynamic pressure profiles shown in Figure 2.7A,B in Chapter 2. These points reflect the movement of the rim positions toward lower absolute radial regions.

regions over time, and their magnitude at a given radial coordinate becomes larger than the one for a previous curve (at an earlier time). Here, this phenomenon is shown until the jump-in point ($t = 0.9951$ sec for toluene and $t = 0.8023$ sec for pentol) in Figure A.4. The maximum shear stresses at the critical film thickness for toluene and pentol are 7.69 and 7.54 Pa, respectively, which occur at the radial positions of 349.66 and 308.78 nm, respectively. When the water droplets are at very close separations, the attractive surface forces pull them together to induce the jump-in and coalescence. As a result of this pulling, the heads of the droplets sharpen, and the rim moves towards the center or lower radial values over time. This movement of the position of the rim r_m is illustrated in Figure A.5 over time for both toluene and pentol cases. This phenomenon can also be observed by the shifts in the position of maximum shear stresses in Figure A.4 (shown

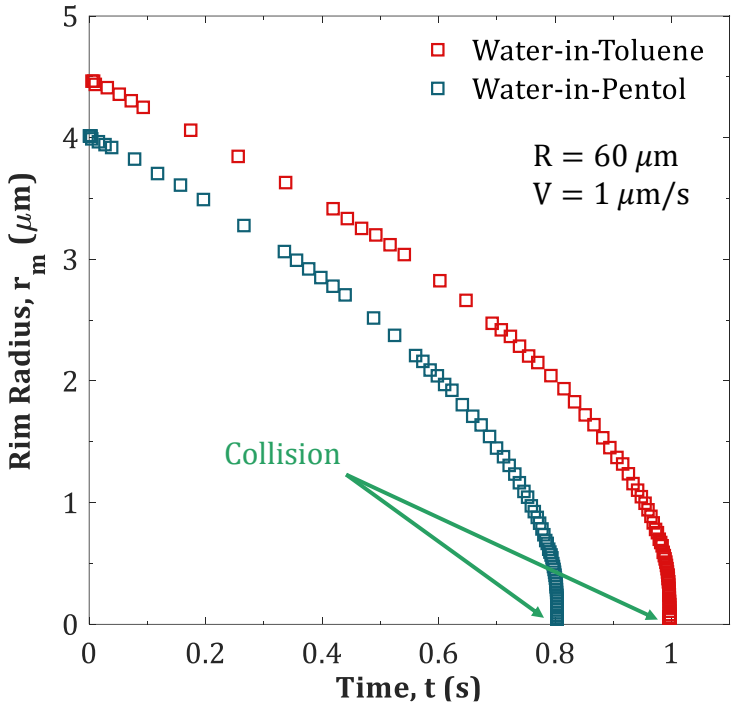

Figure A.5 Theoretical curves of the position of the rim (r_m) along the radial coordinate at various instants of time for water droplets immersed in pure toluene (red squares) and pure pentol (blue squares).

by circles) or the inflection points in the hydrodynamic pressure curves in Figure 2.7A,B (circles) in Chapter 2 toward lower absolute radial positions on each side of the drop (for $r > 0$, the shift is toward left and for $r < 0$, the shift is toward right). The shear stress calculations have similar trends in terms of profile shape and movement of the position of the rim (either toward higher or lower radial values) to the results of previous studies on droplets or bubbles that had vdW forces as the only attractive force;[A42,A43] however, the results of our calculations differ numerically since we included CD attraction.

A.11 References

(A1) Klaseboer, E.; Chevaillier, J. P.; Gourdon, C.; Masbernat, O. Film Drainage between Colliding Drops at Constant Approach Velocity: Experiments and Modeling. *J. Colloid Interface Sci.* **2000**, *229* (1), 274–285.

(A2) Carnie, S. L.; Chan, D. Y. C.; Lewis, C.; Manica, R.; Dagastine, R. R. Measurement of Dynamical Forces between Deformable Drops Using the Atomic Force Microscope. I. Theory. *Langmuir* **2005**, *21* (7), 2912–2922.

(A3) Atkinson, K. E. *An Introduction to Numerical Analysis*, 2nd ed.; John Wiley & Sons, 1991.

(A4) Jin, H.; Wang, W.; Liu, F.; Yu, Z.; Chang, H.; Li, K.; Gong, J. Roles of Interfacial Dynamics in the Interaction Behaviours between Deformable Oil Droplets. *Int. J. Multiph. Flow* **2017**, *94*, 44–52.

(A5) Kestin, J.; Khalifa, H. E.; Correia, R. J. Tables of the Dynamic and Kinematic Viscosity of Aqueous NaCl Solutions in the Temperature Range 20–150 °C and the Pressure Range 0.1–35 MPa. *J. Phys. Chem. Ref. Data* **1981**, *10* (1), 71–88.

(A6) Aleksandrov, A. A.; Dzhuraeva, E. V.; Utenkov, V. F. Viscosity of Aqueous Solutions of Sodium Chloride. *High Temp.* **2012**, *50* (3), 354–358.

(A7) Shi, C. Understanding Interaction Mechanism of Deformable Droplets in Oil Production, University of Alberta, 2016.

(A8) Shi, C.; Zhang, L.; Xie, L.; Lu, X.; Liu, Q.; Mantilla, C. A.; Van Den Berg, F. G. A.; Zeng, H. Interaction Mechanism of Oil-in-Water Emulsions with Asphaltenes Determined Using

Droplet Probe AFM. *Langmuir* **2016**, *32* (10), 2302–2310.

(A9) Manica, R.; Connor, J. N.; Dagastine, R. R.; Carnie, S. L.; Horn, R. G.; Chan, D. Y. C. Hydrodynamic Forces Involving Deformable Interfaces at Nanometer Separations. *Phys. Fluids* **2008**, *20* (3), 032101.

(A10) Katz, M.; Lobo, P. W.; Miñano, A. S.; Sólimo, H. Viscosities, Densities, and Refractive Indices of Binary Liquid Mixtures. *Can. J. Chem.* **1971**, *49* (15), 2605–2609.

(A11) Asfour, A. F. A.; Dullien, F. A. L. Viscosities and Densities of Four Binary Liquid Systems at 25.00 °C. *J. Chem. Eng. Data* **1981**, *26* (3), 312–316.

(A12) Aucejo, A.; Part, E.; Medina, P.; Sancho-Tello, M. Viscosity of Some N-Alkane/1-Chloroalkane Binary Liquid Mixtures. *J. Chem. Eng. Data* **1986**, *31* (2), 143–145.

(A13) Avgeri, S.; Assael, M. J.; Huber, M. L.; Perkins, R. A. Reference Correlation of the Viscosity of Toluene from the Triple Point to 675 K and up to 500 MPa. *J. Phys. Chem. Ref. Data* **2015**, *44* (3), 033101.

(A14) PubChem. *National Center for Biotechnology Information (2022). PubChem Compound Summary for CID 1140, Toluene.* https://pubchem.ncbi.nlm.nih.gov/compound/Toluene (accessed 2022-04-13).

(A15) PubChem. *National Center for Biotechnology Information (2022). PubChem Compound Summary for CID 8003, Pentane.* https://pubchem.ncbi.nlm.nih.gov/compound/Pentane (accessed 2022-04-13).

(A16) Krall, A. H.; Sengers, J. V.; Kestin, J. Viscosity of Liquid Toluene at Temperatures from

25 to 150°C and at Pressures up to 30 MPa. *J. Chem. Eng. Data* **1992**, *37* (3), 349–355.

(A17) Santos, F. J. V.; Nieto de Castro, C. A.; Dymond, J. H.; Dalaouti, N. K.; Assael, M. J.; Nagashima, A. Standard Reference Data for the Viscosity of Toluene. *J. Phys. Chem. Ref. Data* **2006**, *35* (1), 1–8.

(A18) Das, A.; Frenkel, M.; Gadalla, N.; Marsh, K.; Wilhoit, R. C. *TRC Thermodynamic Tables*; Thermodynamic Research Center, Texas A&M University: College Station, TX., 1994.

(A19) Zahabi, A. Flocculation of Silica Particles in a Model Oil Solution: Effect of Adsorbed Asphaltene, University of Alberta, 2011.

(A20) D. A. G. Bruggeman. Berechnung Verschiedener Physikalischer Konstanten von Heterogenen Substanzen. I. Dielektrizitätskonstanten Und Leitfähigkeiten Der Mischkörper Aus Isotropen Substanzen. *Ann. Phys.* **1935**, *416* (7), 636–664.

(A21) Gric, T.; Hess, O. Electromagnetics of Metamaterials. In *Phenomena of Optical Metamaterials, Micro and Nano Technologies*; 2019; pp 41–73.

(A22) Ritzoulis, G.; Papadopoulos, N.; Jannakoudakis, D. Densities, Viscosities, and Dielectric Constants of Acetonitrile + Toluene at 15, 25, and 35 °C. *J. Chem. Eng. Data* **1986**, *31* (2), 146–148.

(A23) Sastry, N. V.; Valand, M. K. Densities, Viscosities, and Relative Permittivities for Pentane + 1-Alcohols (C1 to C12) at 298.15 K. *J. Chem. Eng. Data* **1998**, *43* (2), 152–157.

(A24) Lifshitz, E. M. The Theory of Molecular Attractive Forces between Solids. *Zhurnal Eksp. Teor. Fiz.* **1955**, *29*, 94–110.

(A25) Lifshitz, E. M.; Hamermesh, M. The Theory of Molecular Attractive Forces between Solids. In *Perspectives in Theoretical Physics*; Pergamon Press plc, 1992; pp 329–349.

(A26) Jacob N. Israelachvili. *Intermolecular and Surface Forces*, 3rd ed.; Academic Press, 2011.

(A27) Hale, G. M.; Querry, M. R. Optical Constants of Water in the 200-Nm to 200-Mm Wavelength Region. *Appl. Opt.* **1973**, *12* (3), 555–563.

(A28) Malmberg, C. G.; Maryott, A. A. Dielectric Constant of Water from 0° to 100°C. *J. Res. Natl. Inst. Stand. Technol.* **1956**, *56* (1), 1–8.

(A29) Spieweck, F.; Bettin, H. Review: Solid and Liquid Density Determination / Übersicht: Bestimmung Der Dichte von Festkörpern Und Flüssigkeiten. *tm - Tech. Mess.* **1992**, *59* (7–8), 285–292.

(A30) Cohen, E. R.; Cvitaš, T.; Frey, J. G.; Holmstrőm, B.; Kuchitzu, K.; Marquardt, R.; Mills, I.; Pavese, F.; Quack, M.; Stohner, J.; Strauss, H. L.; Takami, M.; Thor, A. J. *Quantities, Units and Symbols in Physical Chemistry*, 3rd ed.; International Union of Pure and Applied Chemistry, The Royal Society of Chemistry, 2007.

(A31) PubChem. *National Center for Biotechnology Information (2022). PubChem Compound Summary for CID 962, Water.* https://pubchem.ncbi.nlm.nih.gov/compound/962 (accessed 2022-04-13).

(A32) Shi, C.; Zhang, L.; Xie, L.; Lu, X.; Liu, Q.; He, J.; Mantilla, C. A.; Van Den Berg, F. G. A.; Zeng, H. Surface Interaction of Water-in-Oil Emulsion Droplets with Interfacially Active Asphaltenes. *Langmuir* **2017**, *33* (5), 1265–1274.

(A33) Gregory, J. K.; Clary, D. C.; Liu, K.; Brown, M. G.; Saykally, R. J. The Water Dipole Moment in Water Clusters. *Science (80-.).* **1997**, *275* (5301), 814–817.

(A34) Bai, C.; Kale, S.; Herzfeld, J. Chemistry with Semi-Classical Electrons: Reaction Trajectories Auto-Generated by Sub-Atomistic Force Fields. *Chem. Sci.* **2017**, *8* (6), 4203–4210.

(A35) Bakó, I.; Csókás, D.; Mayer, I.; Pothoczki, S.; Pusztai, L. The Influence of Cations on the Dipole Moments of Neighboring Polar Molecules. *Int. J. Quantum Chem.* **2021**, *122* (8), e26758.

(A36) Xie, L.; Lu, Q.; Tan, X.; Liu, Q.; Tang, T.; Zeng, H. Interfacial Behavior and Interaction Mechanism of Pentol/Water Interface Stabilized with Asphaltenes. *J. Colloid Interface Sci.* **2019**, *553*, 341–349.

(A37) Schoeler, A. M.; Josephides, D. N.; Sajjadi, S.; Lorenz, C. D.; Mesquida, P. Charge of Water Droplets in Non-Polar Oils. *J. Appl. Phys.* **2013**, *114* (14), 144903.

(A38) Leunissen, M. E.; Zwanikken, J.; van Roij, R.; Chaikin, P. M.; van Blaaderen, A. Ion Partitioning at the Oil–Water Interface as a Source of Tunable Electrostatic Effects in Emulsions with Colloids. *Phys. Chem. Chem. Phys.* **2007**, *9* (48), 6405–6414.

(A39) Zwanikken, J.; van Roij, R. Charged Colloidal Particles and Small Mobile Ions near the Oil-Water Interface: Destruction of Colloidal Double Layer and Ionic Charge Separation. *Phys. Rev. Lett.* **2007**, *99* (17), 178301.

(A40) de Graaf, J.; Zwanikken, J.; Bier, M.; Baarsma, A.; Oloumi, Y.; Spelt, M.; van Roij, R.

Spontaneous Charging and Crystallization of Water Droplets in Oil. *J. Chem. Phys.* **2008**, *129* (19), 194701.

(A41) Shi, C.; Cui, X.; Xie, L.; Liu, Q.; Chan, D. Y. C.; Israelachvili, J. N.; Zeng, H. Measuring Forces and Spatiotemporal Evolution of Thin Water Films between an Air Bubble and Solid Surfaces of Different Hydrophobicity. *ACS Nano* **2015**, *9* (1), 95–104.

(A42) Manica, R.; Connor, J. N.; Carnie, S. L.; Horn, R. G.; Chan, D. Y. C. Dynamics of Interactions Involving Deformable Drops: Hydrodynamic Dimpling under Attractive and Repulsive Electrical Double Layer Interactions. *Langmuir* **2007**, *23* (2), 626–637.

(A43) Zhang, X.; Manica, R.; Tchoukov, P.; Liu, Q.; Xu, Z. Effect of Approach Velocity on Thin Liquid Film Drainage between an Air Bubble and a Flat Solid Surface. *J. Phys. Chem. C* **2017**, *121* (10), 5573–5584.